Supplementary Information

for

Introducing dibenzocyclooctatetraene into actinide chemistry: isolation of rare trivalent uranium sandwich complexes

Ernesto Castellanos, Wei Su, and Selvan Demir*

Department of Chemistry, Michigan State University, 578 South Shaw Lane, East Lansing, Michigan 48824, USA

*Correspondence to: sdemir@chemistry.msu.edu (S.D.)

Table of Contents

1 X-ray Crystallography

Table S1. Crystallographic data and structural refinements of $[K(DME)_2][U(dbCOT)_2]$, **1**, [K(crypt-222)][$U(dbCOT)_2$], **2**, and [K(crypt-222)][$U(dbCOT)_2$(THF)], **3**.

	1	**2**	**3**
Empirical formula	$C_{40}H_{44}KO_4U$	$C_{50}H_{60}KN_2O_6U$	$C_{54}H_{68}KN_2O_7U$
Formula weight	865.88	1062.13	1134.23
Temperature/K	100.00(10)	100.01(10)	99.98(10)
Crystal system	monoclinic	monoclinic	monoclinic
Space group	$P2_1/n$	$P2_1/n$	$P2_1/c$
a/Å	10.50500(10)	13.17900(10)	18.39050(10)
b/Å	22.4291(2)	19.76760(10)	10.59960(10)
c/Å	14.54230(10)	18.17180(10)	26.3529(2)
α/°	90	90	90
β/°	92.7560(10)	105.9300(10)	108.9470(10)
γ/°	90	90	90
Volume/Å3	3422.46(5)	4552.27(5)	4858.69(7)
Z	4	4	4
ρ_{calc}g/cm3	1.680	1.550	1.551
μ/mm-1	14.754	11.256	10.601
F(000)	1708.0	2132.0	2292.0
Crystal size/mm3	0.11 × 0.08 × 0.06	0.156 × 0.06 × 0.055	0.25 × 0.08 × 0.08
Radiation	Cu Kα (λ = 1.54184)	Cu Kα (λ = 1.54184)	Cu Kα (λ = 1.54184)
2Θ range for data collection/°	7.25 to 160.67	6.752 to 160.692	5.08 to 160.924
Index ranges	-13 ≤ h ≤ 13, -28 ≤ k ≤ 21, -18 ≤ l ≤ 18	-16 ≤ h ≤ 14, -25 ≤ k ≤ 25, -23 ≤ l ≤ 23	-22 ≤ h ≤ 23, -12 ≤ k ≤ 13, -33 ≤ l ≤ 30
Reflections collected	36784	95067	53270
Independent reflections	7388 [R_{int} = 0.0309, R_{sigma} = 0.0217]	9910 [R_{int} = 0.0431, R_{sigma} = 0.0202]	10454 [R_{int} = 0.0434, R_{sigma} = 0.0297]
Data/restraints/parameters	7388/0/464	9910/0/589	10454/0/618
Goodness-of-fit on F2	1.098	1.169	1.137
Final R indexes [I>=2σ (I)]	R_1 = 0.0329, wR_2 = 0.0884	R_1 = 0.0216, wR_2 = 0.0562	R_1 = 0.0248, wR_2 = 0.0625
Final R indexes [all data]	R_1 = 0.0375, wR_2 = 0.0911	R_1 = 0.0233, wR_2 = 0.0569	R_1 = 0.0275, wR_2 = 0.0641
Largest diff. peak/hole / e $Å^{-3}$	1.54/-1.69	0.76/-1.24	1.22/-1.23

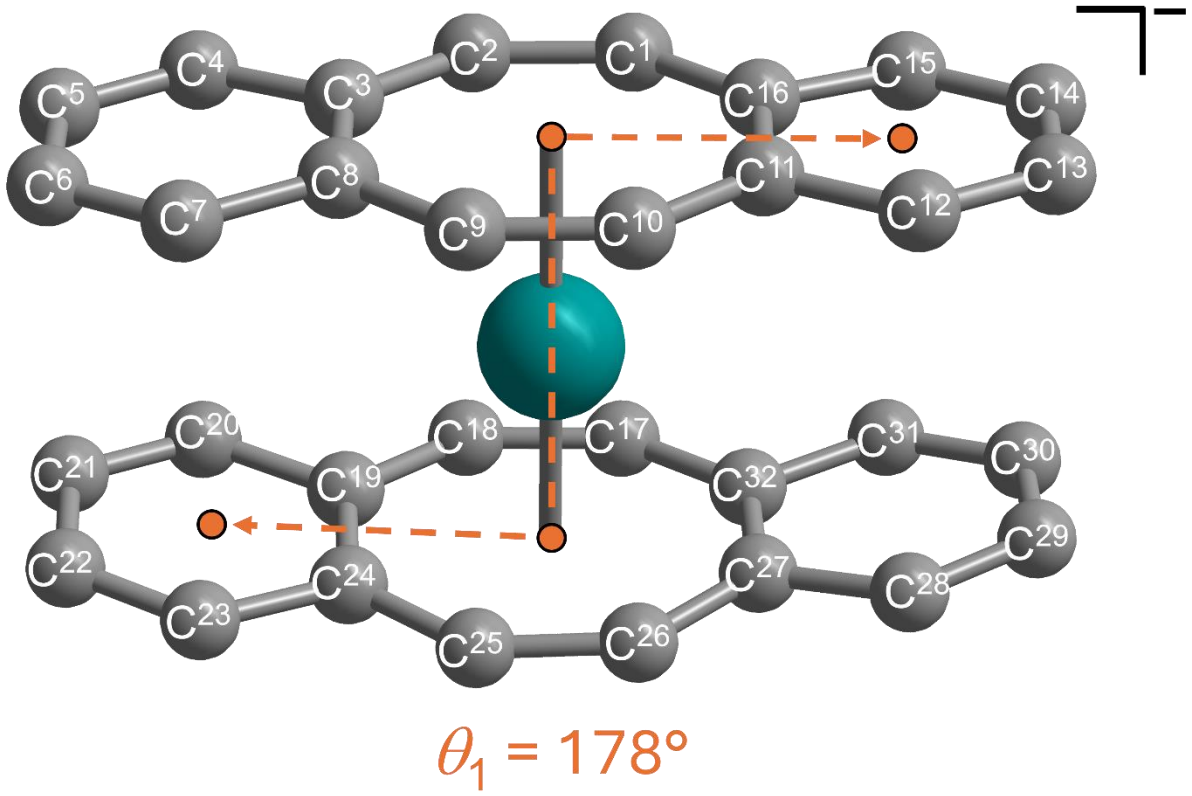

Figure S1. Structure of the $[U(dbCOT)_2]^-$ anion in a crystal of $[K(DME)_2][U(dbCOT)_2]$, **1**, with corresponding atom labels. The dihedral angles (θ_1 = 178° and θ_2 = 2°) were calculated using the benzo– and COT ring centroids. Teal and grey spheres represent U and C atoms, respectively. H atoms and the coordinating $[K(DME)_2]^+$ countercation are omitted for clarity.

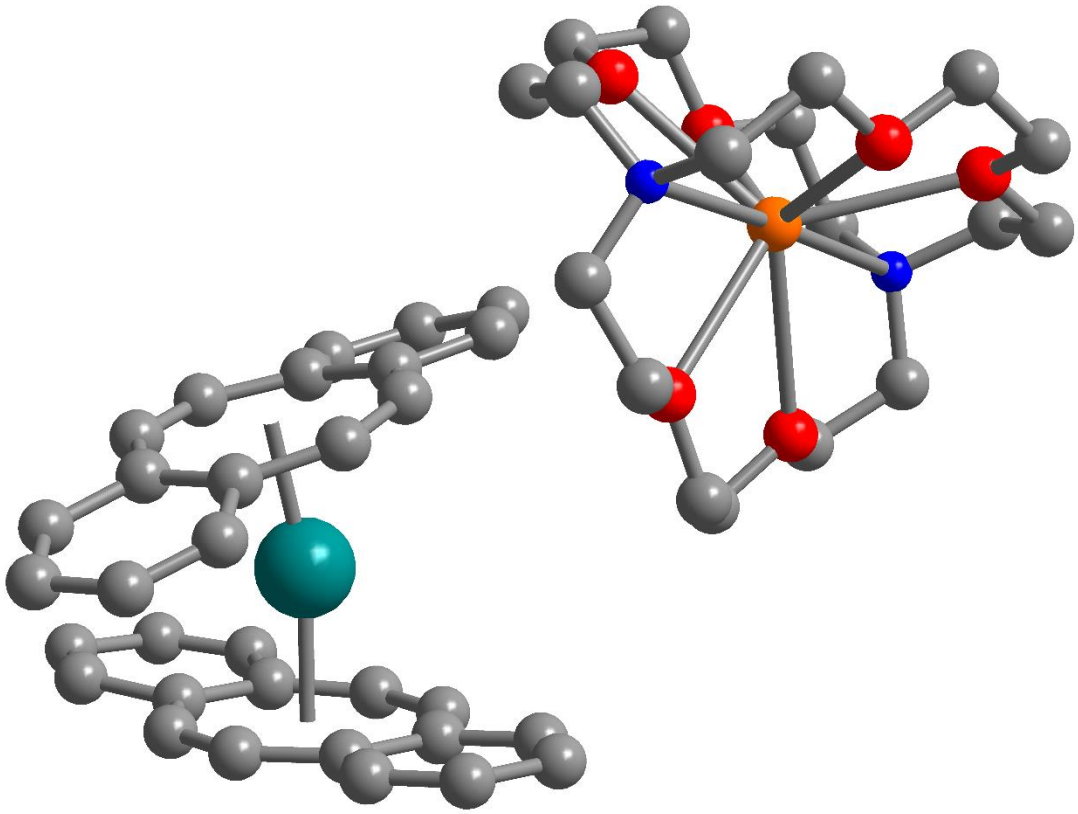

Figure S2. Structure of [K(crypt-222)][U(dbCOT)$_2$], **2**. Teal, orange, red, blue, and grey spheres represent U, K, O, N, and C atoms, respectively. H atoms are omitted for clarity.

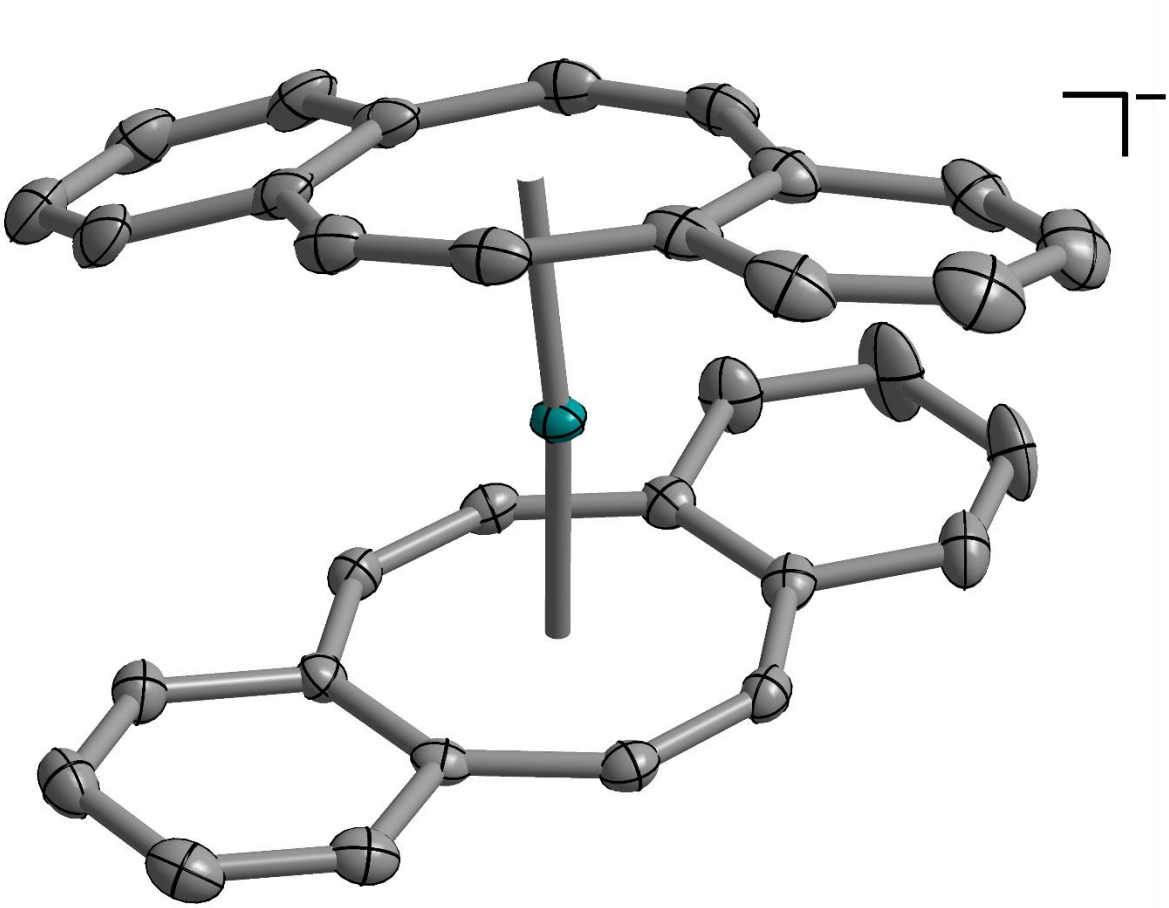

Figure S3. Structure of the $[U(dbCOT)_2]^-$ anion in a crystal of $[K(crypt\text{-}222)][U(dbCOT)_2]$, **2**, with thermal ellipsoids drawn at the 50% probability level. Teal and grey ellipsoids represent U and C atoms, respectively. H atoms and the $[K(crypt\text{-}222)]^+$ countercation are omitted for clarity.

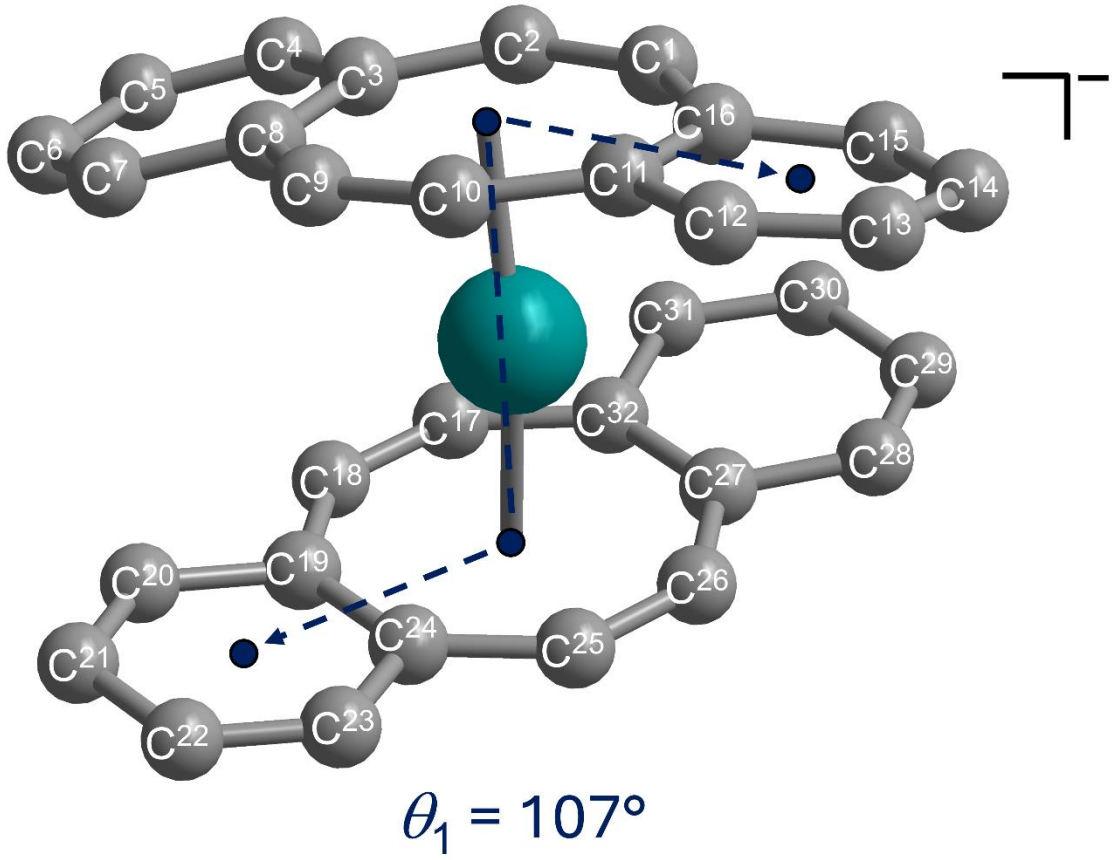

Figure S4. Structure of the $[U(dbCOT)_2]^-$ anion in a crystal of [K(crypt-222)][$U(dbCOT)_2$], **2**, in a crystal of [K(crypt-222)][$U(dbCOT)_2$], with corresponding atom labels. Teal and grey spheres represent U and C atoms, respectively. H atoms and the $[K(crypt\text{-}222)]^+$ countercation are omitted for clarity.

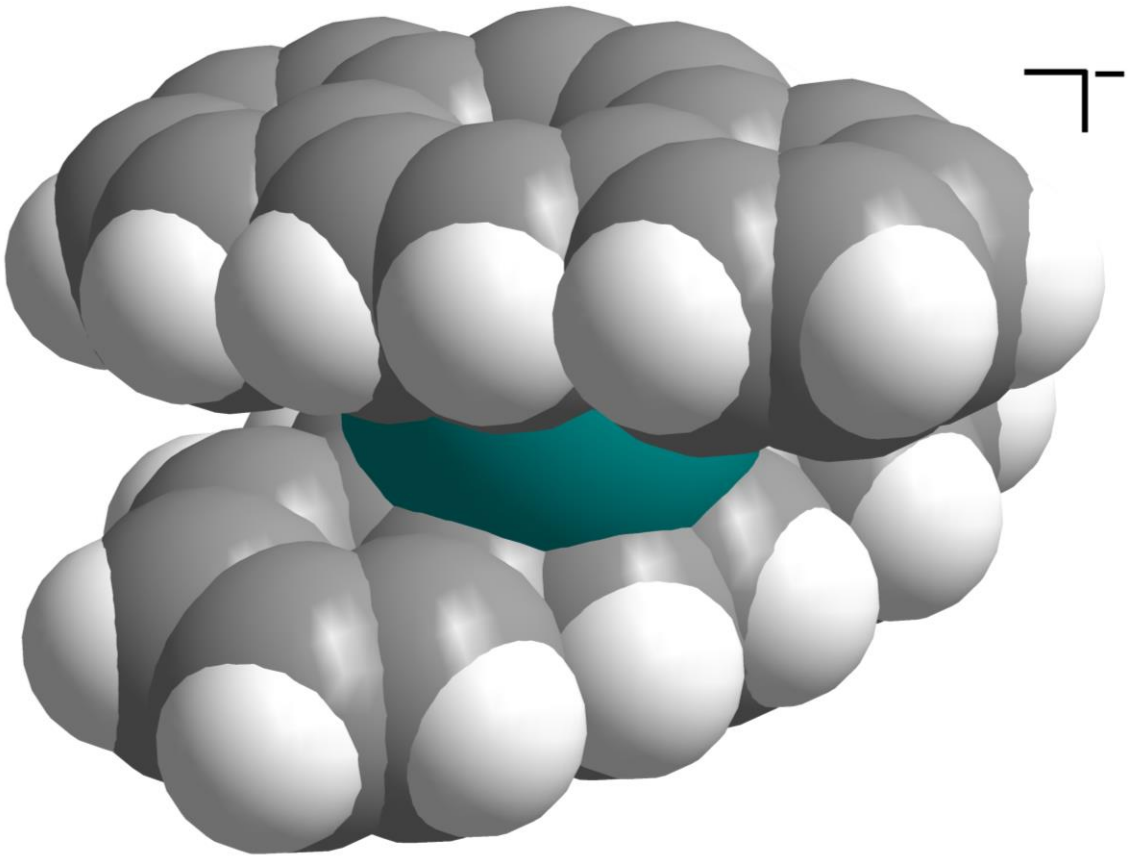

Figure S5. Space filling model of the $[U(dbCOT)_2]^-$ anion in a crystal of [K(crypt-222)][U(dbCOT)$_2$], **2**. Teal, grey, and white-grey spheres represent U, C, and H atoms, respectively. The $[K(crypt\text{-}222)]^+$ countercation is omitted for clarity.

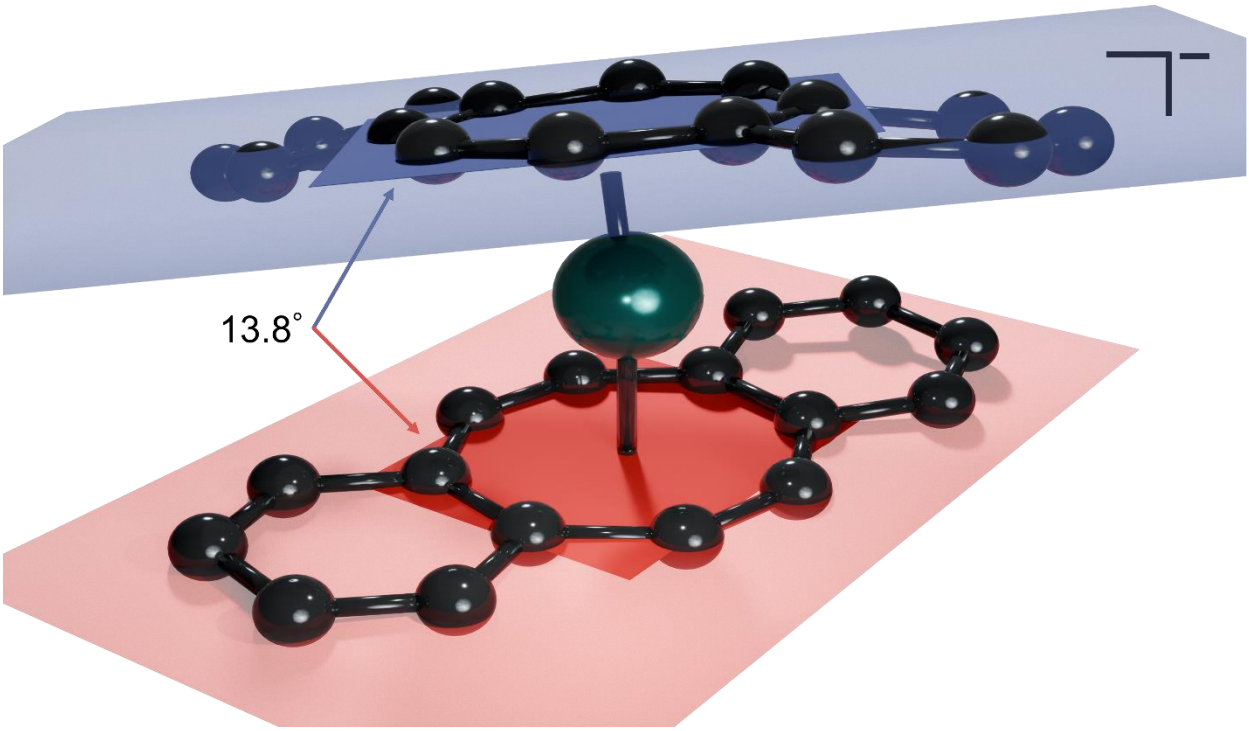

Figure S6. Structure of the $[U(dbCOT)_2]^-$ anion in a crystal of $[K(crypt\text{-}222)][U(dbCOT)_2]$, **2**, with planes bisecting the central COT rings of each $dbCOT^{2-}$ ligand, where the angle between planes is 13.8°. Teal and black spheres represent U and C atoms, respectively. H atoms and the $[K(crypt\text{-}222)]^+$ countercation are omitted for clarity.

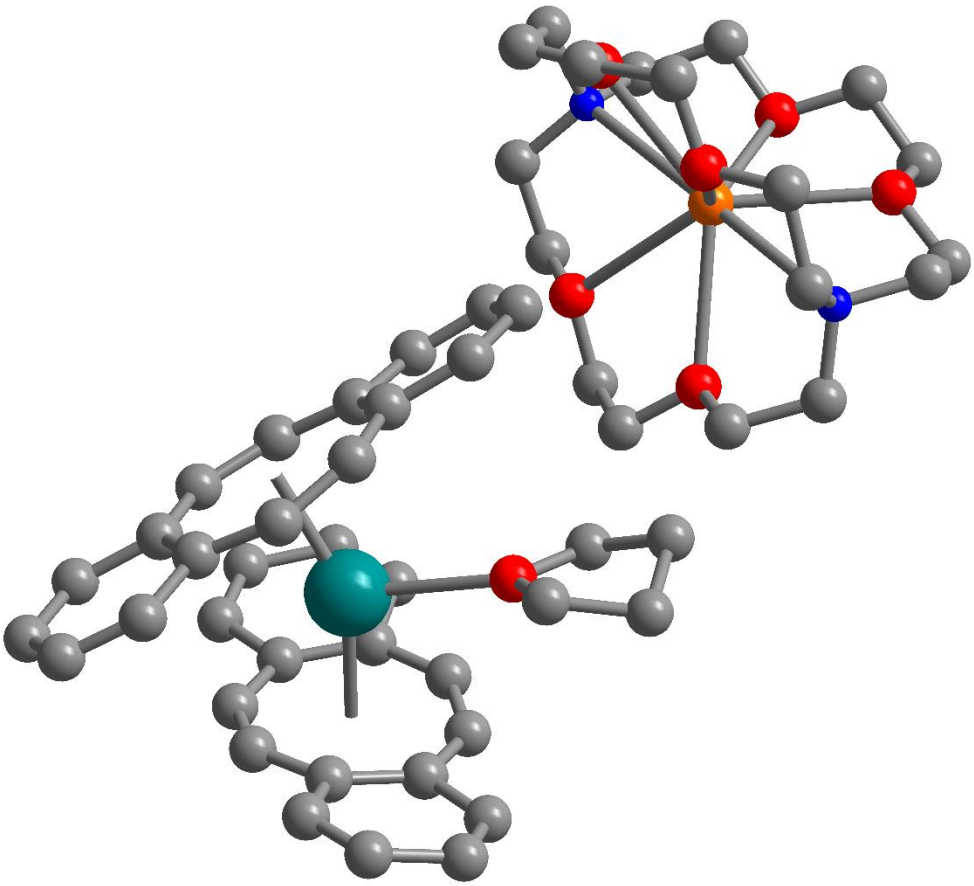

Figure S7. Structure of [K(crypt-222)][U(dbCOT)$_2$(THF)], **3**. Teal, orange, red, blue, and grey spheres represent U, K, O, N, and C atoms, respectively. H atoms are omitted for clarity.

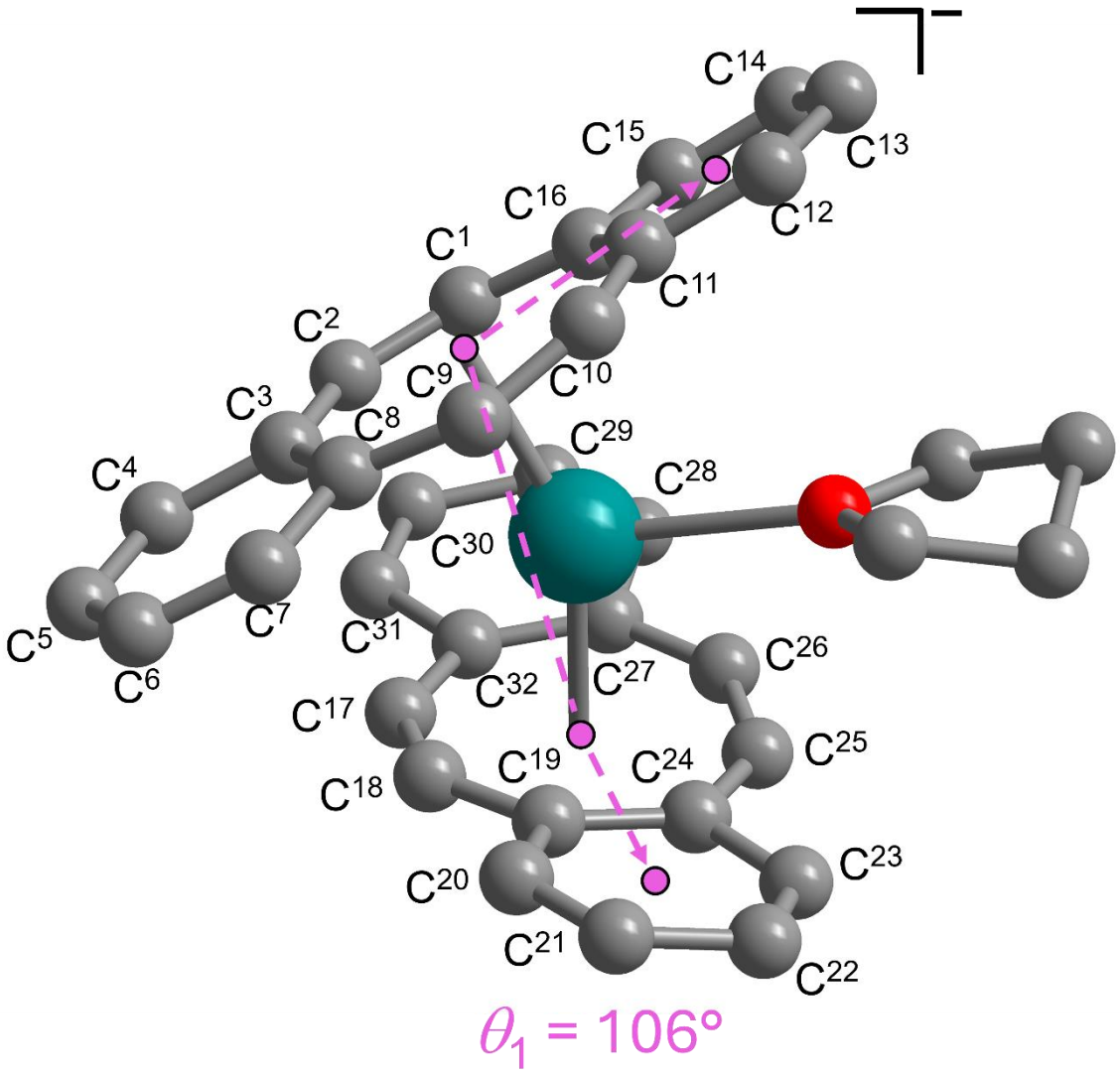

Figure S8. Structure of the $[U(dbCOT)_2(THF)]^-$ anion in a crystal of [K(crypt-222)][U(dbCOT)$_2$(THF)], **3**, with corresponding atom labels. The dihedral angles (θ_1 = 106° and θ_2 = 74°) were calculated using the benzo and COT ring centroids. Teal, red, and grey spheres represent U, O, and C atoms, respectively. H atoms and the $[K(crypt-222)]^+$ countercation are omitted for clarity.

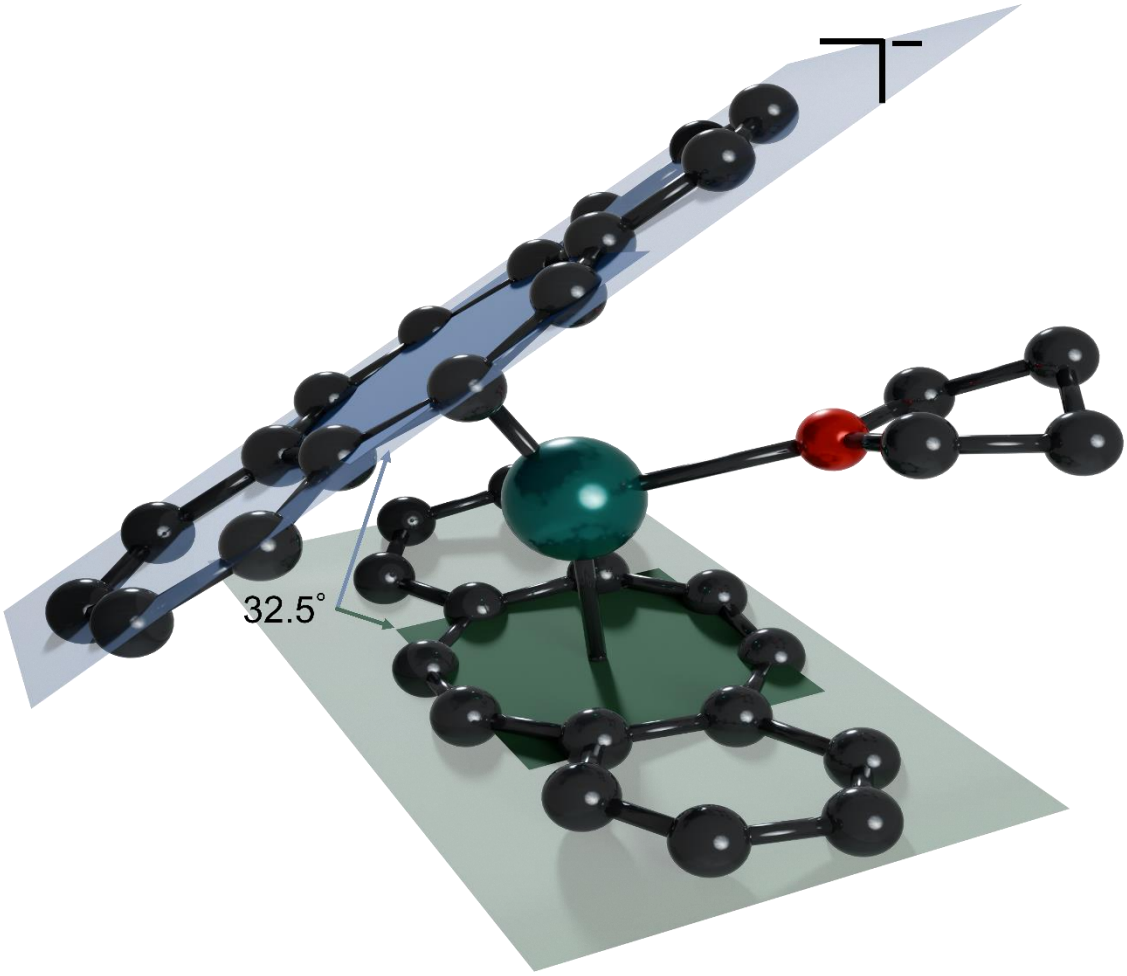

Figure S9. Structure of the $[U(dbCOT)_2(THF)]^-$ anion in a crystal of [K(crypt-222)][$U(dbCOT)_2(THF)$], **3**, with planes bisecting the central COT rings of each $dbCOT^{2-}$ ligand, where the angle between planes is 32.5°. Teal, red, and black spheres represent U, O, and C atoms, respectively. H atoms and the $[K(crypt\text{-}222)]^+$ countercation are omitted for clarity.

Table S2. Metrical parameters for the C–C distances of the cyclooctatetraenyl (COT) moieties in $[K(DME)_2][U(dbCOT)_2]$, **1**, [K(crypt-222)][$U(dbCOT)_2$], **2**, and [K(crypt-222)][$U(dbCOT)_2(THF)$], **3**. Atom labels for **1**, **2**, and **3** correspond to those given in Figures S1, S4, and S8, respectively.

C_{COT}–C_{COT} Distances (Å)			
	1	**2**	**3**
C1–C2	1.416(6)	1.407(4)	1.412(5)
C2–C3	1.437(6)	1.432(4)	1.422(5)
C3–C8	1.455(6)	1.454(4)	1.457(5)
C8–C9	1.437(6)	1.436(4)	1.419(4)
C9–C10	1.409(6)	1.419(4)	1.419(5)
C10–C11	1.431(6)	1.430(4)	1.423(5)
C11–C16	1.453(6)	1.457(4)	1.454(5)
C16–C1	1.432(6)	1.432(5)	1.426(4)
C17–C18	1.415(6)	1.409(3)	1.415(5)
C18–C19	1.434(6)	1.432(4)	1.426(5)
C19–C24	1.452(6)	1.453(4)	1.449(5)
C24–C25	1.431(6)	1.430(3)	1.421(5)
C25–C26	1.413(6)	1.421(3)	1.415(5)
C26–C27	1.431(6)	1.426(4)	1.422(5)
C27–C32	1.456(6)	1.449(4)	1.450(4)
C32–C17	1.432(6)	1.429(3)	1.424(5)

COT = cyclooctatetraenyl rings of the $dbCOT^{2-}$ ligands in **1**.

Table S3. Metrical parameters for the C–C distances of the benzo moieties of $[K(DME)_2][U(dbCOT)_2]$, **1**, $[K(crypt\text{-}222)][U(dbCOT)_2]$, **2**, and $[K(crypt\text{-}222)][U(dbCOT)_2(THF)]$, **3**. Atom labels for **1**, **2**, and **3** correspond to those given in Figures S1, S4, and S8, respectively.

C_{benzo}–C_{benzo} Distances (Å)			
	1	**2**	**3**
C3–C4	1.450(6)	1.443(5)	1.443(4)
C4–C5	1.352(6)	1.353(5)	1.357(4)
C5–C6	1.414(6)	1.426(5)	1.413(7)
C6–C7	1.356(7)	1.349(5)	1.354(5)
C7–C8	1.446(6)	1.449(4)	1.442(5)
C8–C3	1.455(6)	1.454(4)	1.457(5)
C11–C12	1.442(6)	1.454(5)	1.442(4)
C12–C13	1.352(6)	1.350(5)	1.365(6)
C13–C14	1.413(6)	1.420(5)	1.409(7)
C14–C15	1.353(6)	1.351(5)	1.366(5)
C15–C16	1.448(6)	1.444(4)	1.441(5)
C16–C11	1.453(6)	1.457(4)	1.454(5)
C3'–C4'	1.439(6)	1.437(4)	1.444(5)
C4'–C5'	1.358(6)	1.354(4)	1.352(5)
C5'–C6'	1.419(7)	1.426(5)	1.427(6)
C6'–C7'	1.359(6)	1.350(4)	1.351(6)
C7'–C8'	1.452(6)	1.443(4)	1.448(5)
C8'–C3'	1.451(6)	1.453(4)	1.449(5)
C11'–C12'	1.440(6)	1.449(4)	1.442(5)
C12'–C13'	1.352(6)	1.343(4)	1.360(5)
C13'–C14'	1.416(6)	1.417(6)	1.418(5)
C14'–C15'	1.348(6)	1.352(4)	1.362(6)
C15'–C16'	1.446(6)	1.441(4)	1.445(5)
C16'–C11'	1.456(6)	1.450(4)	1.450(4)

Table S4. Metrical parameters for the U–C distances and angles in the crystal structure of $[K(DME)_2][U(dbCOT)_2]$, **1**. Atom labels for **1**, **2**, and **3** correspond to those given in Figures S1, S4, and S8, respectively.

U–C_{COT} Distances (Å)			
	1	**2**	**3**
U–C1	2.716(4)	2.691(3)	2.723(4)
U–C2	2.707(4)	2.715(3)	2.786(4)
U–C3	2.823(4)	2.769(3)	2.908(3)
U–C8	2.825(4)	2.746(3)	2.859(3)
U–C9	2.732(4)	2.690(3)	2.734(3)
U–C10	2.737(4)	2.732(3)	2.814(3)
U–C11	2.856(4)	2.803(3)	2.939(3)
U–C16	2.835(4)	2.751(3)	2.855(4)
U–C17	2.723(4)	2.696(3)	2.759(3)
U–C18	2.707(4)	2.692(3)	2.692(3)
U–C19	2.771(4)	2.783(3)	2.802(3)
U–C24	2.782(4)	2.783(2)	2.920(4)
U–C25	2.716(4)	2.717(3)	2.864(3)
U–C26’	2.698(4)	2.714(3)	2.773(3)
U–C27’	2.745(4)	2.775(3)	2.812(3)
U–C32’	2.782(4)	2.765(3)	2.850(3)
Cnt Distances (Å)			
U–Cnt^1	2.004	2.000	2.106
U–Cnt^2	2.055	2.003	2.128
Cnt Angles (°)			
Cnt–U–Cnt	177.1	167.2	150.4
Cnt–U—Cnt–K	19.0	154.3	126.9
θ_1	177.7	107.1	106.1
θ_2	2.3	72.9	73.9

COT = cyclooctatetraenyl rings of the $dbCOT^{2-}$ ligands in **1**. Cnt = COT ring centroid. The dihedral angles (θ_1 = 177.7° and θ_2 = 2.3°) were calculated using the benzo and COT ring centroids (see Figure S1, S4, and S8).

2 NMR Spectroscopy

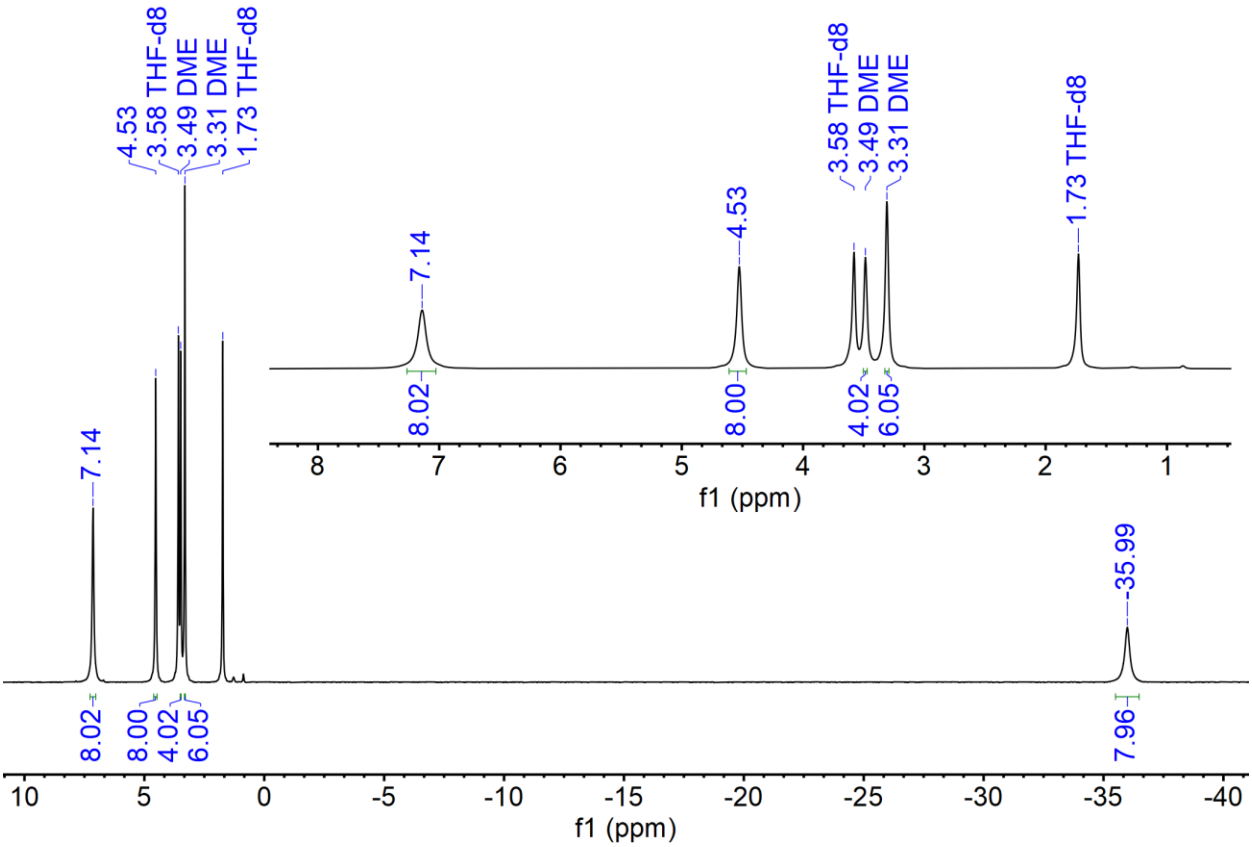

Figure S10. ^{1}H NMR spectrum of [K(DME)$_2$][U(dbCOT)$_2$], **1**, (500 MHz, THF-d_8, 25 °C): δ 7.14 (br s, 8 H, COT(C*H*(CH)$_2$C*H*)$_2$), 4.53 (br s, 8 H, COT(CH(C*H*)$_2$CH)$_2$), 3.49 (s, 4 H, H$_3$CO(C*H*$_2$)$_2$OCH$_3$), 3.49 (s, 6 H, *H*$_3$CO(CH$_2$)$_2$OC*H*$_3$), –35.99 (br s, 8 H (COT–*H*).

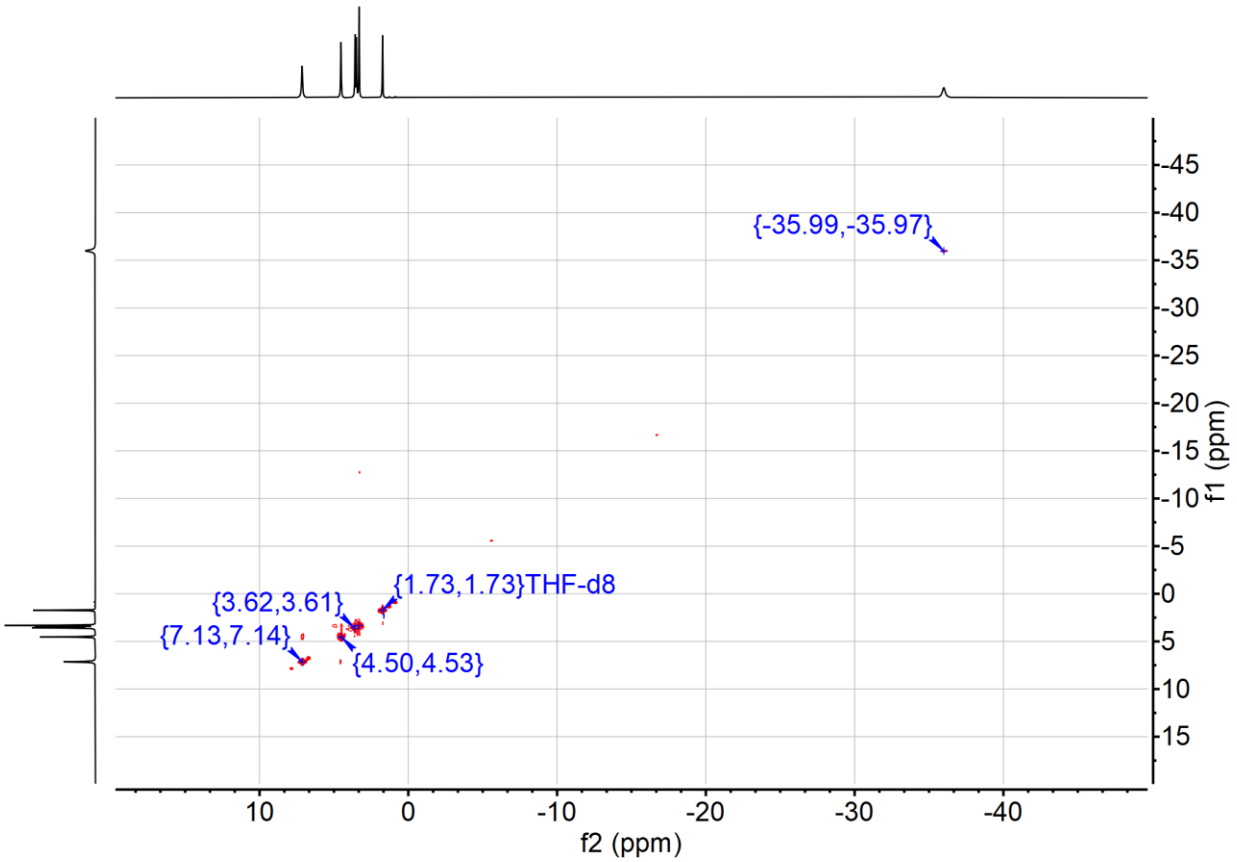

Figure S11. ^{1}H–^{1}H gCOSY spectrum of [K(DME)$_2$][U(dbCOT)$_2$], **1**, (500 MHz, THF-d_8, 25 °C).

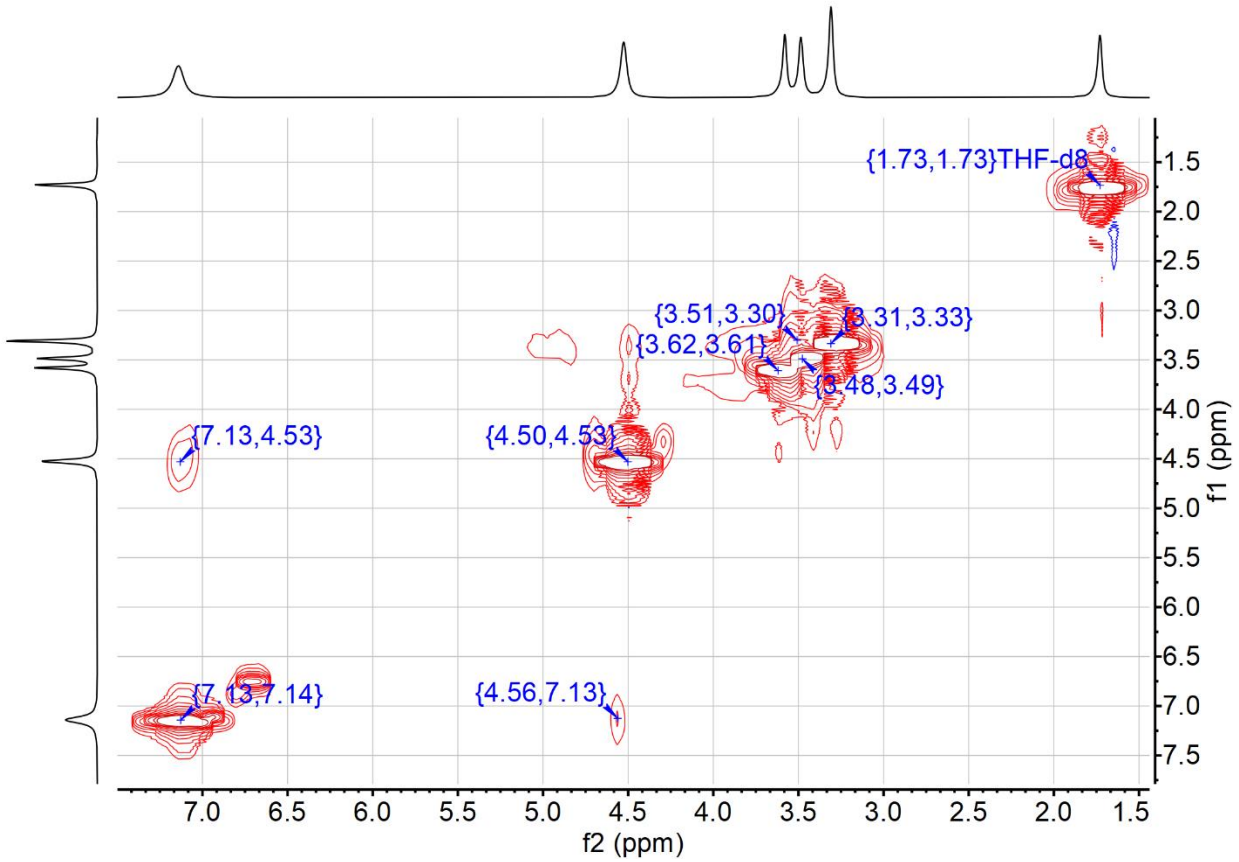

Figure S12. Magnification of the ^{1}H–^{1}H gCOSY spectrum of [K(DME)$_2$][U(dbCOT)$_2$], **1**, (500 MHz, THF-d_8, 25 °C).

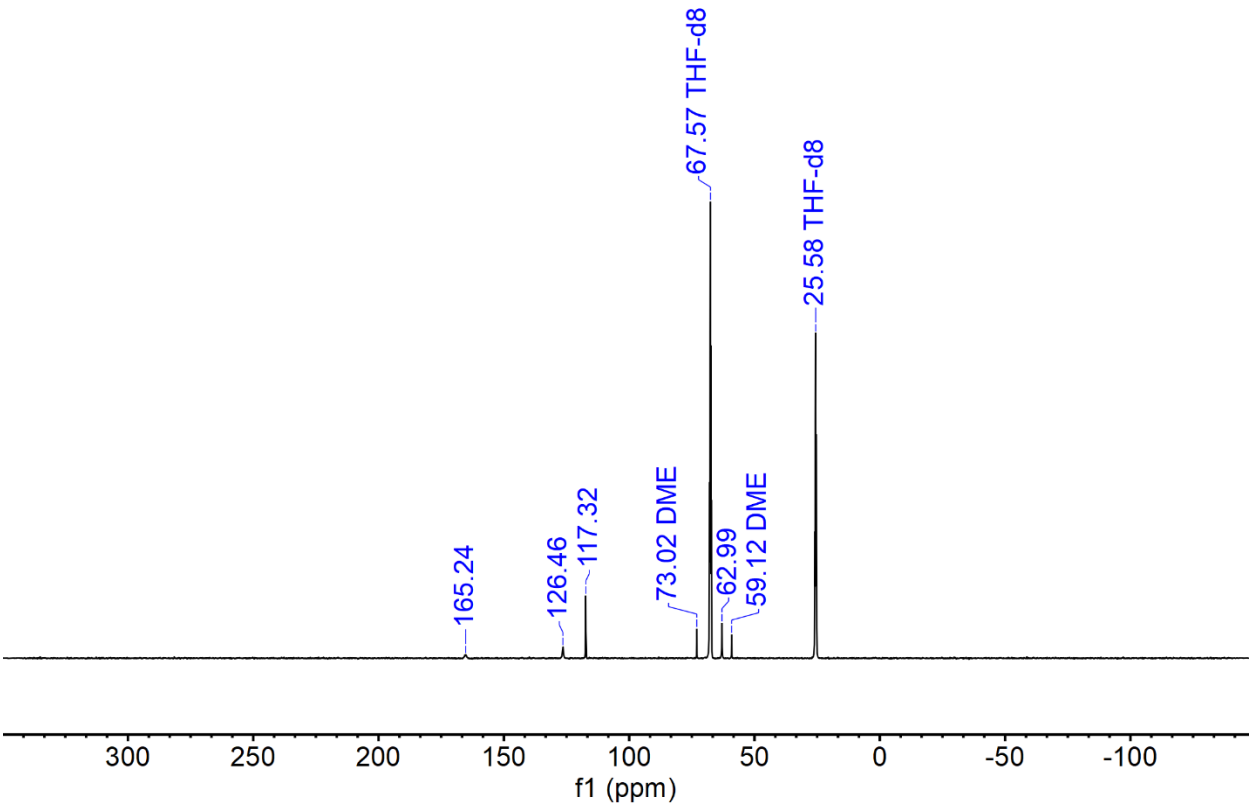

Figure S13. ^{13}C NMR spectrum of [K(DME)$_2$][U(dbCOT)$_2$], **1**, (126 MHz, THF-*d*$_8$, 25 °C): δ 165.24 (*C*$_8$H$_4$), 126.46 (*C*$_8$H$_4$), 117.32 (*C*$_6$H$_4$) 73.02 (H$_3$CO(*C*H$_2$)$_2$OCH$_3$), 62.99 (*C*$_6$H$_4$), 59.12 (H$_3$*C*O(CH$_2$)$_2$O*C*H$_3$).

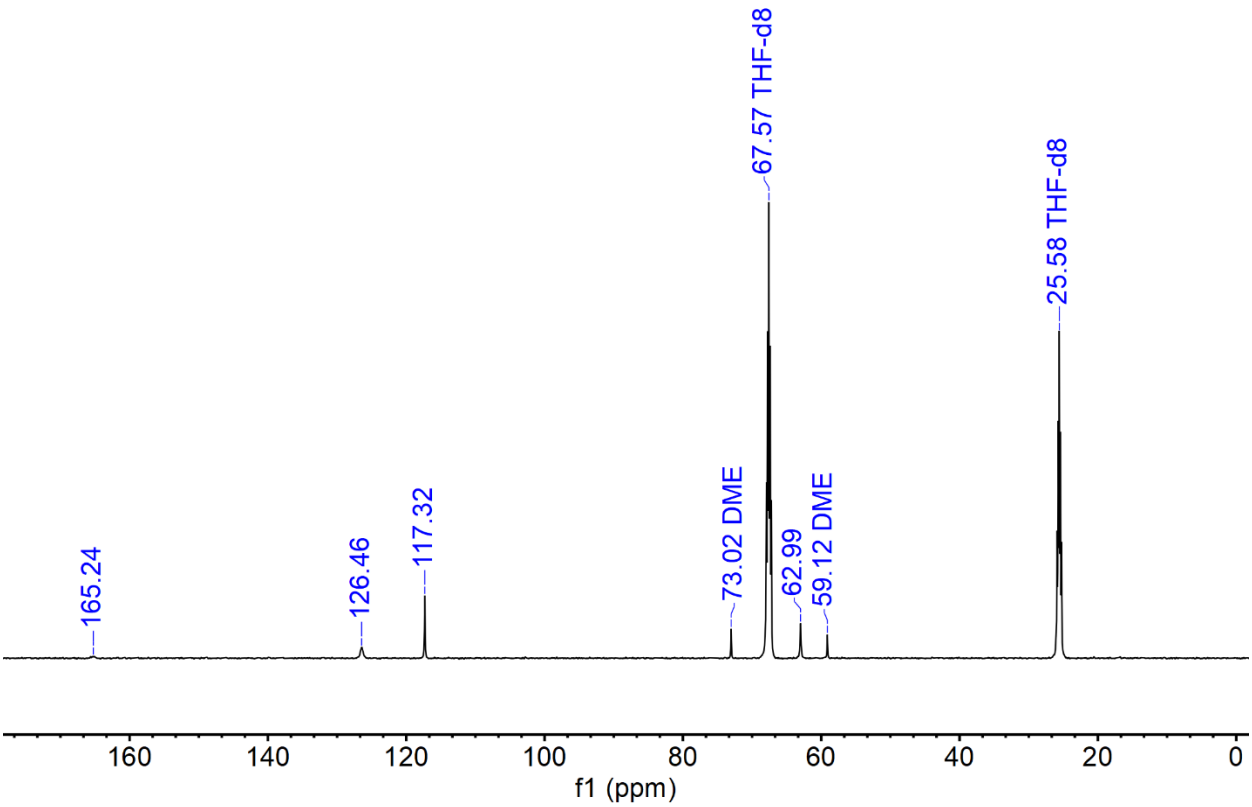

Figure S14. Magnification of the ^{13}C NMR spectrum of $[K(DME)_2][U(dbCOT)_2]$, **1**, (126 MHz, THF-d_8, 25 °C): δ 165.24 ($\underline{C}_8H_4$), 126.46 ($\underline{C}_8H_4$), 117.32 ($\underline{C}_6H_4$) 73.02 ($H_3CO(\underline{C}H_2)_2OCH_3$), 62.99 ($\underline{C}_6H_4$), 59.12 ($H_3\underline{C}O(CH_2)_2O\underline{C}H_3$).

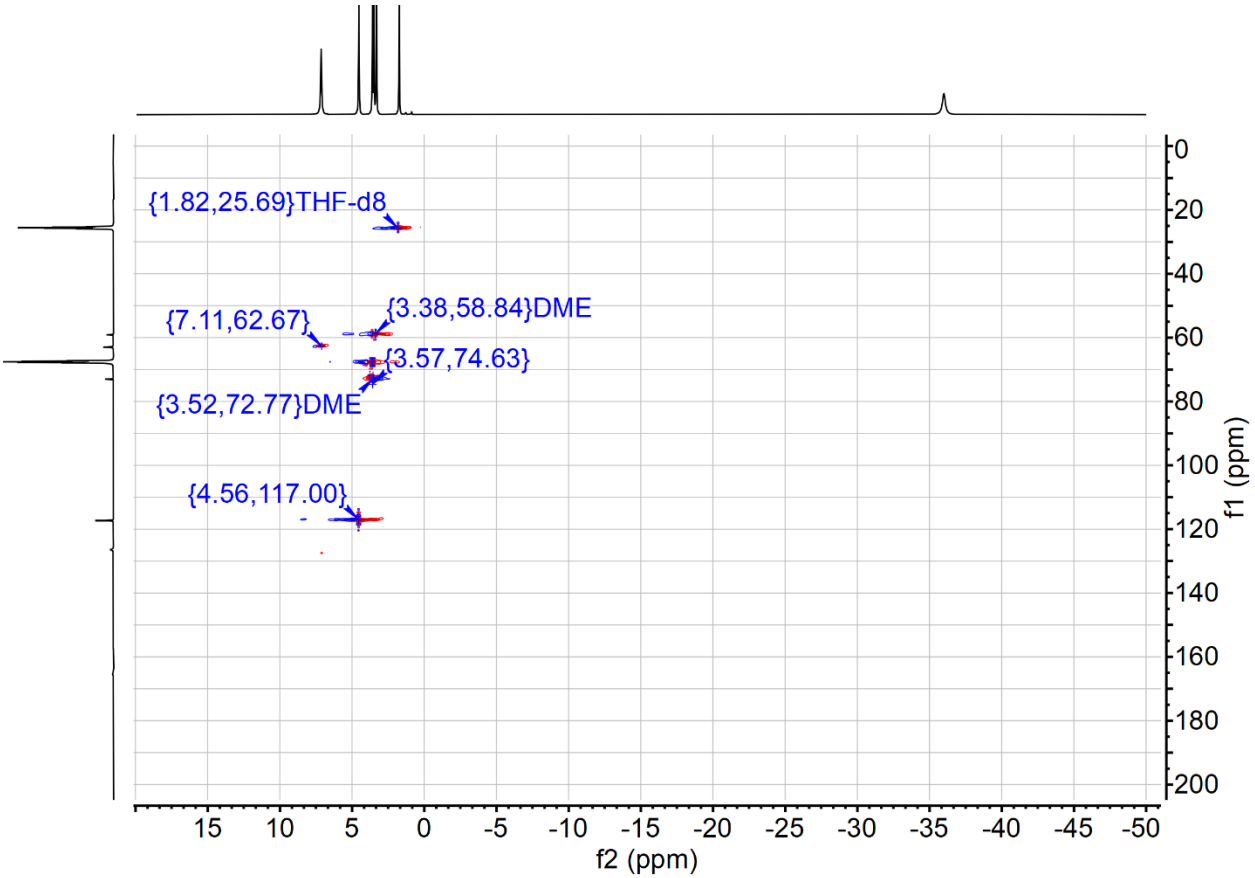

Figure S15. $^{1}H–^{13}C$ gHSQCAD spectrum of $[K(DME)_2][U(dbCOT)_2]$, **1**, (^{1}H 500 MHz, ^{13}C 126 MHz, THF-d_8, 25 °C).

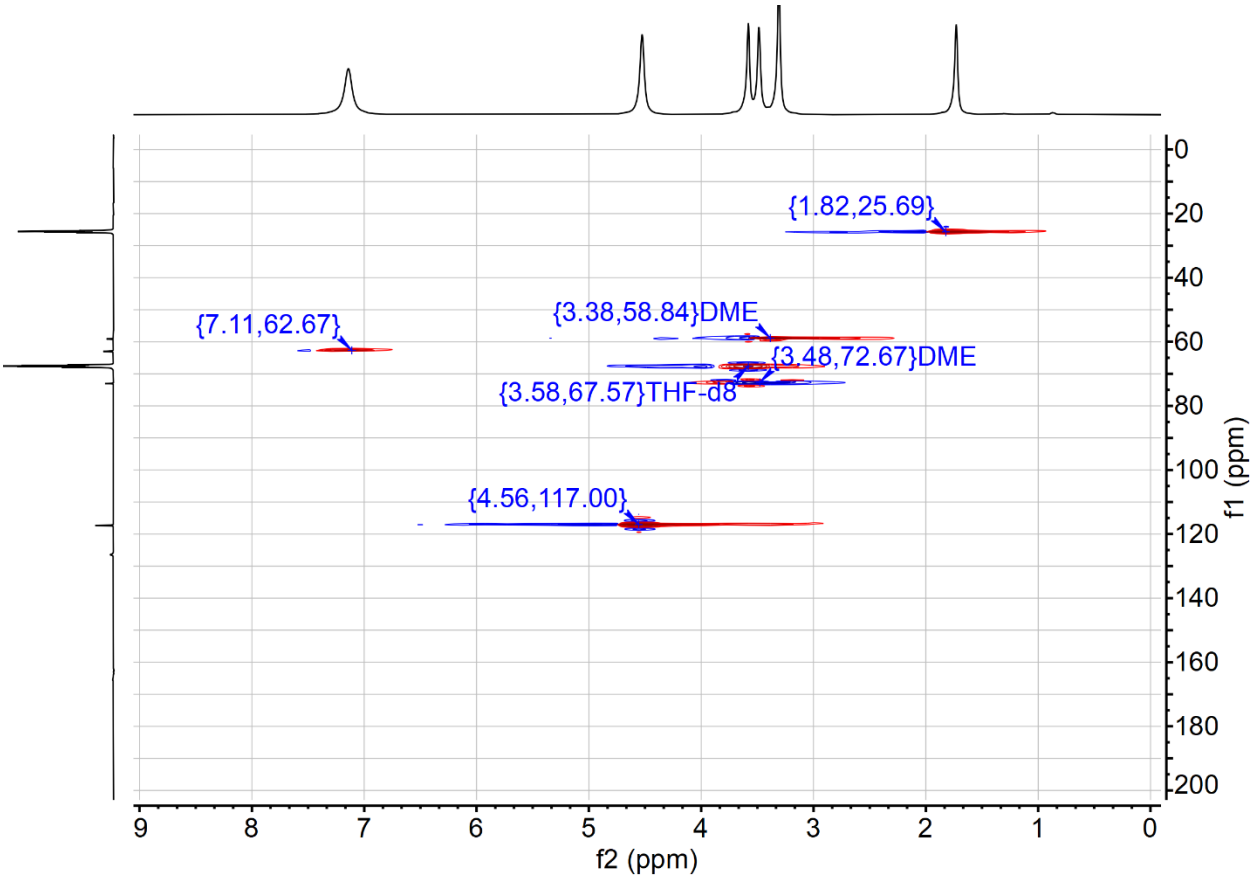

Figure S16. Magnification of the ^{1}H–^{13}C gHSQCAD spectrum of $[K(DME)_2][U(dbCOT)_2]$, **1**, (^{1}H 500 MHz, ^{13}C 126 MHz, THF-d_8, 25 °C).

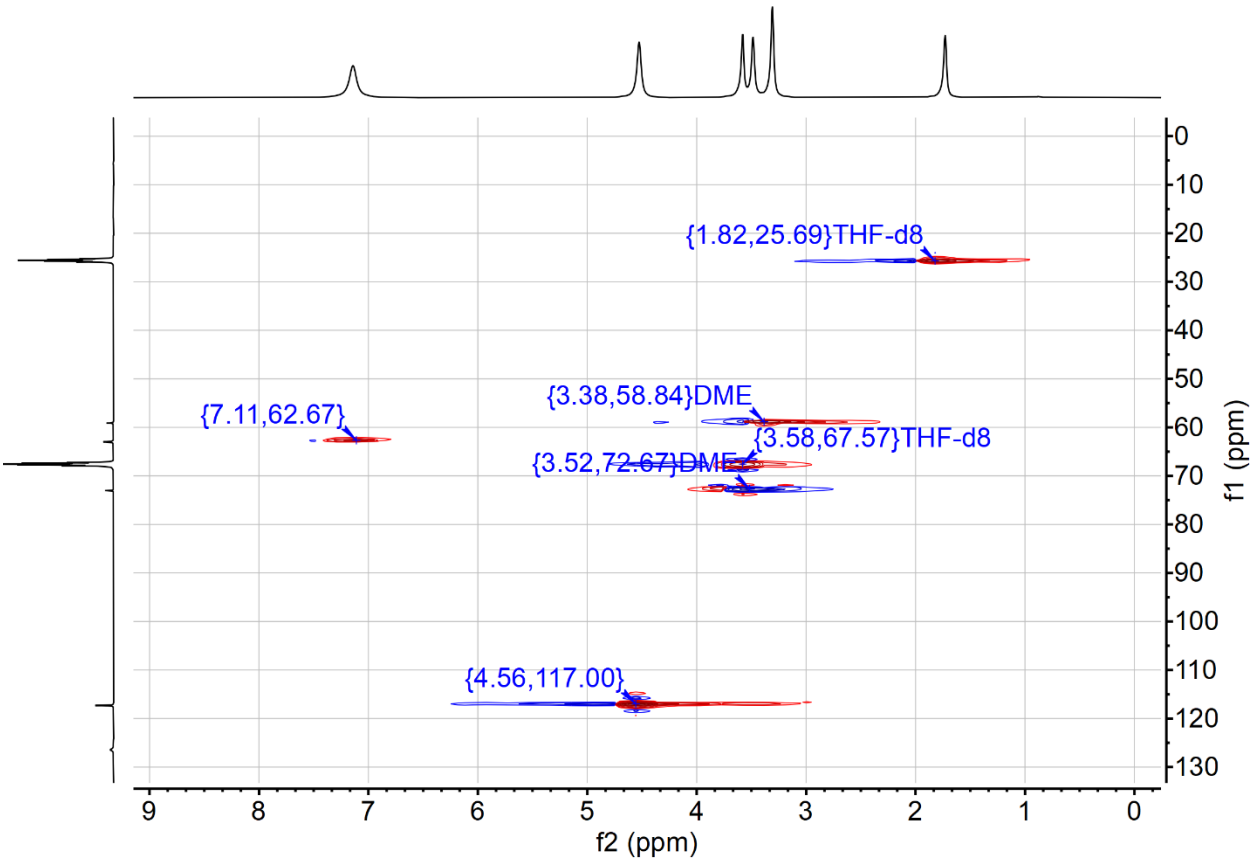

Figure S17. Magnification of the ^{1}H–^{13}C gHSQCAD spectrum of $[K(DME)_2][U(dbCOT)_2]$, **1**, (^{1}H 500 MHz, ^{13}C 126 MHz, THF-d_8, 25 °C).

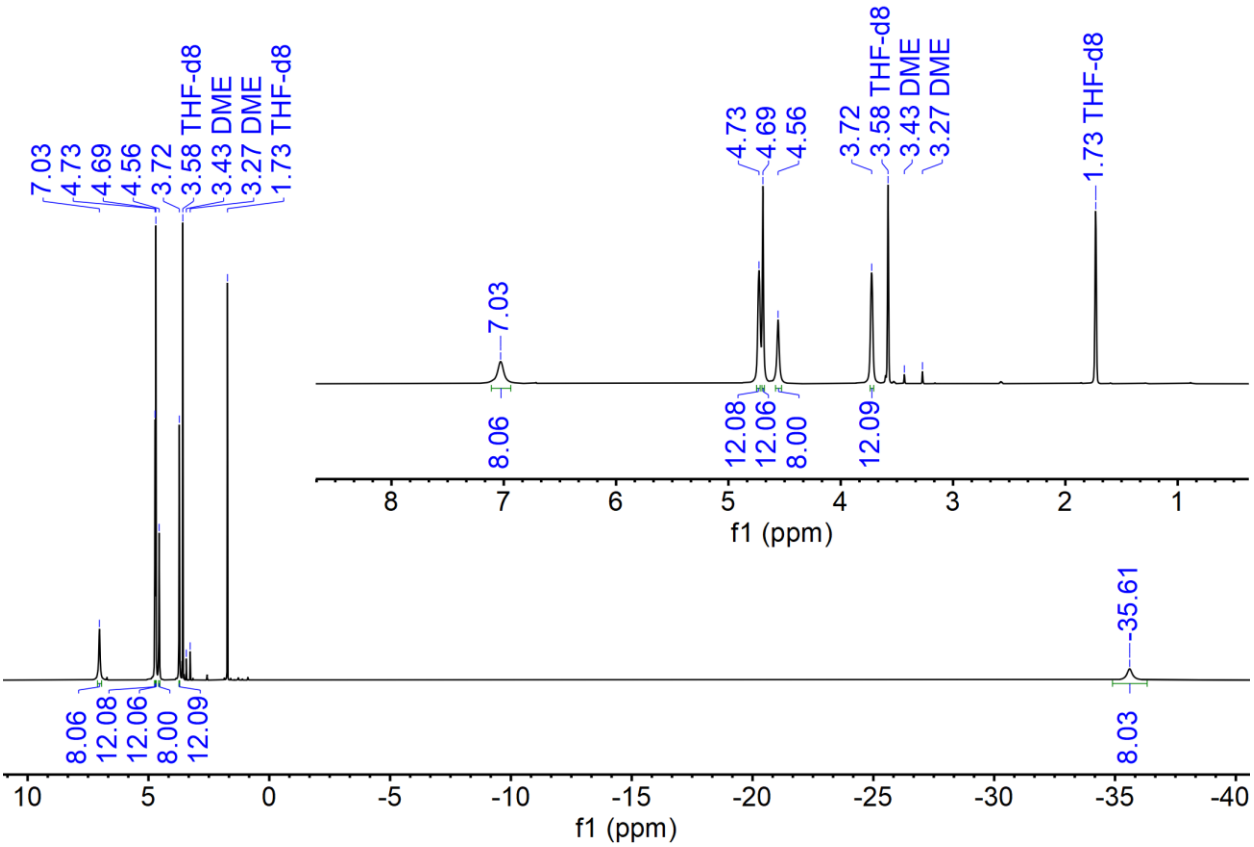

Figure S18. ^{1}H NMR spectrum of [K(crypt-222)][U(dbCOT)$_2$], **2**, (500 MHz, THF-d_8, 25 °C): 7.03 (br s, 8 H, COT(C<u>*H*</u>(CH)$_2$C<u>*H*</u>)$_2$), 4.73 (s, 12 H, OC<u>*H*</u>$_2$CH$_2$N), 4.69 (s, 12 H, O(C<u>*H*</u>$_2$)$_2$O), 4.56 (br s, 8 H, COT(CH(C<u>*H*</u>)$_2$CH)$_2$), 3.72 (s, 12 H, OCH$_2$C<u>*H*</u>$_2$N), –35.61 (br s, 8 H (COT–<u>*H*</u>).

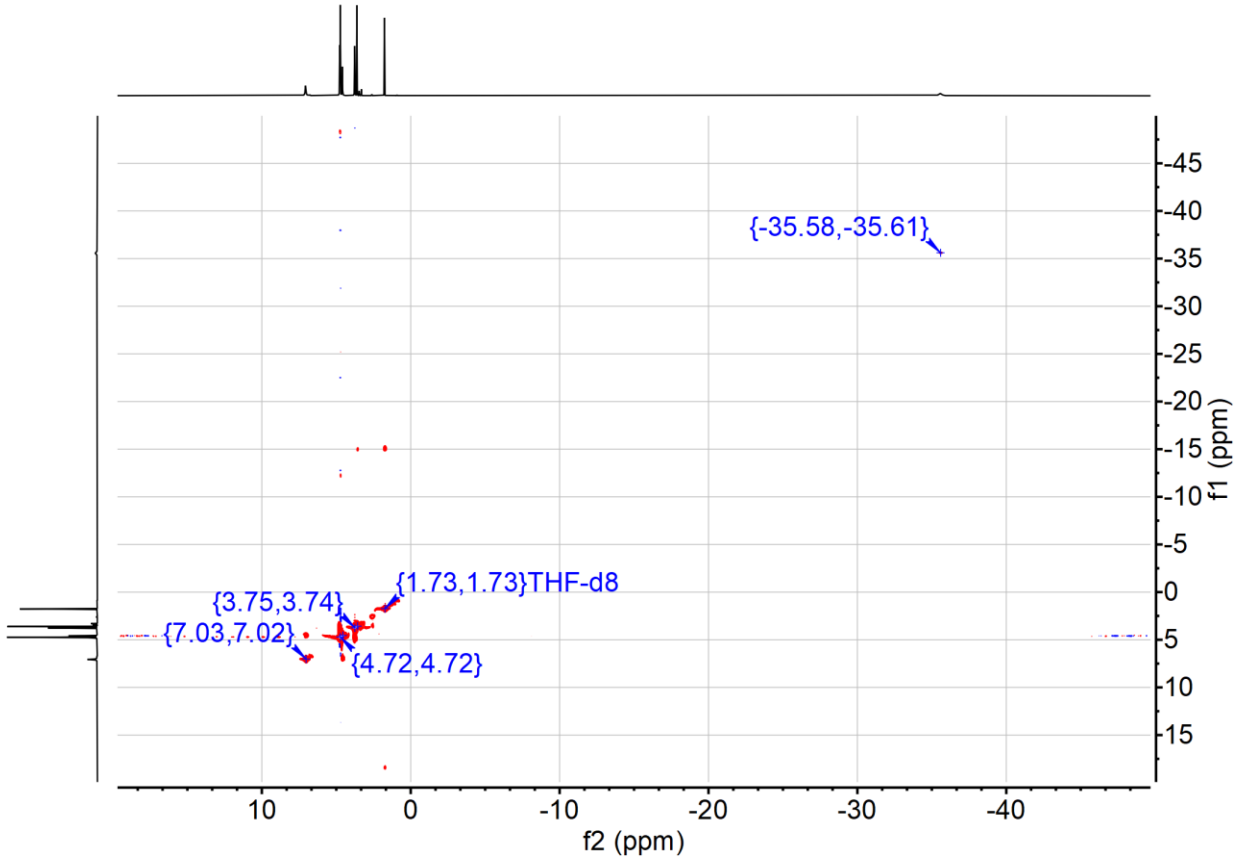

Figure S19. ^{1}H–^{1}H gCOSY spectrum of [K(crypt-222)][U(dbCOT)$_2$], **2**, (500 MHz, THF-d_8, 25 °C).

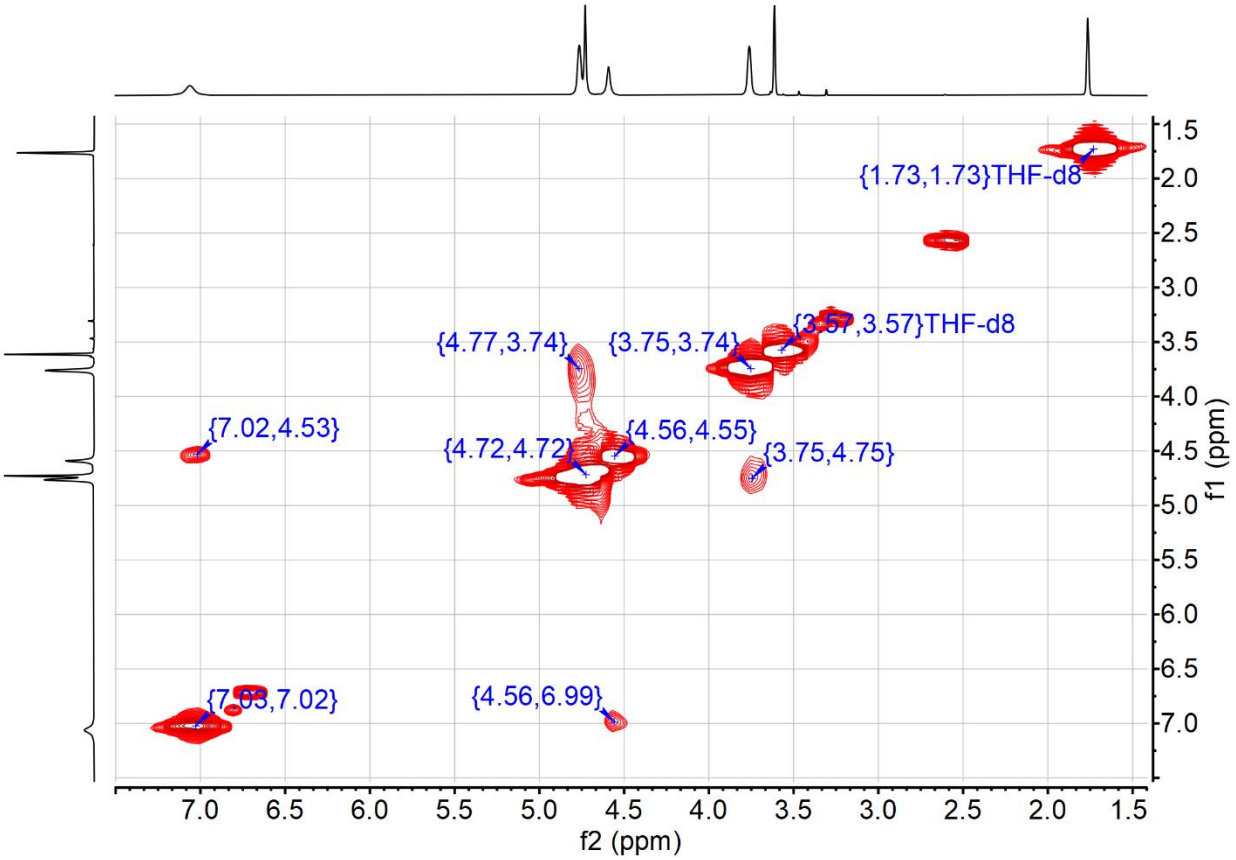

Figure S20. Magnification of the ^{1}H–^{1}H gCOSY spectrum of [K(crypt-222)][U(dbCOT)$_2$], **2**, (500 MHz, THF-d_8, 25 °C).

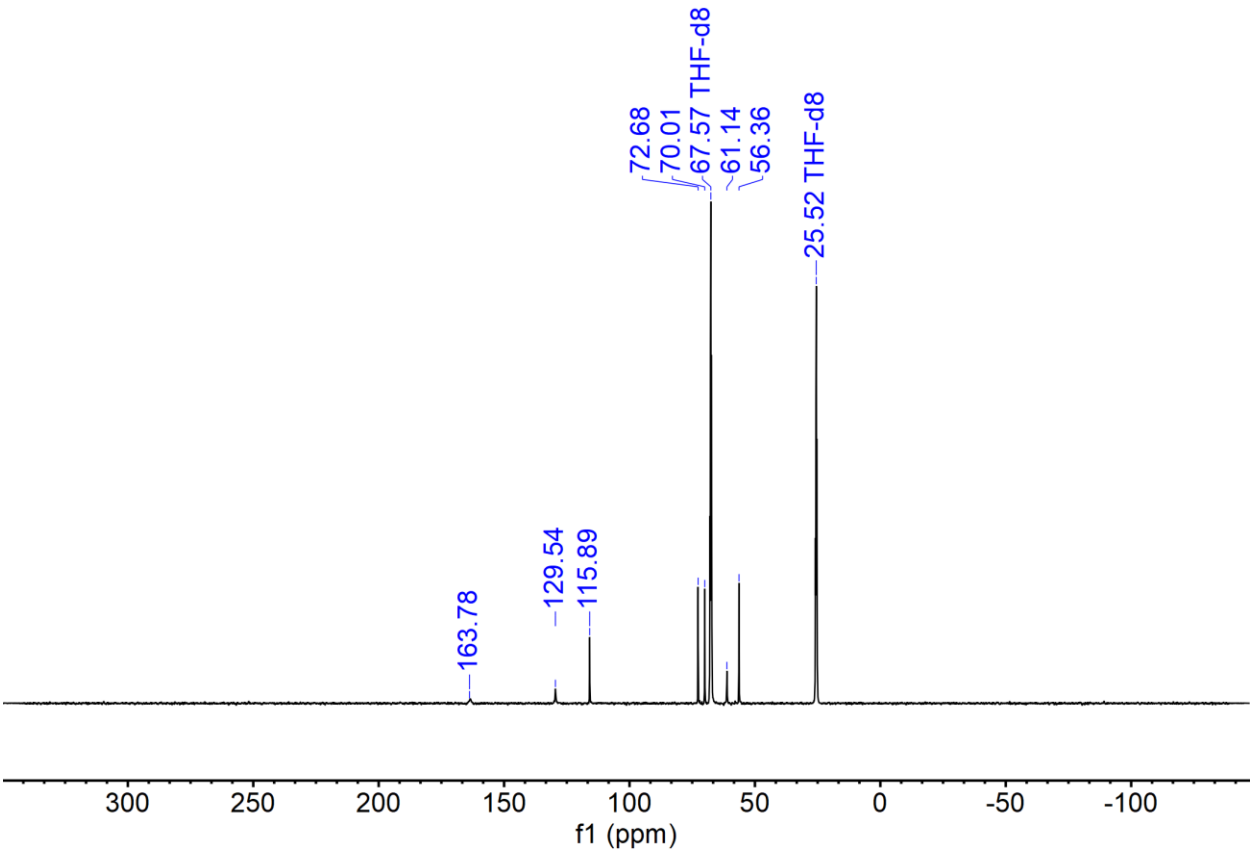

Figure S21. ^{13}C NMR spectrum of [K(crypt-222)][U(dbCOT)$_2$], **2**, (126 MHz, THF-d_8, 25 °C): δ 163.78 (*C*$_8$H$_4$), 129.54 (*C*$_8$H$_4$), 115.89 (*C*$_6$H$_4$) 72.68 (O(*C*H$_2$)$_2$O), 70.01 (O*C*H$_2$CH$_2$N), 61.14 (*C*$_6$H$_4$), 56.36 (OCH$_2$*C*H$_2$N).

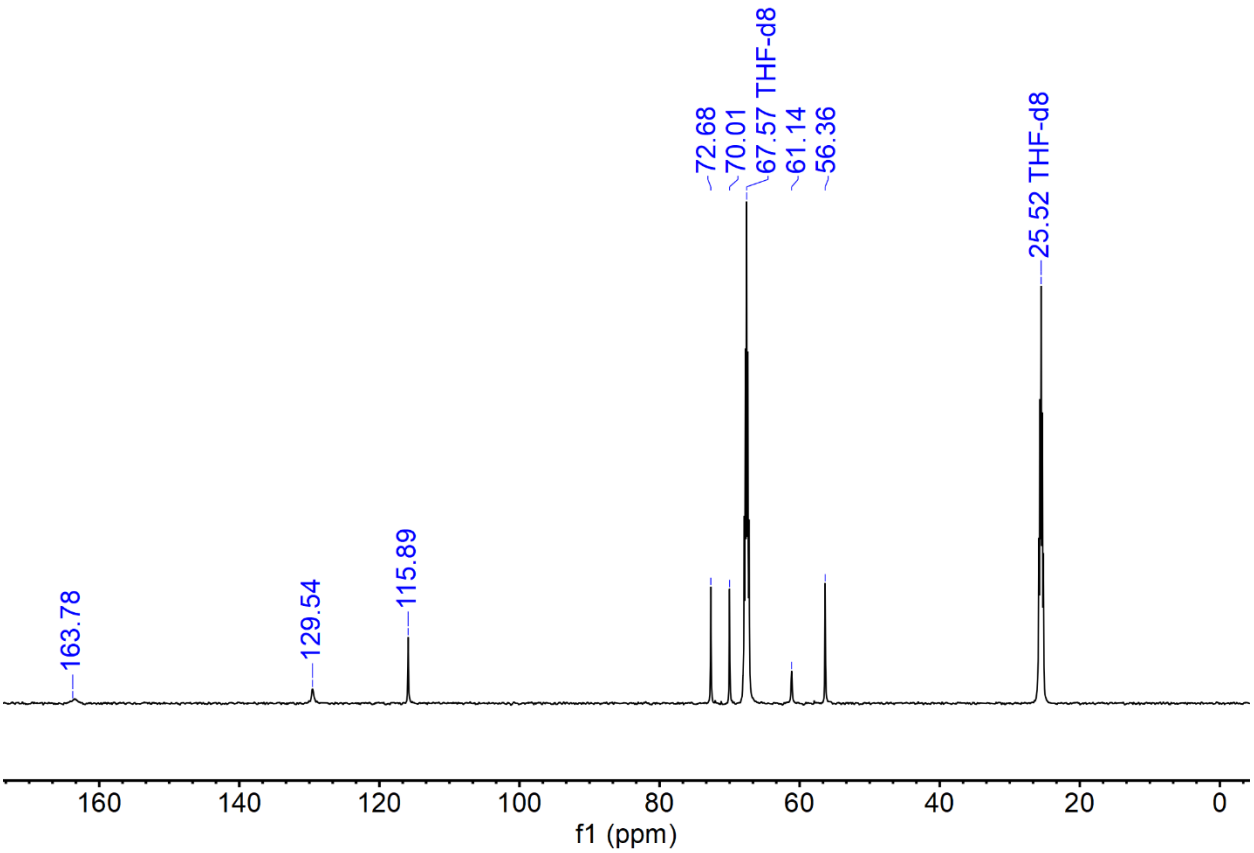

Figure S22. Magnification of the ^{13}C NMR spectrum of [K(crypt-222)][U(dbCOT)$_2$], **2**, (126 MHz, THF-d_8, 25 °C): δ 163.78 ($\underline{C}_8H_4$), 129.54 ($\underline{C}_8H_4$), 115.89 ($\underline{C}_6H_4$) 72.68 (O($\underline{C}H_2$)$_2$O), 70.01 (O$\underline{C}H_2CH_2N$), 61.14 ($\underline{C}_6H_4$), 56.36 (OCH$_2\underline{C}H_2$N).

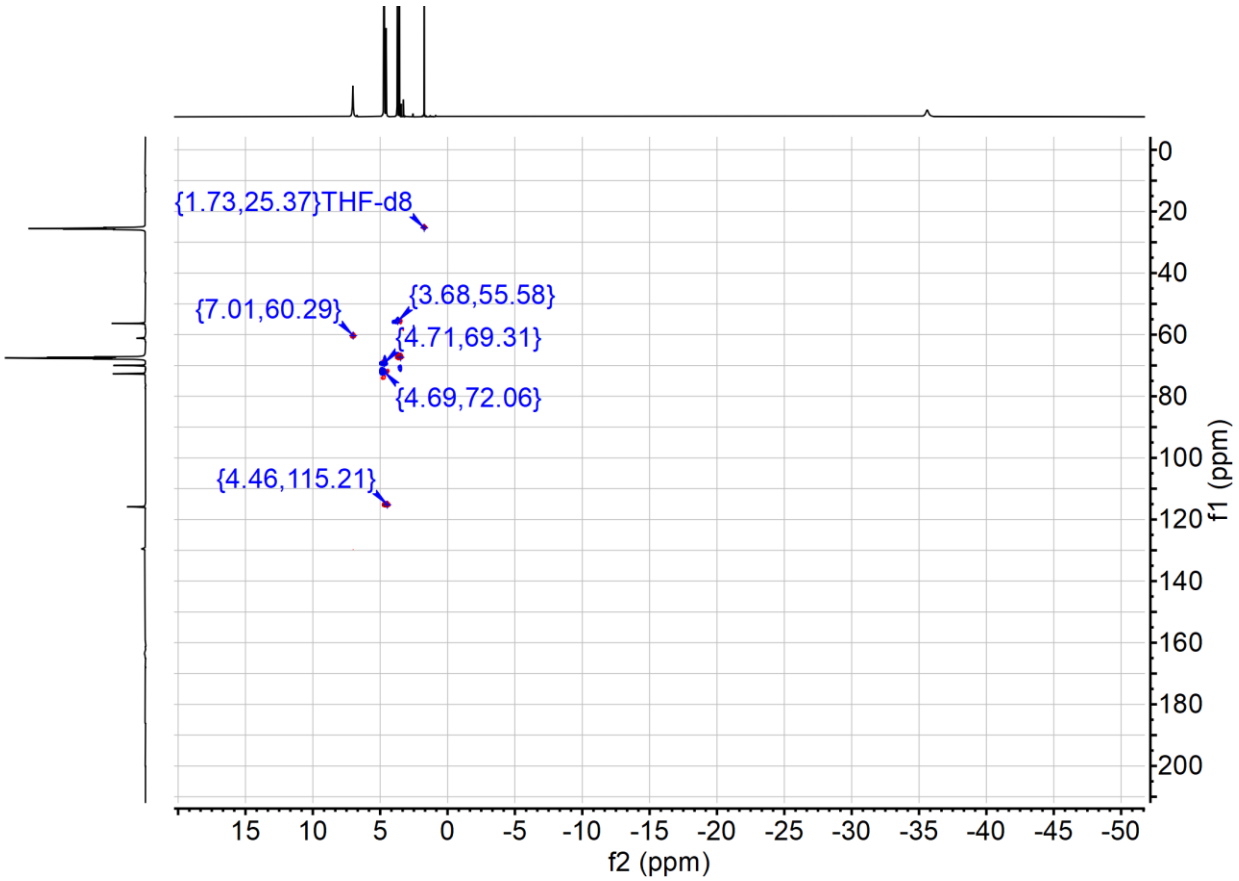

Figure S23. ^{1}H–^{13}C gHSQCAD spectrum of [K(crypt-222)][U(dbCOT)$_2$], **2**, (^{1}H 500 MHz, ^{13}C 126 MHz, THF-d_8, 25 °C).

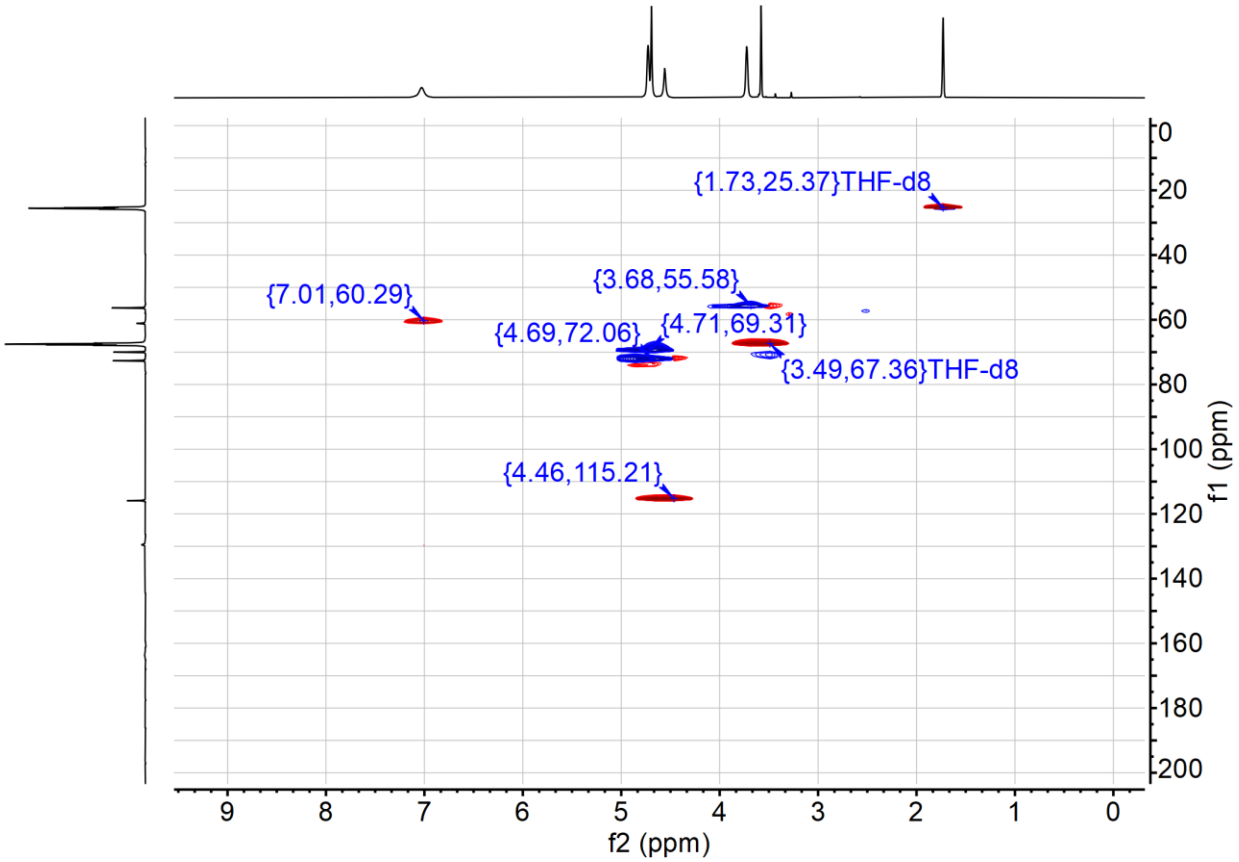

Figure S24. Magnification of the ^{1}H–^{13}C gHSQCAD spectrum of [K(crypt-222)][U(dbCOT)$_2$], **2**, (^{1}H 500 MHz, ^{13}C 126 MHz, THF-d_8, 25 °C).

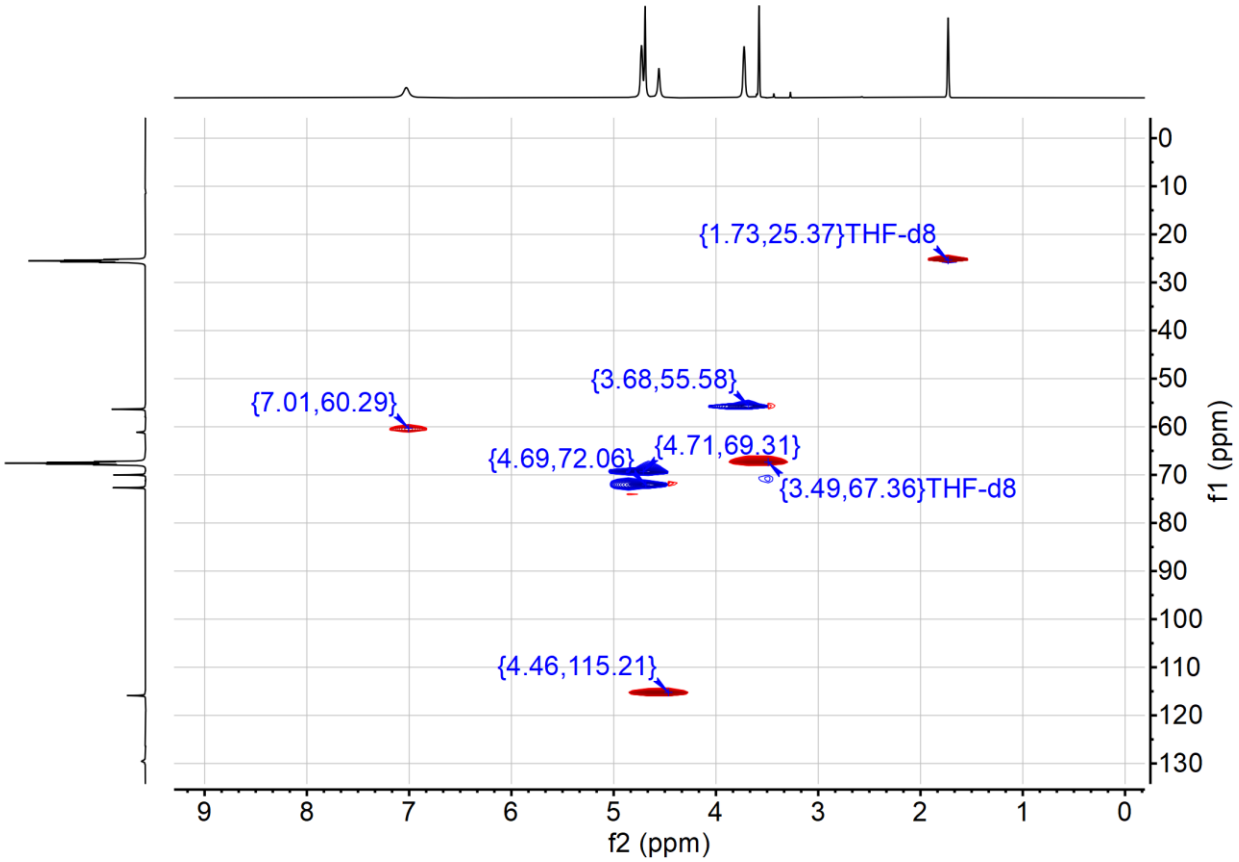

Figure S25. Magnification of the ^{1}H–^{13}C gHSQCAD spectrum of [K(crypt-222)][U(dbCOT)$_2$], **2**, (^{1}H 500 MHz, ^{13}C 126 MHz, THF-d_8, 25 °C).

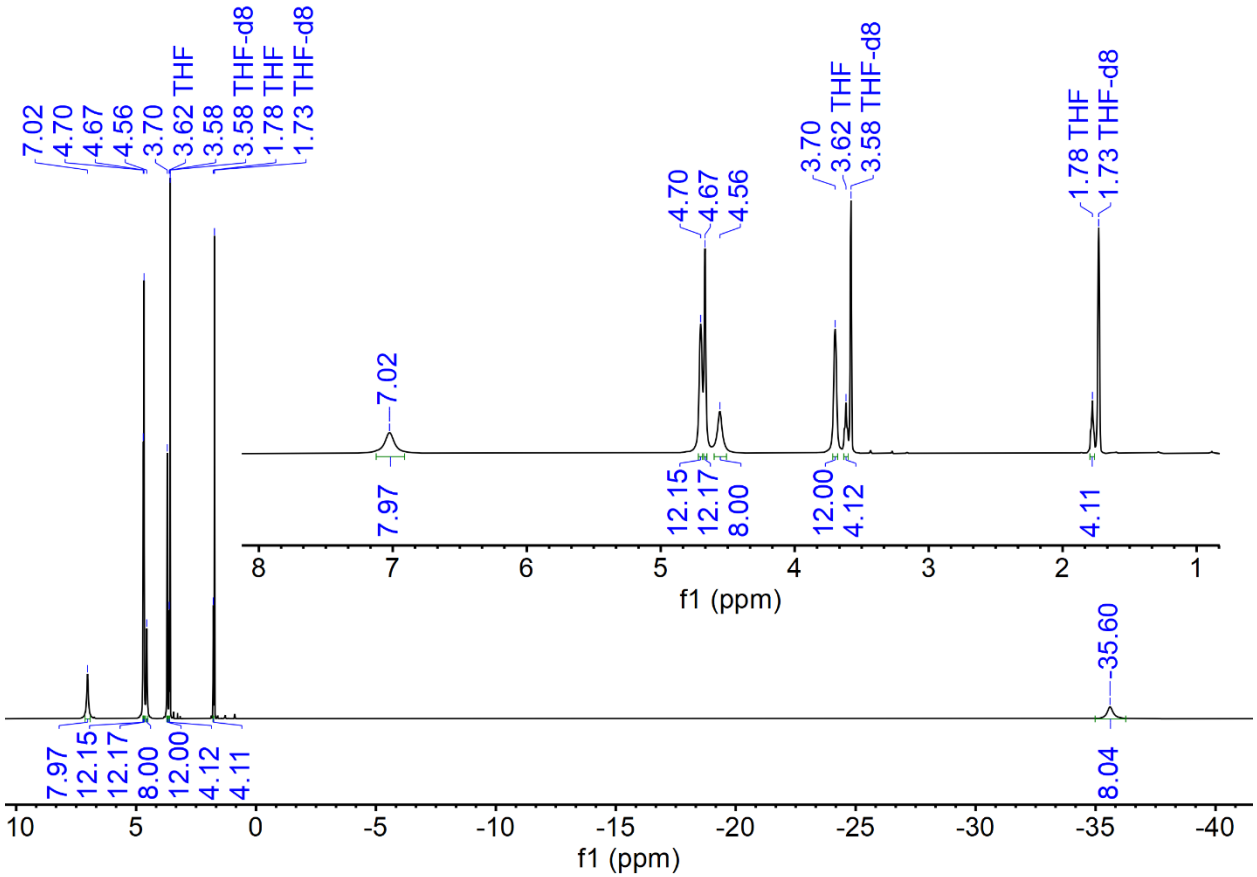

Figure S26. ^{1}H NMR spectrum of [K(crypt-222)][U(dbCOT)$_2$(THF)], **3**, (500 MHz, THF-d_8, 25 °C): δ 7.02 (br s, 8 H, COT(C*H*(CH)$_2$C*H*)$_2$), 4.70 (s, 12 H, OC*H*$_2$CH$_2$N), 4.67 (s, 12 H, O(C*H*$_2$)$_2$O), 4.56 (br s, 8 H, COT(CH(C*H*)$_2$CH)$_2$), 3.70 (s, 12 H, OCH$_2$C*H*$_2$N), 3.62 (br, t, 4 H, THF–*H*$_2$COC*H*$_2$), 1.78 (br, t, 4 H, THF–H$_2$C(C*H*$_2$)$_2$CH$_2$), –35.60 (br s, 8 H (COT–*H*).

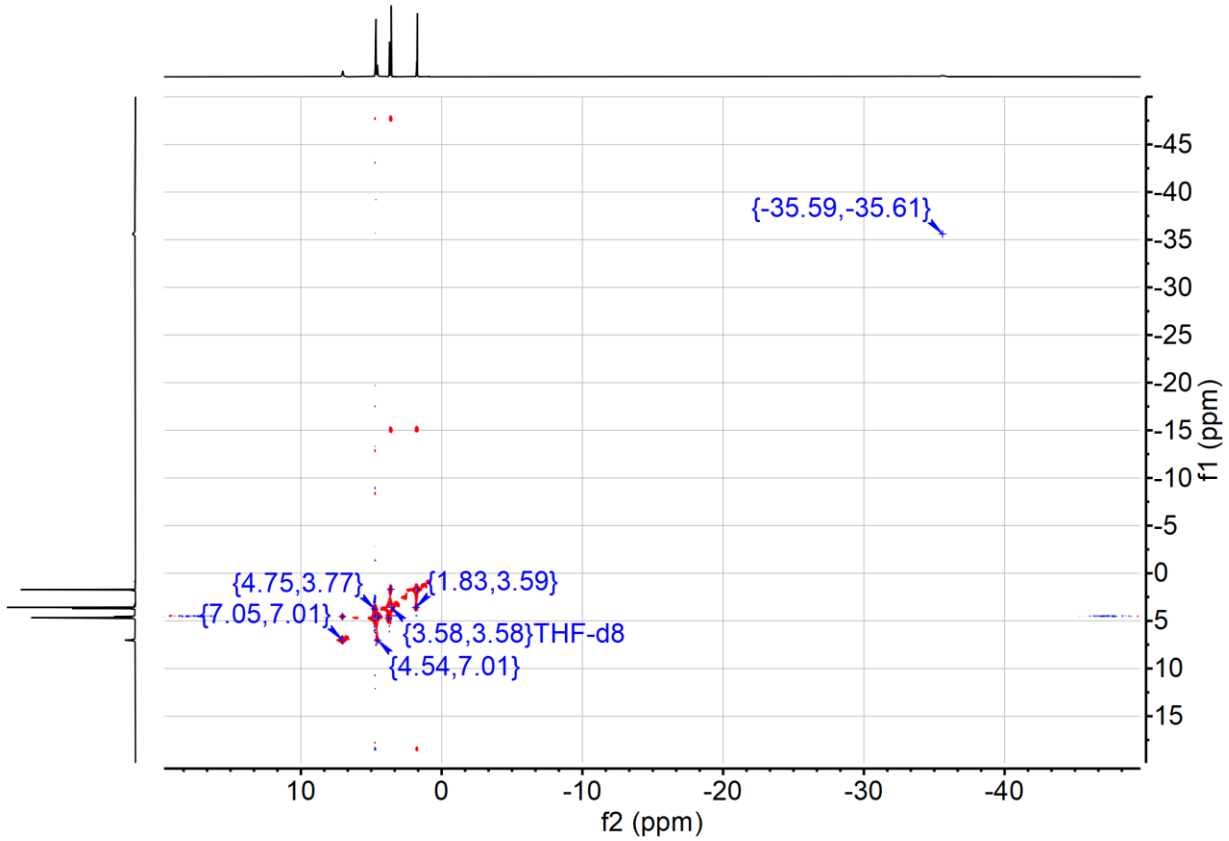

Figure S27. ^{1}H–^{1}H gCOSY spectrum of [K(crypt-222)][U(dbCOT)$_2$(THF)], **3**, (500 MHz, THF-d_8, 25 °C).

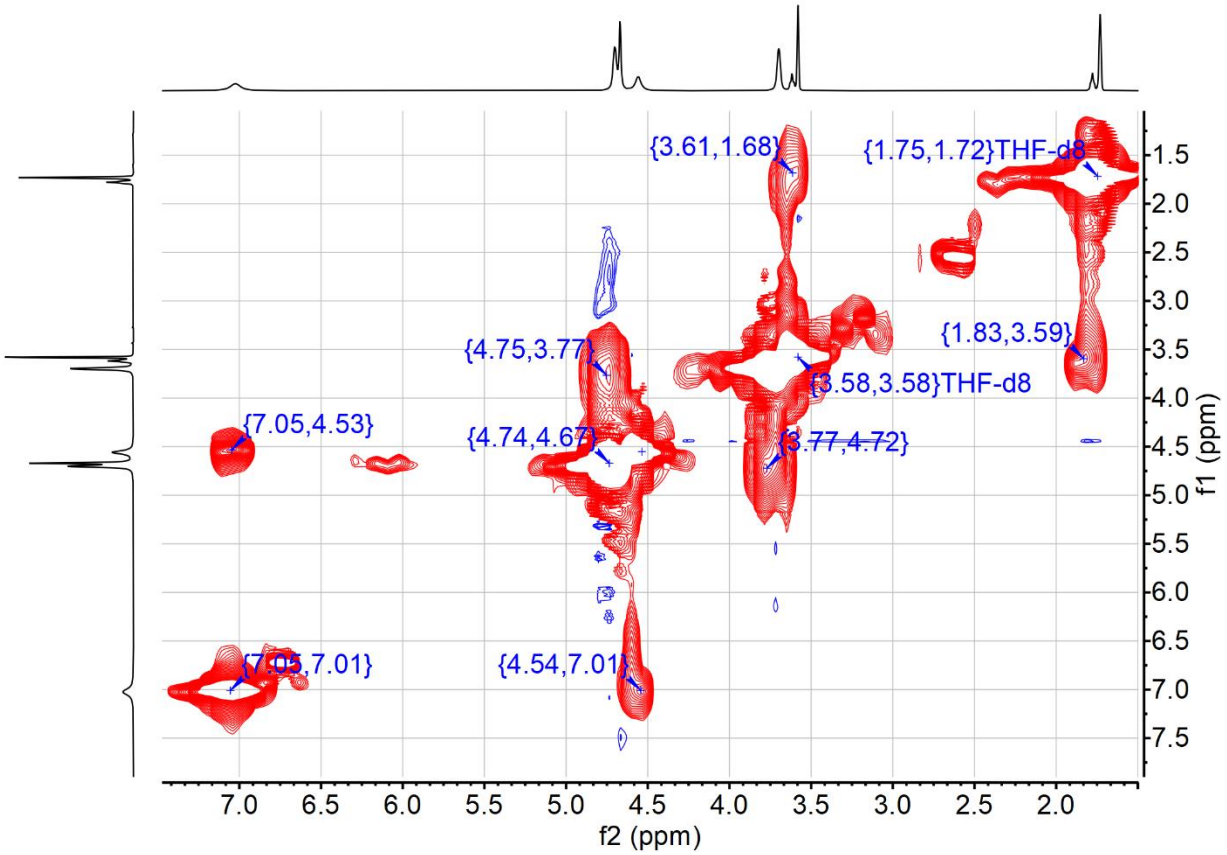

Figure S28. Magnification of the ^{1}H–^{1}H gCOSY spectrum of [K(crypt-222)][U(dbCOT)$_2$(THF)], **3**, (500 MHz, THF-d_8, 25 °C).

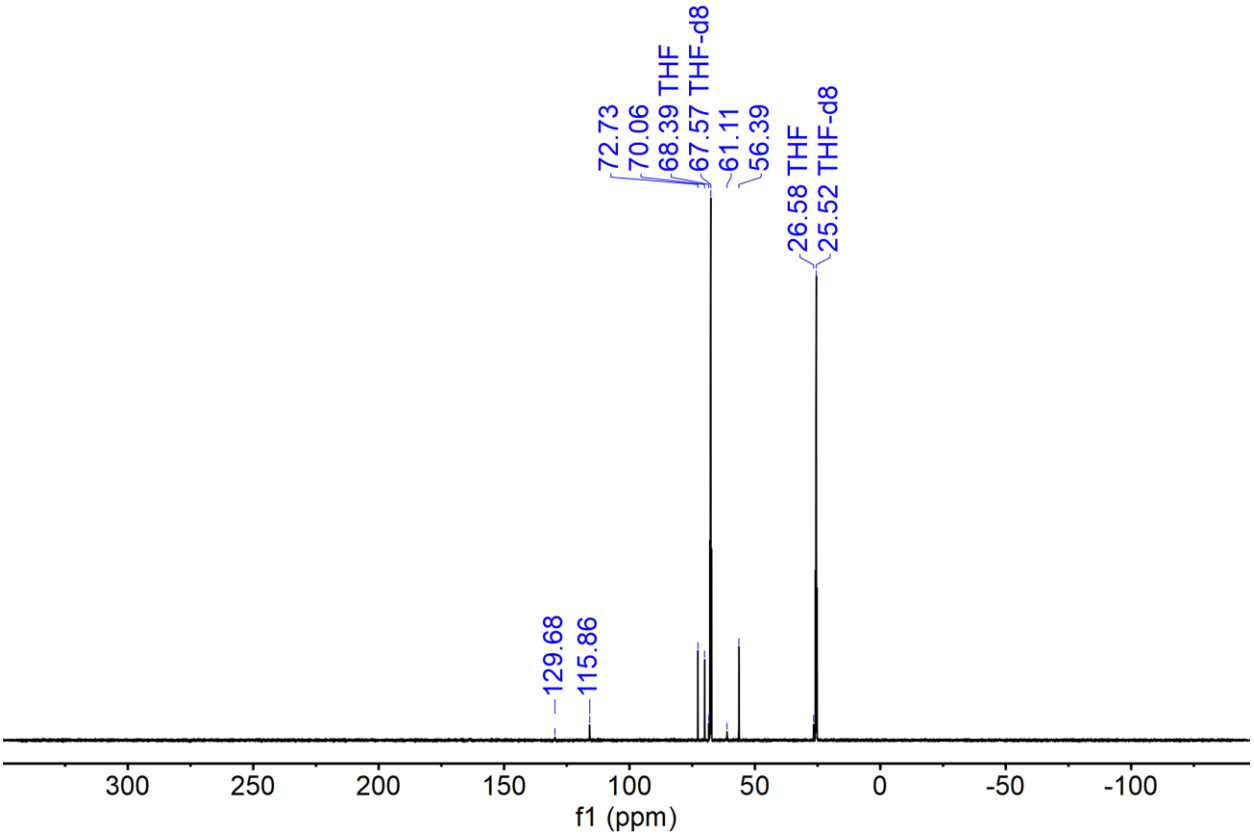

Figure S29. ^{13}C NMR spectrum of [K(crypt-222)][U(dbCOT)$_2$(THF)], **3**, (126 MHz, THF-d_8, 25 °C): δ 129.68 ($\underline{C}_8H_4$), 115.86 ($\underline{C}_6H_4$) 72.73 (O($\underline{C}H_2$)$_2$O), 70.06 (O$\underline{C}H_2CH_2N$), 68.39 (THF–$H_2\underline{C}O\underline{C}H_2$), 61.11 ($\underline{C}_6H_4$), 56.39 ($OCH_2\underline{C}H_2N$), 28.58 (THF–$H_2C(C\underline{H}_2)_2CH_2$). Owing to the poor solubility of **3** in THF, the ^{13}C resonance expected at approximately 163 ppm is absent, presumably owing to the lower concentration of **3** with regards to **1** and **2**, respectively.

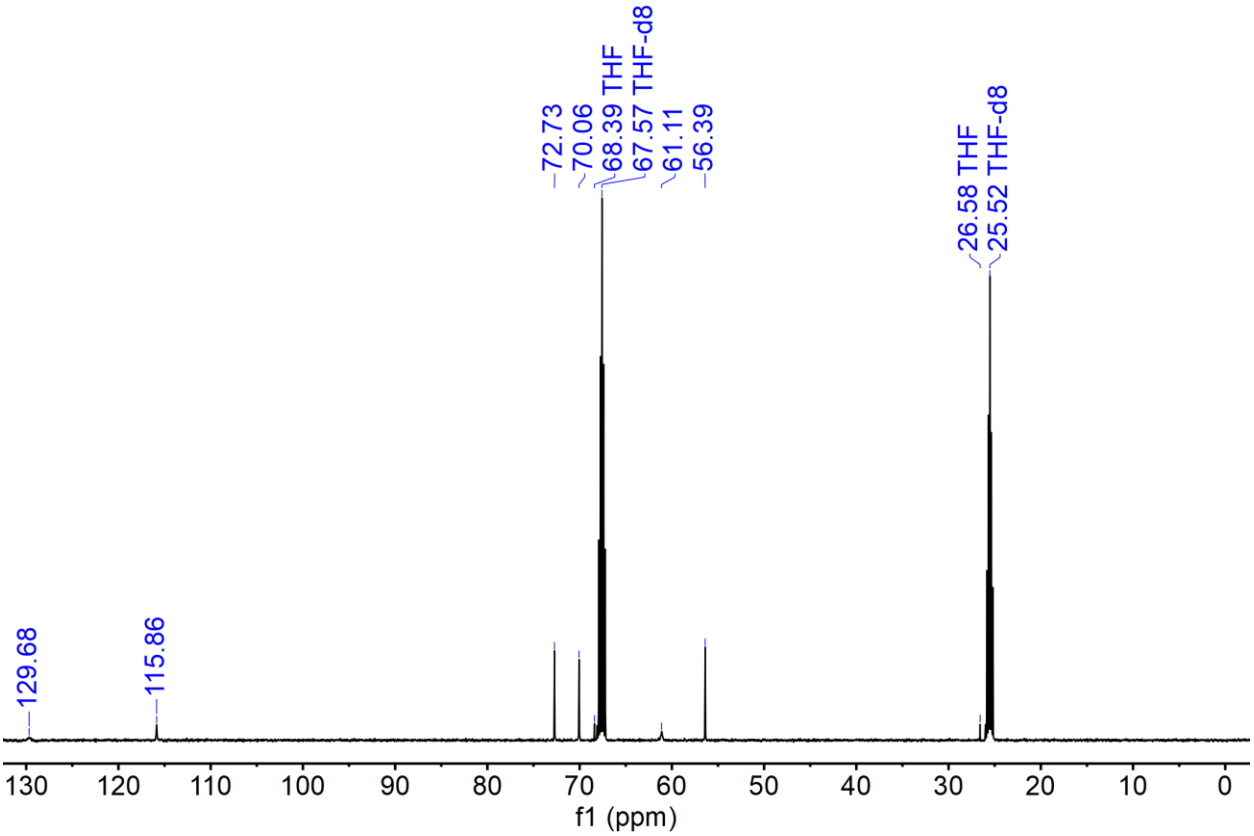

Figure S30. Magnification of the ^{13}C NMR spectrum of [K(crypt-222)][U(dbCOT)$_2$(THF)], **3**, (126 MHz, THF-d_8, 25 °C): δ 129.68 ($\underline{C}_8H_4$), 115.86 ($\underline{C}_6H_4$) 72.73 (O($\underline{C}H_2$)$_2$O), 70.06 (O$\underline{C}H_2CH_2N$), 68.39 (THF–$H_2\underline{C}O\underline{C}H_2$), 61.11 ($\underline{C}_6H_4$), 56.39 ($OCH_2\underline{C}H_2N$), 28.58 (THF–$H_2C(C\underline{H}_2)_2CH_2$). Owing to the poor solubility of **3** in THF, the ^{13}C resonance expected at approximately 163 ppm is absent, presumably owing to the lower concentration of **3** with regards to **1** and **2**, respectively.

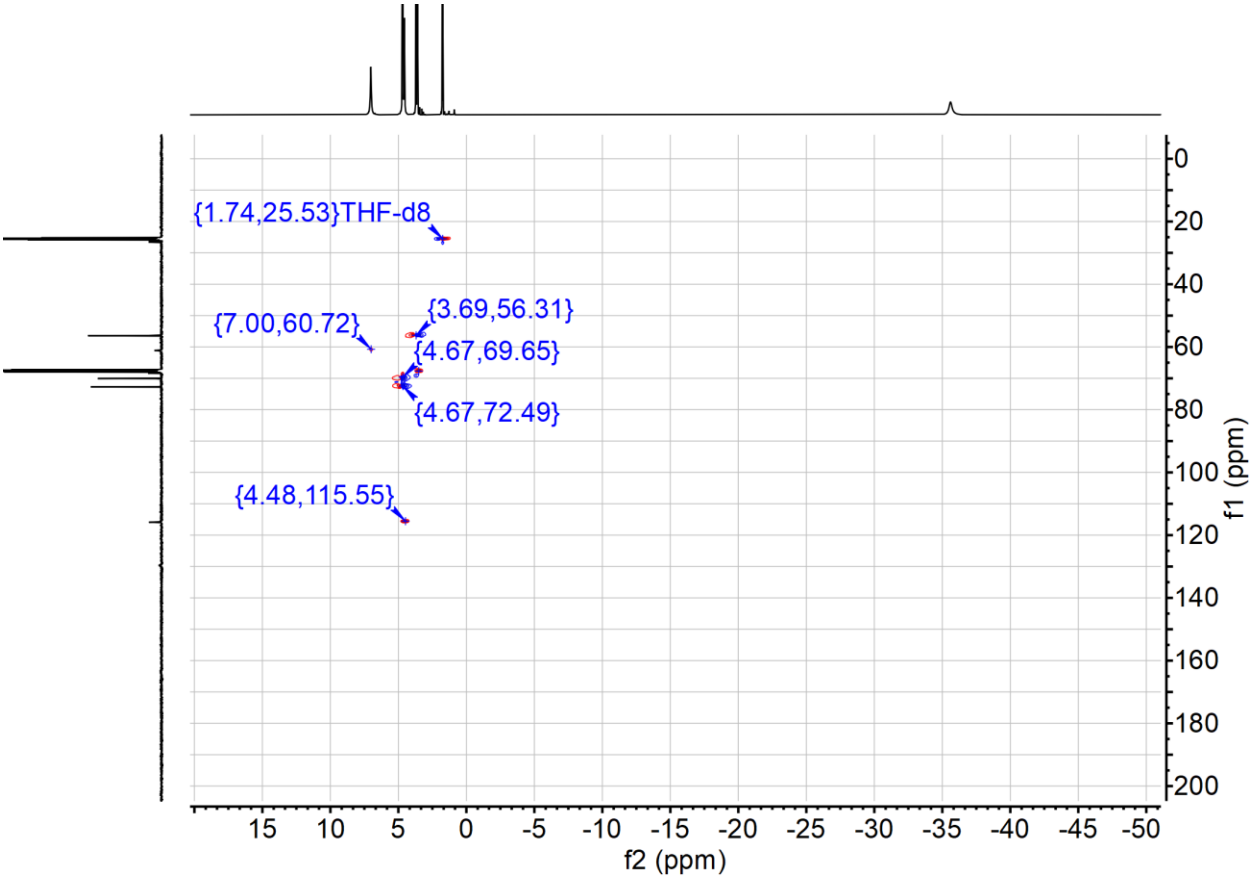

Figure S31. ^{1}H–^{13}C gHSQCAD spectrum of [K(crypt-222)][U(dbCOT)$_2$(THF)], **3**, (^{1}H 500 MHz, ^{13}C 126 MHz, THF-d_8, 25 °C).

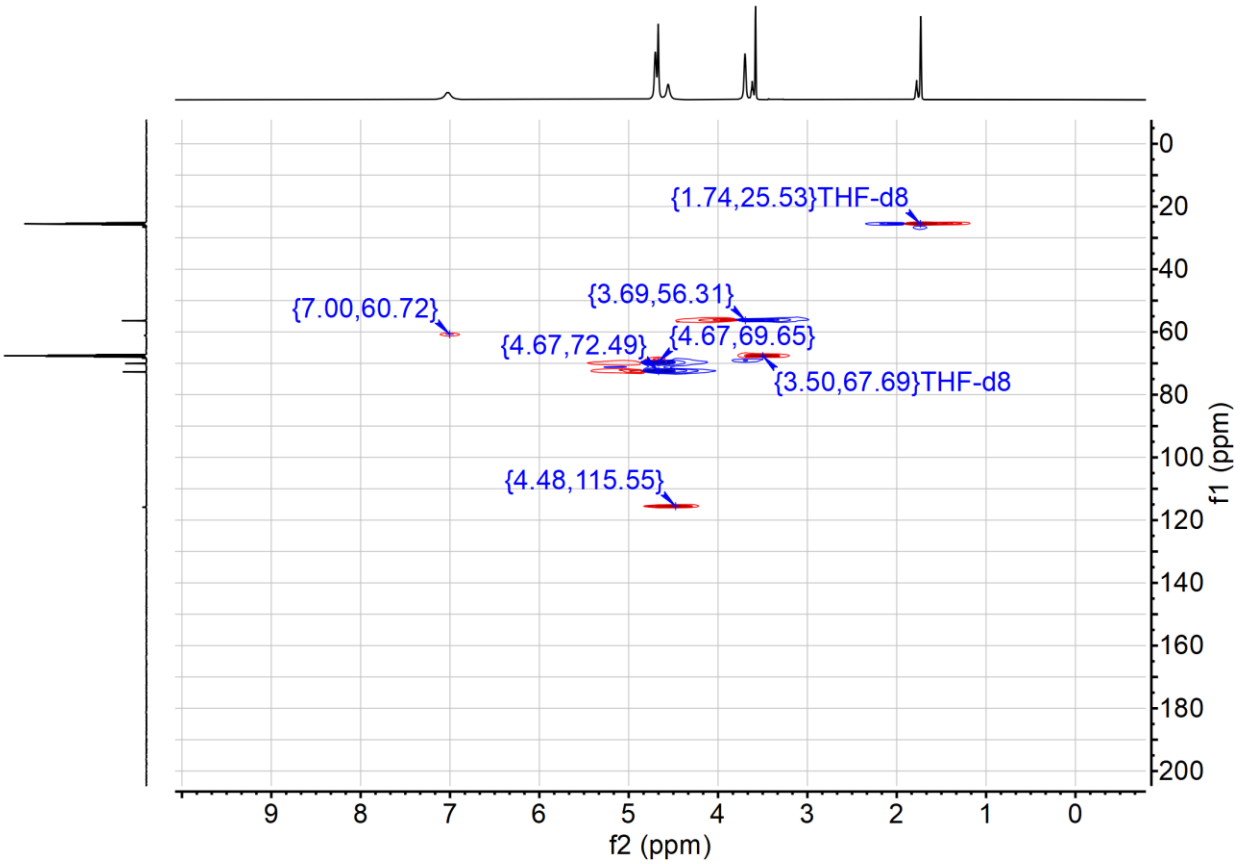

Figure S32. Magnification of the ^{1}H–^{13}C gHSQCAD spectrum of [K(crypt-222)][U(dbCOT)$_2$(THF)], **3**, (^{1}H 500 MHz, ^{13}C 126 MHz, THF-d_8, 25 °C).

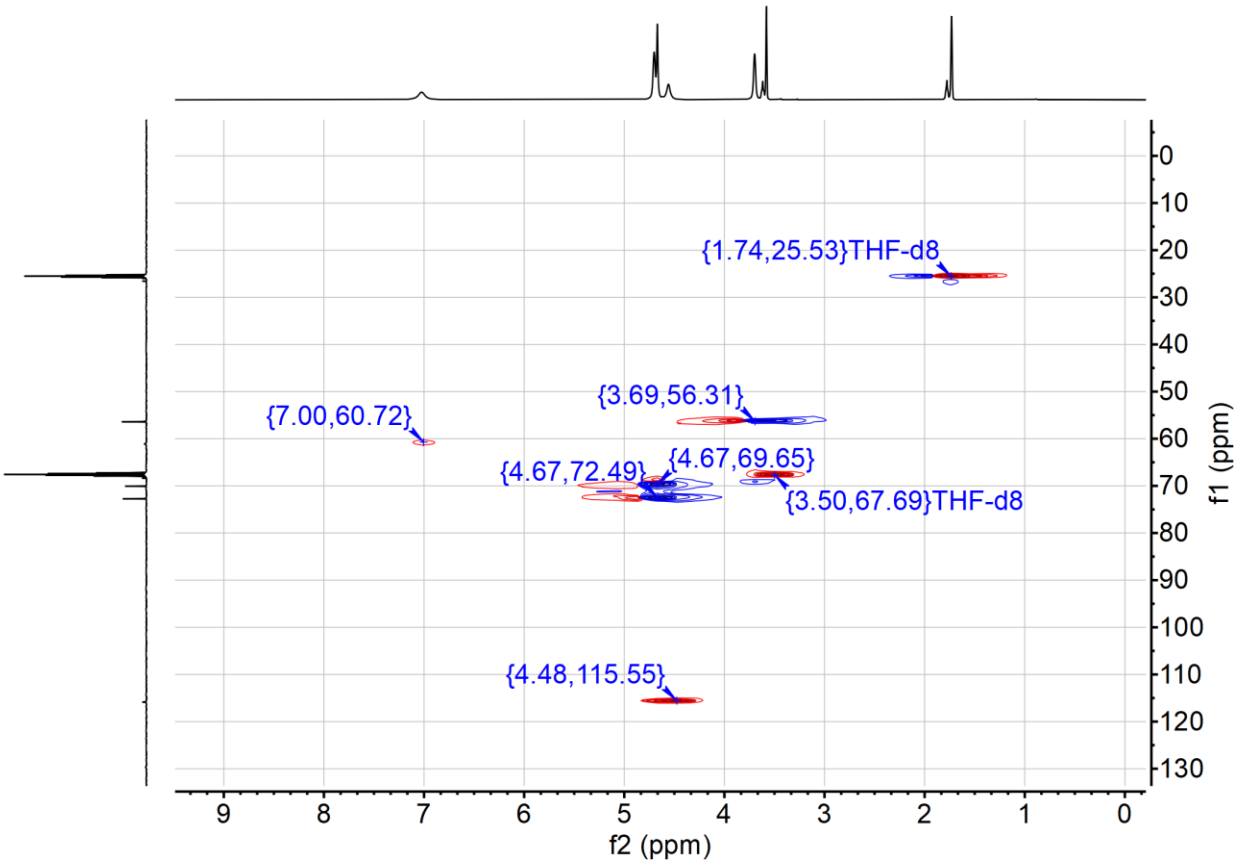

Figure S33. Magnification of the ^{1}H–^{13}C gHSQCAD spectrum of [K(crypt-222)][U(dbCOT)$_2$(THF)], **3**, (^{1}H 500 MHz, ^{13}C 126 MHz, THF-d_8, 25 °C).

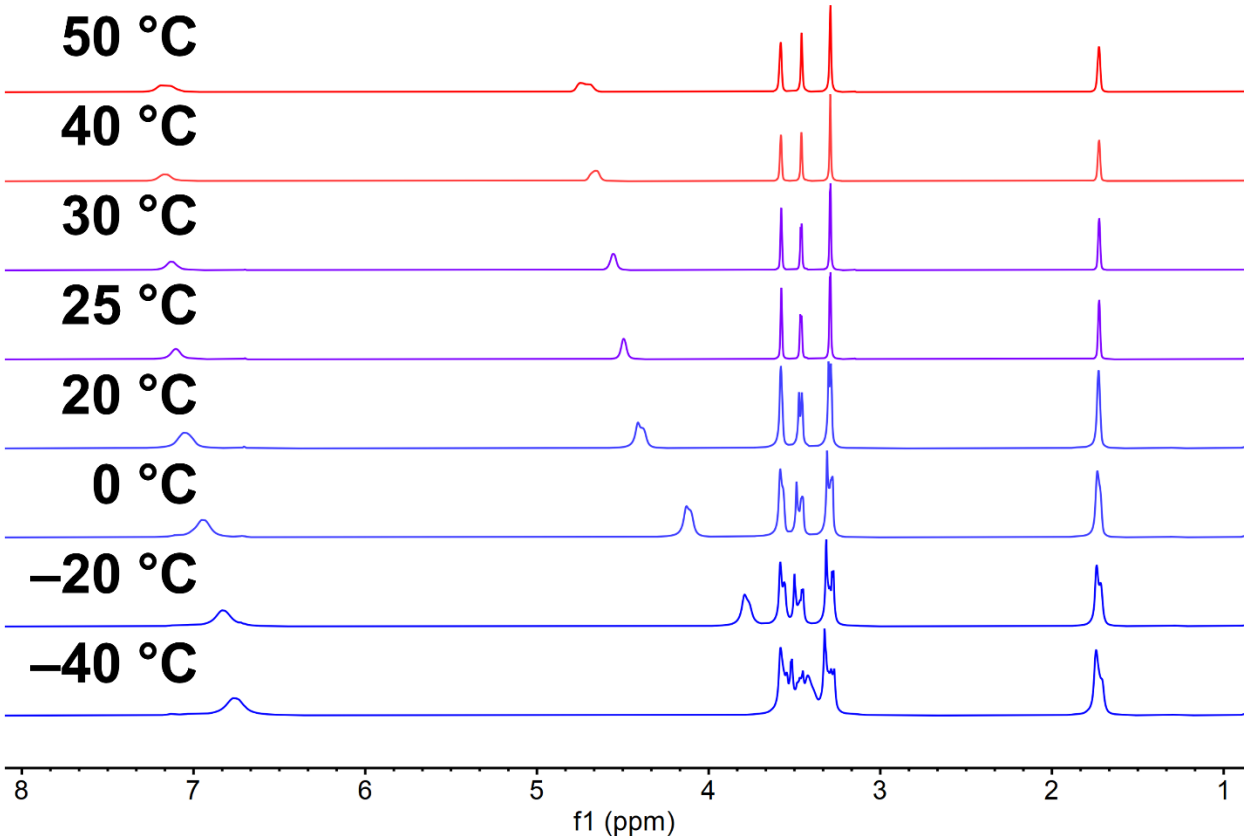

Figure S34. Variable-temperature ^{1}H NMR spectra of [K(DME)$_2$][U(dbCOT)$_2$], **1**, from 1 to 8 ppm in THF-d_8 obtained with a 500 MHz spectrometer.

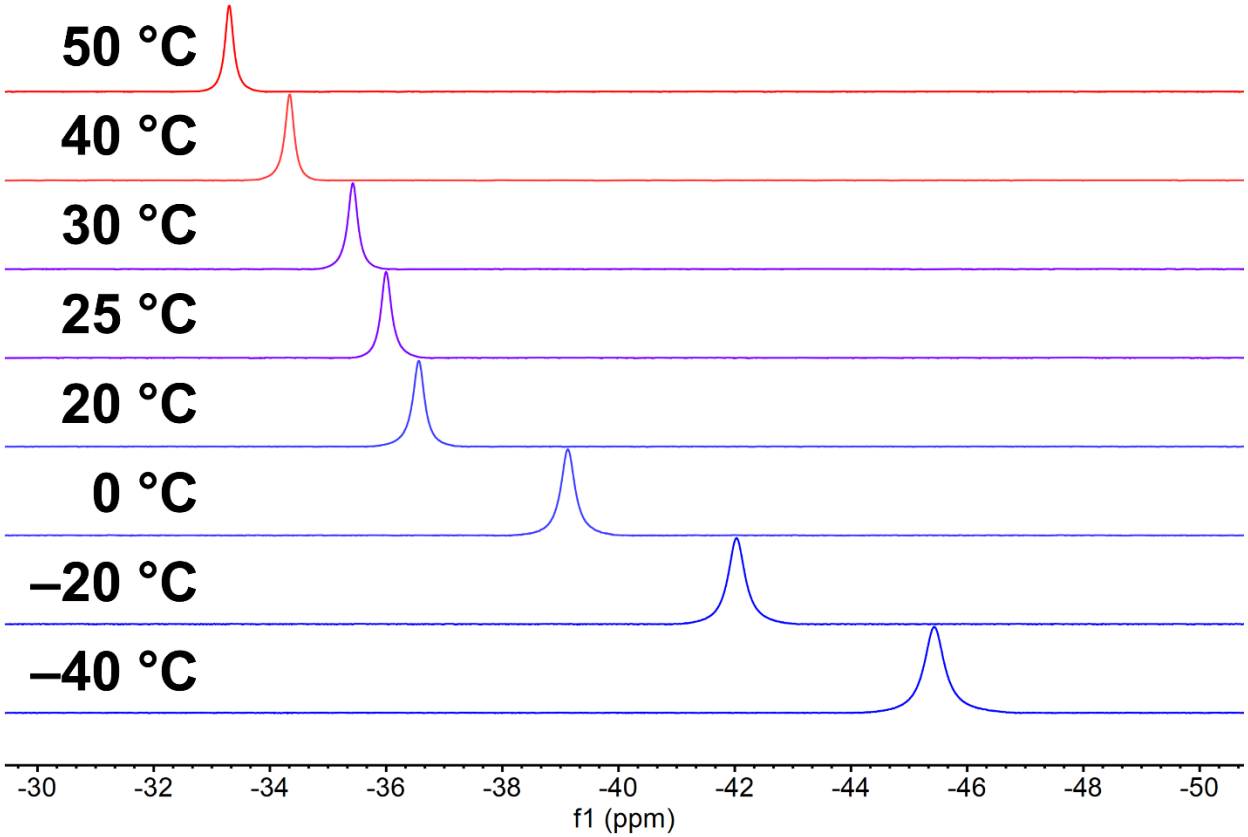

Figure S35. Variable-temperature ^{1}H NMR spectra of [K(DME)$_2$][U(dbCOT)$_2$], **1**, from –30 to –50 ppm in THF-d_8 obtained with a 500 MHz spectrometer.

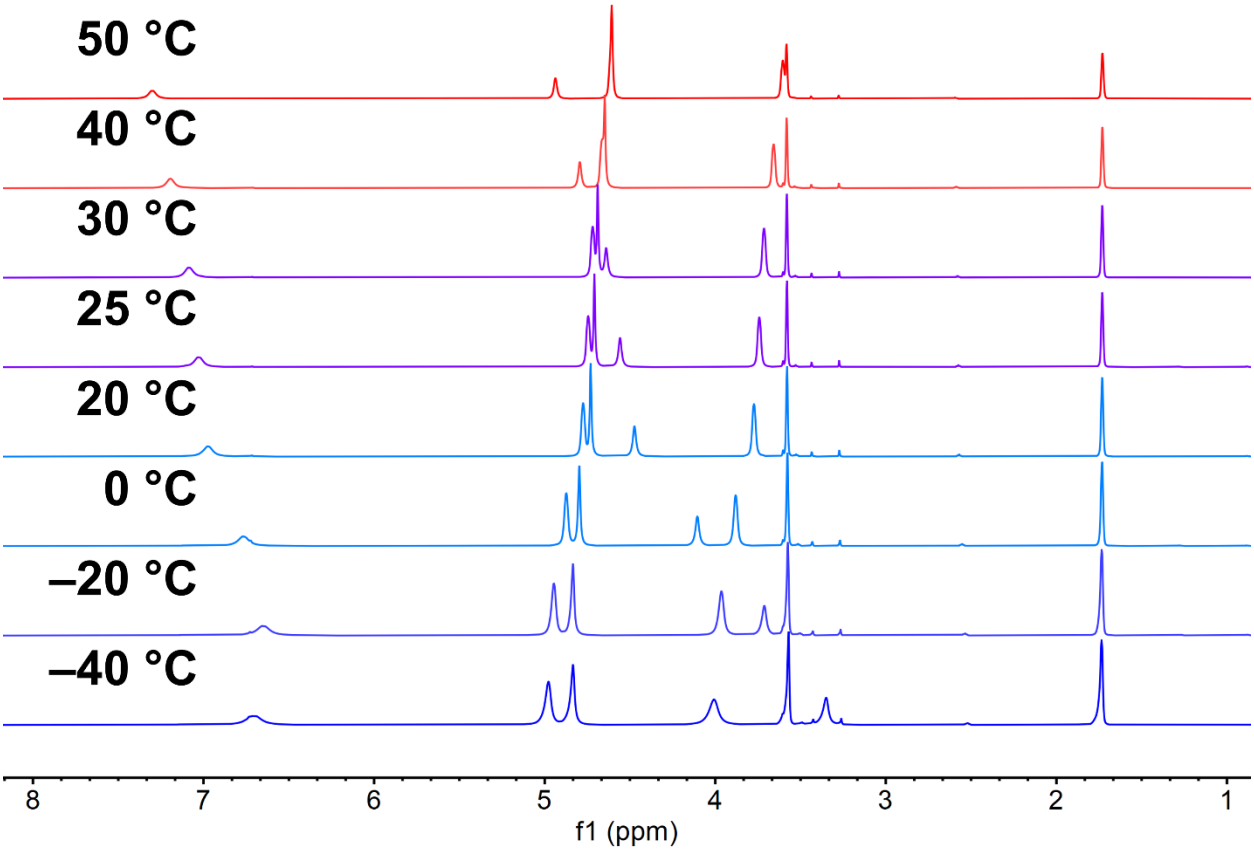

Figure S36. Variable-temperature ^{1}H NMR spectra of [K(crypt-222)][U(dbCOT)$_2$], **2**, from 1 to 8 ppm in THF-d_8 obtained with a 500 MHz spectrometer.

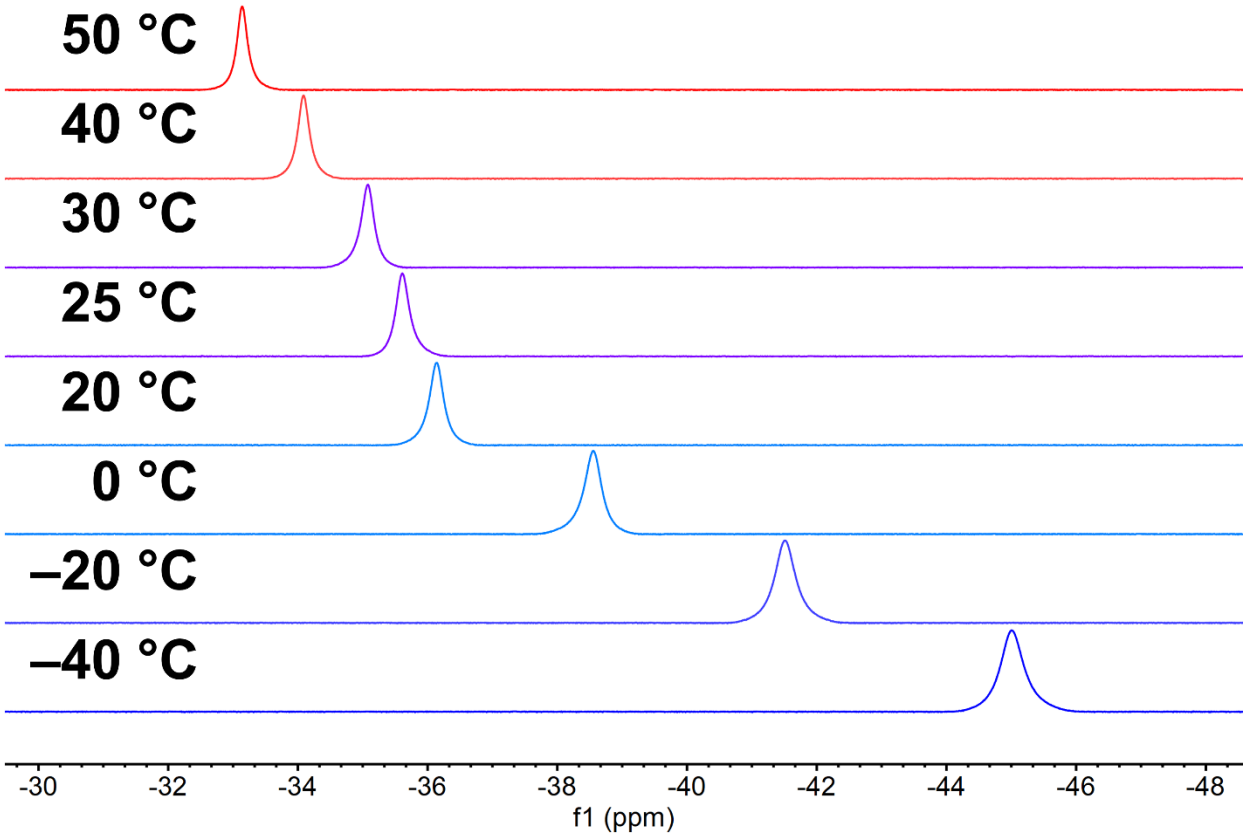

Figure S37. Variable-temperature ^{1}H NMR spectra of [K(crypt-222)][U(dbCOT)$_2$], **2**, from –30 to –48 ppm in THF-d_8 obtained with a 500 MHz spectrometer.

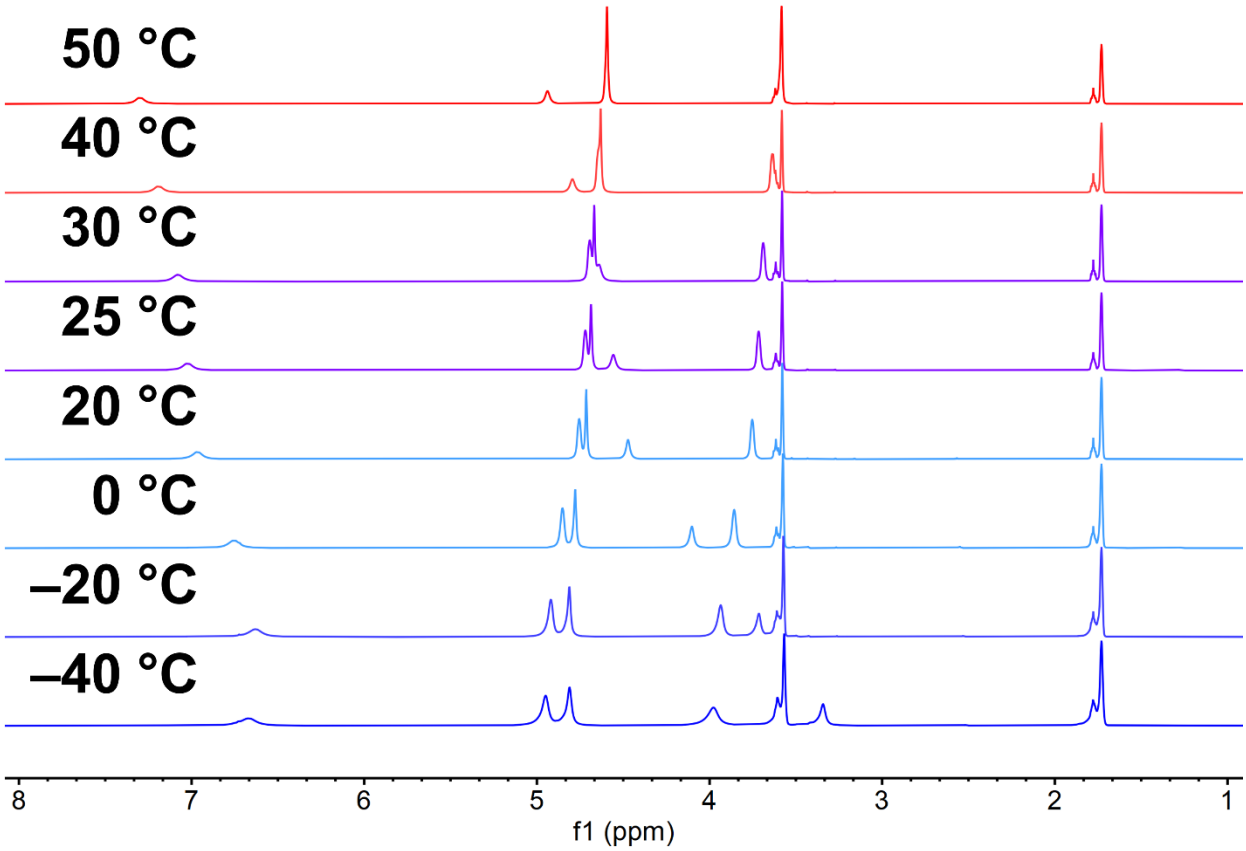

Figure S38. Variable-temperature ^{1}H NMR spectra of [K(crypt-222)][U(dbCOT)$_2$(THF)], **3**, from 1 to 8 ppm in THF-d_8 obtained with a 500 MHz spectrometer.

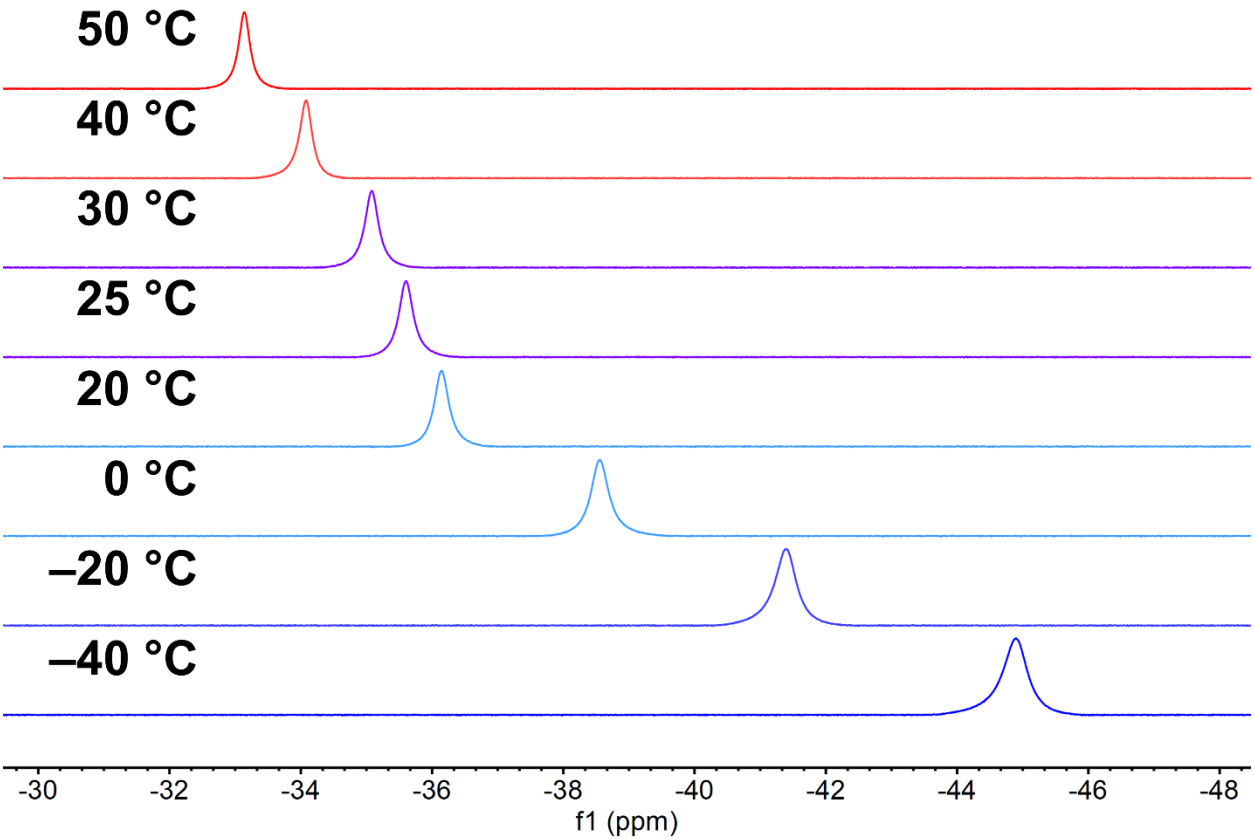

Figure S39. Variable-temperature ^{1}H NMR spectra of [K(crypt-222)][U(dbCOT)$_2$(THF)], **3**, from –30 to –48 ppm in THF-d_8 obtained with a 500 MHz spectrometer.

3 UV-Vis-NIR Spectroscopy

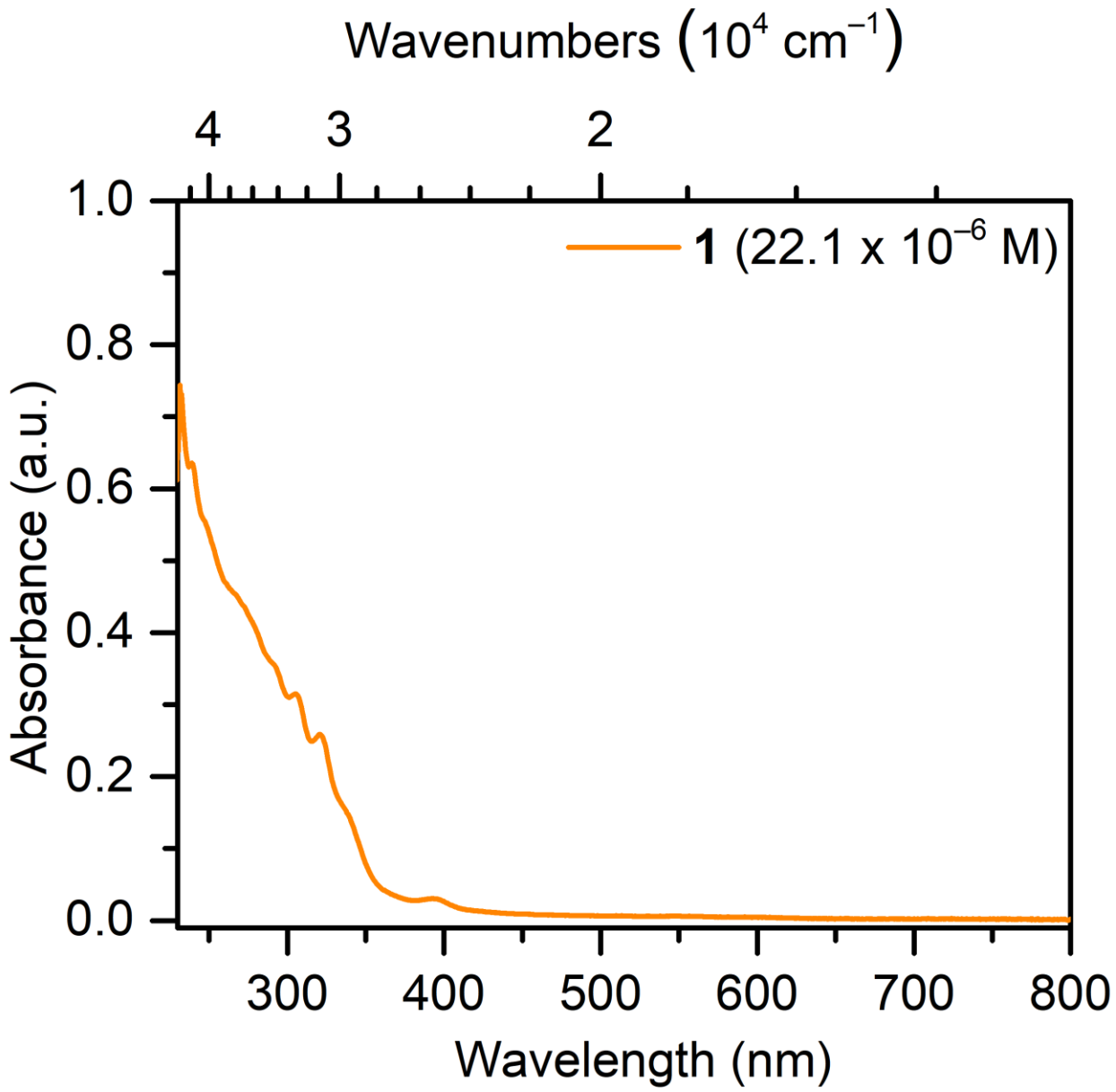

Figure S40. UV-Vis spectrum of $[K(DME)_2][U(dbCOT)_2]$, **1**, taken in 2-MeTHF at 22.1 x 10^{-6} mol/L.

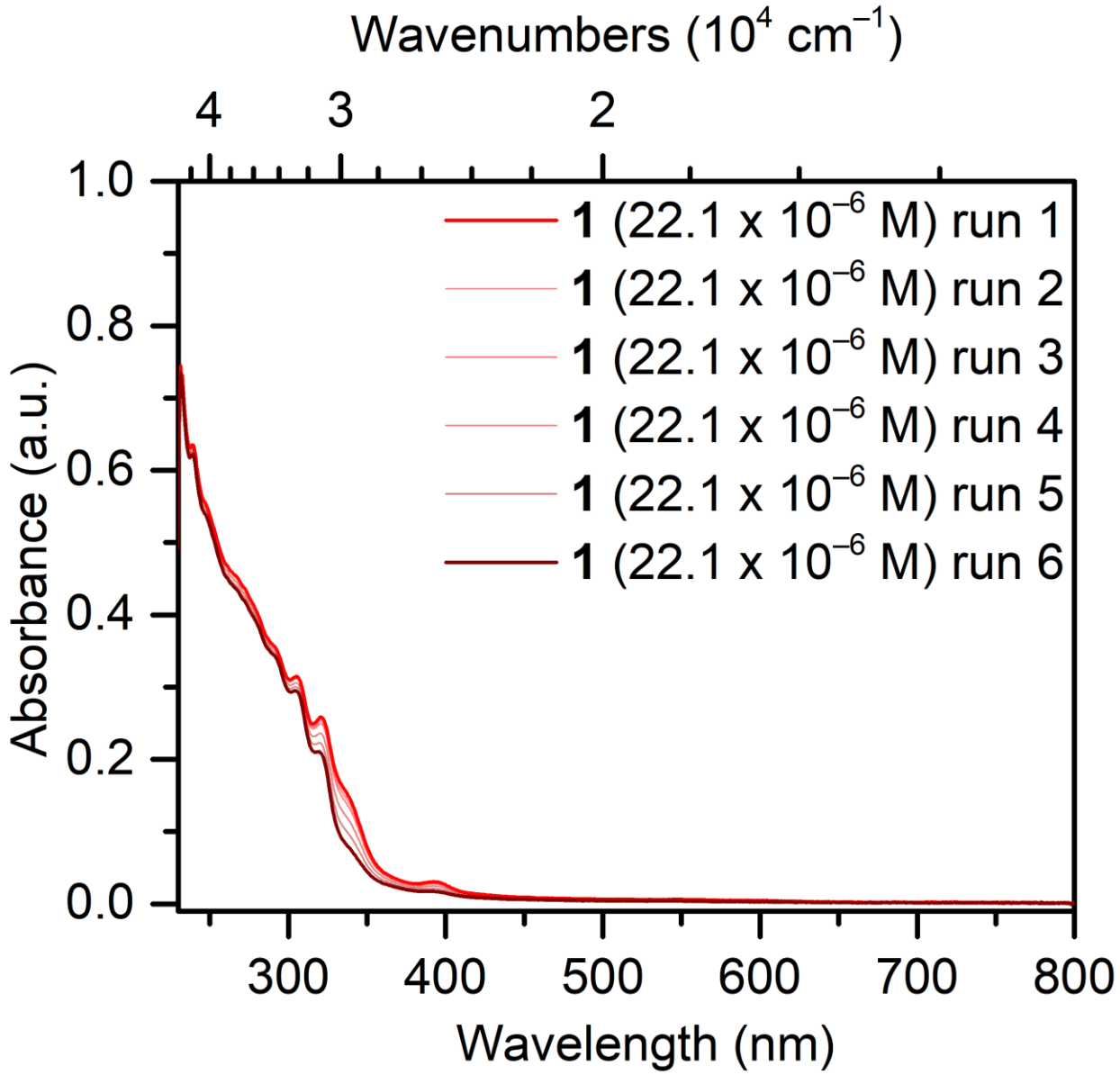

Figure S41. UV-Vis spectra of $[K(DME)_2][U(dbCOT)_2]$, **1**, taken in 2-MeTHF at 22.1 x 10^{-6} mol/L over the course of six scans.

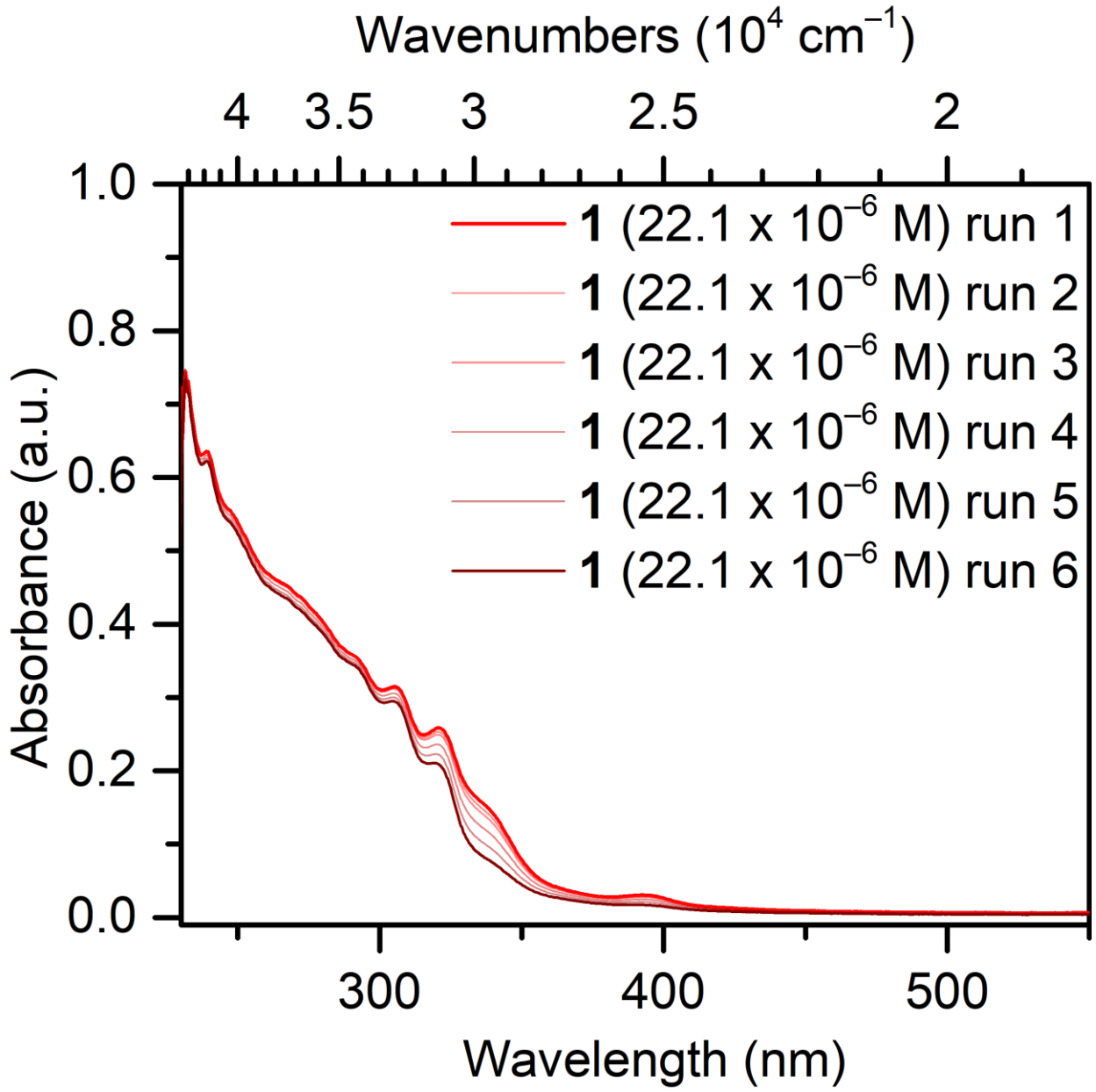

Figure S42. Magnification of the UV-Vis spectra of $[K(DME)_2][U(dbCOT)_2]$, **1**, taken in 2-MeTHF at 22.1 x 10^{-6} mol/L over the course of six scans.

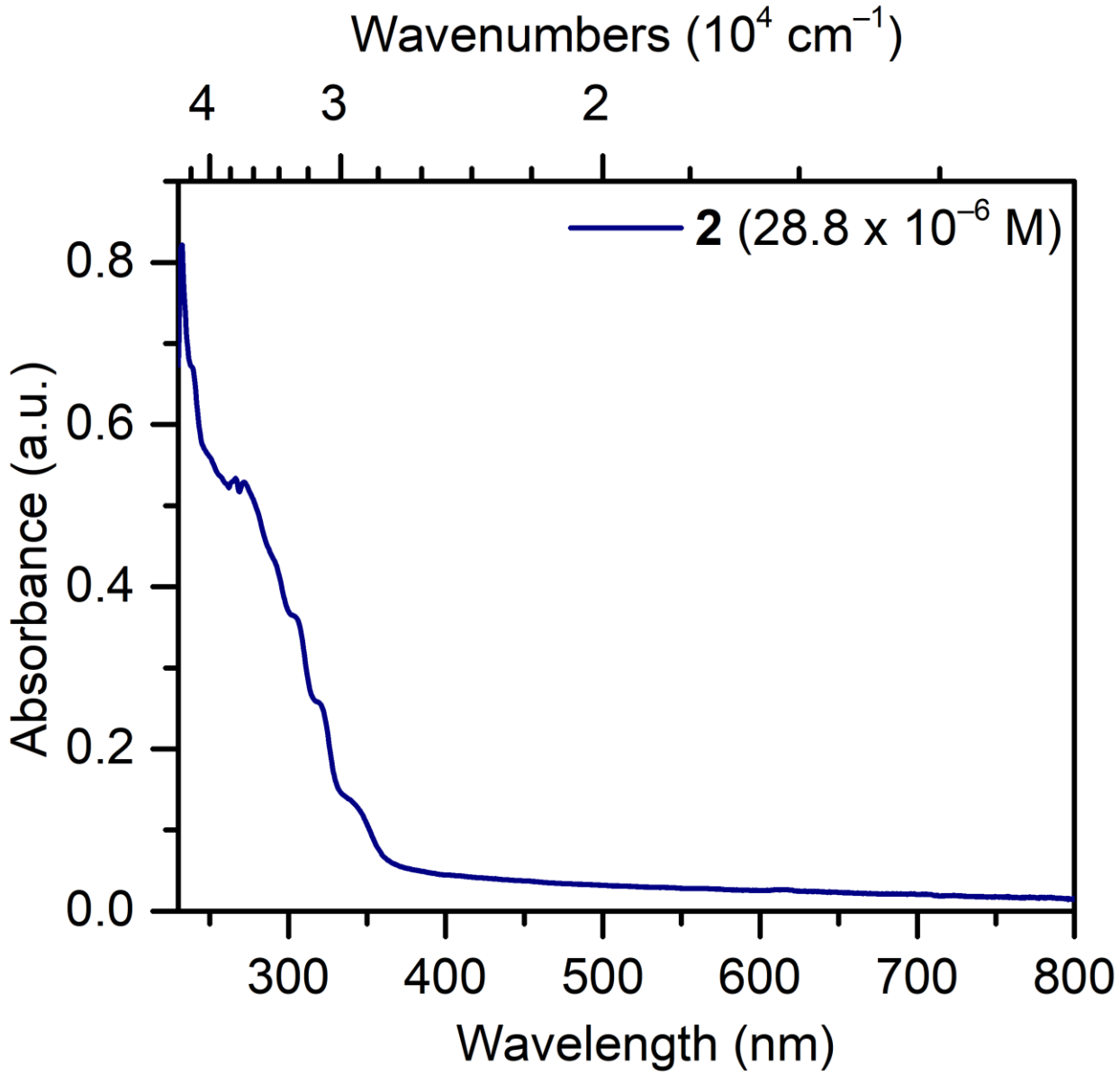

Figure S43. UV-Vis spectrum of [K(crypt-222)][U(dbCOT)$_2$], **2**, taken in 2-MeTHF at 28.8 x 10^{-6} mol/L.

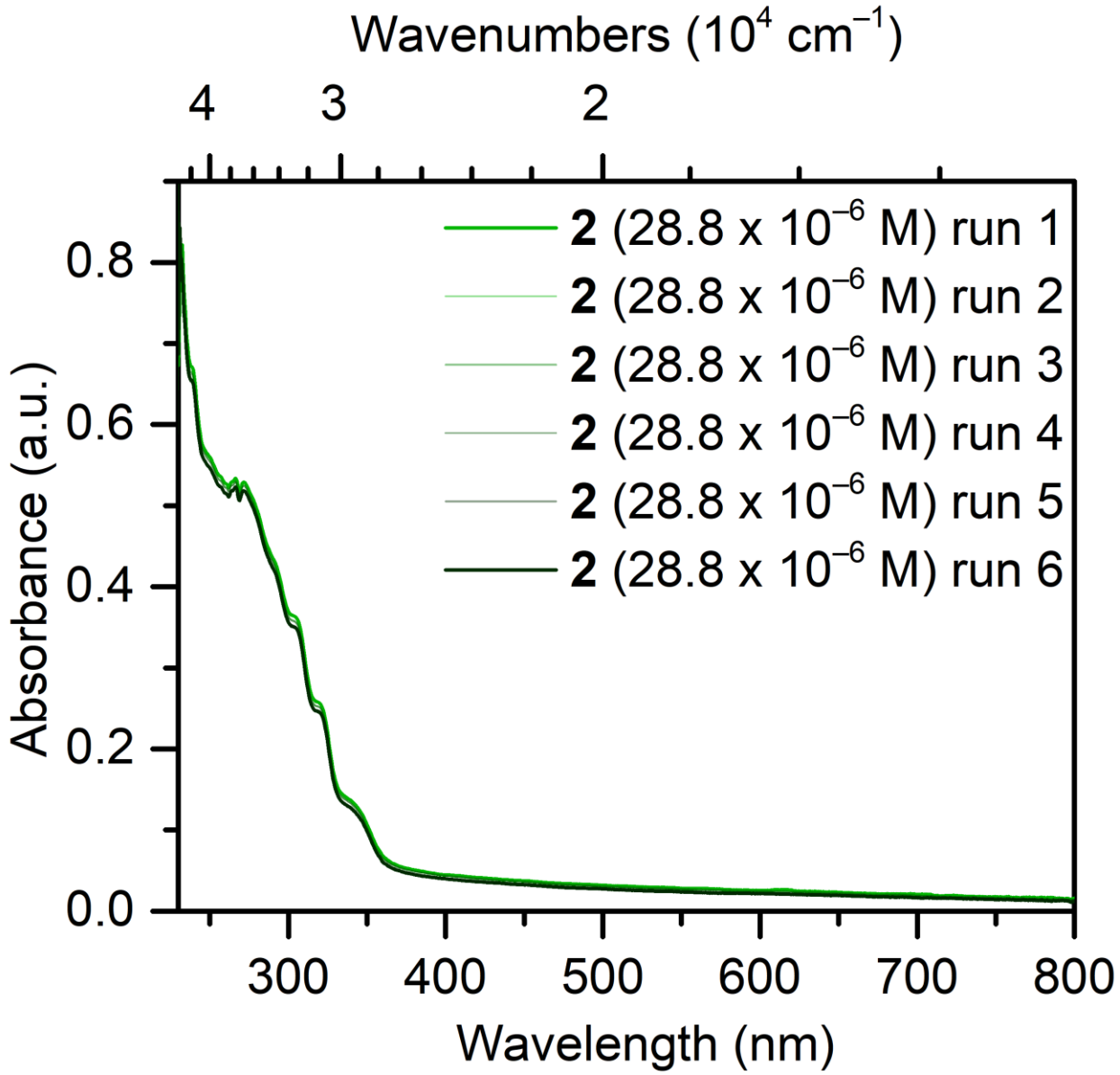

Figure S44. UV-Vis spectra of [K(crypt-222)][U(dbCOT)$_2$], **2**, taken in 2-MeTHF at 28.8 x 10^{-6} mol/L over the course of six scans.

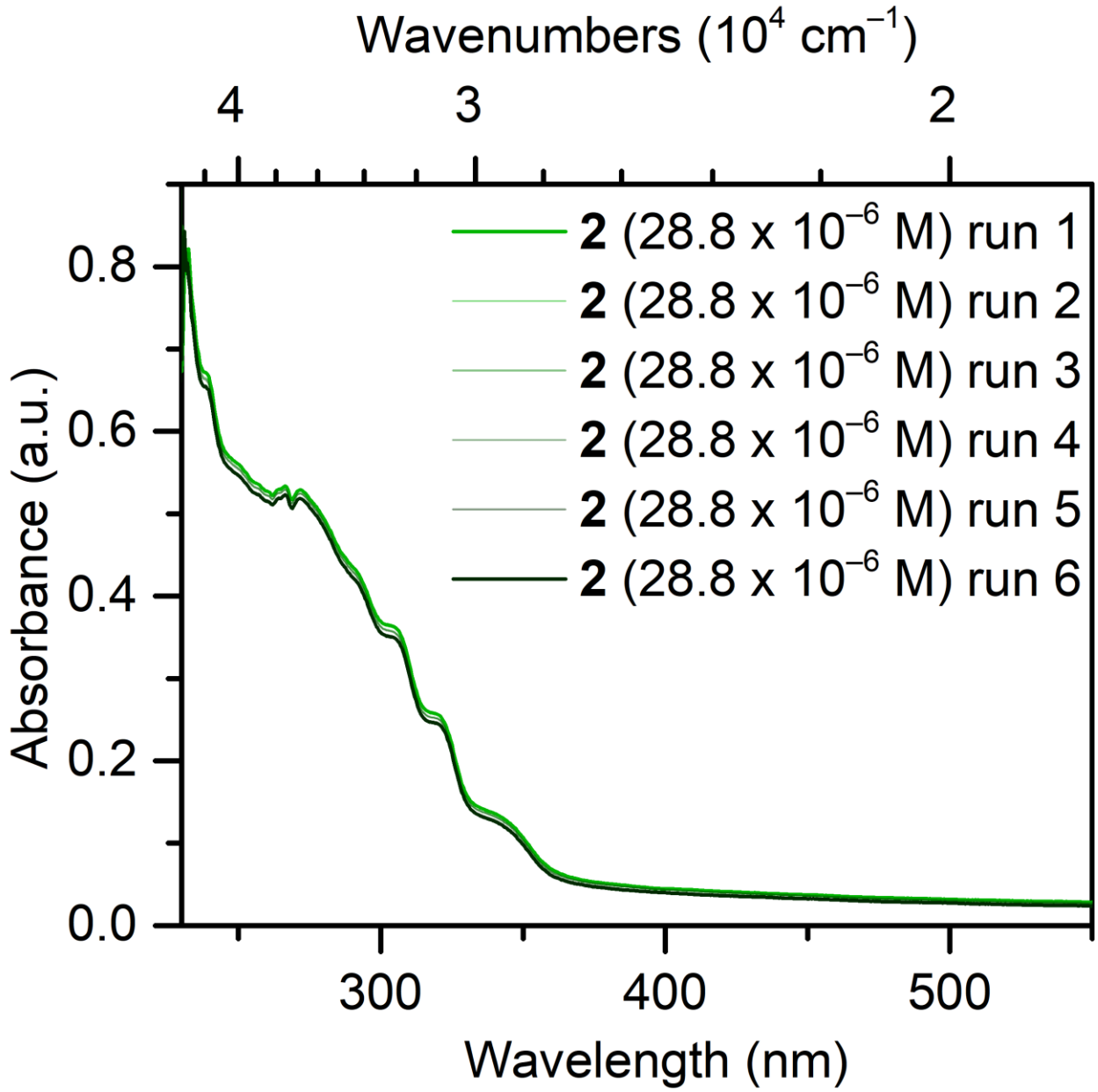

Figure S45. Magnification of the UV-Vis spectra of [K(crypt-222)][U(dbCOT)$_2$], **2**, taken in 2-MeTHF at 28.8 x 10^{-6} mol/L over the course of six scans.

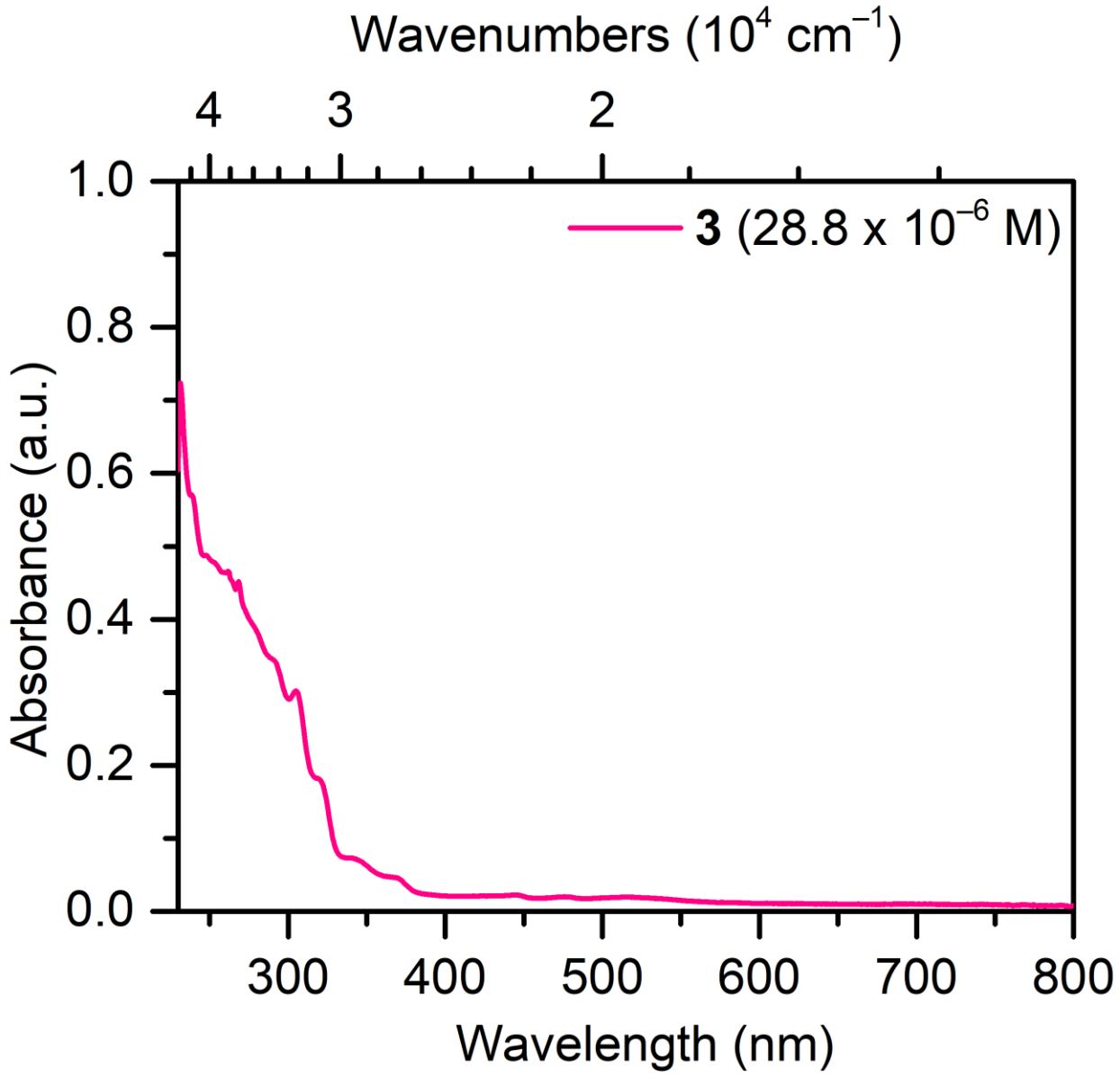

Figure S46. UV-Vis spectrum of K(crypt-222)][U(dbCOT)$_2$(THF)], **3**, taken in 2-MeTHF at 25.0 x 10^{-6} mol/L.

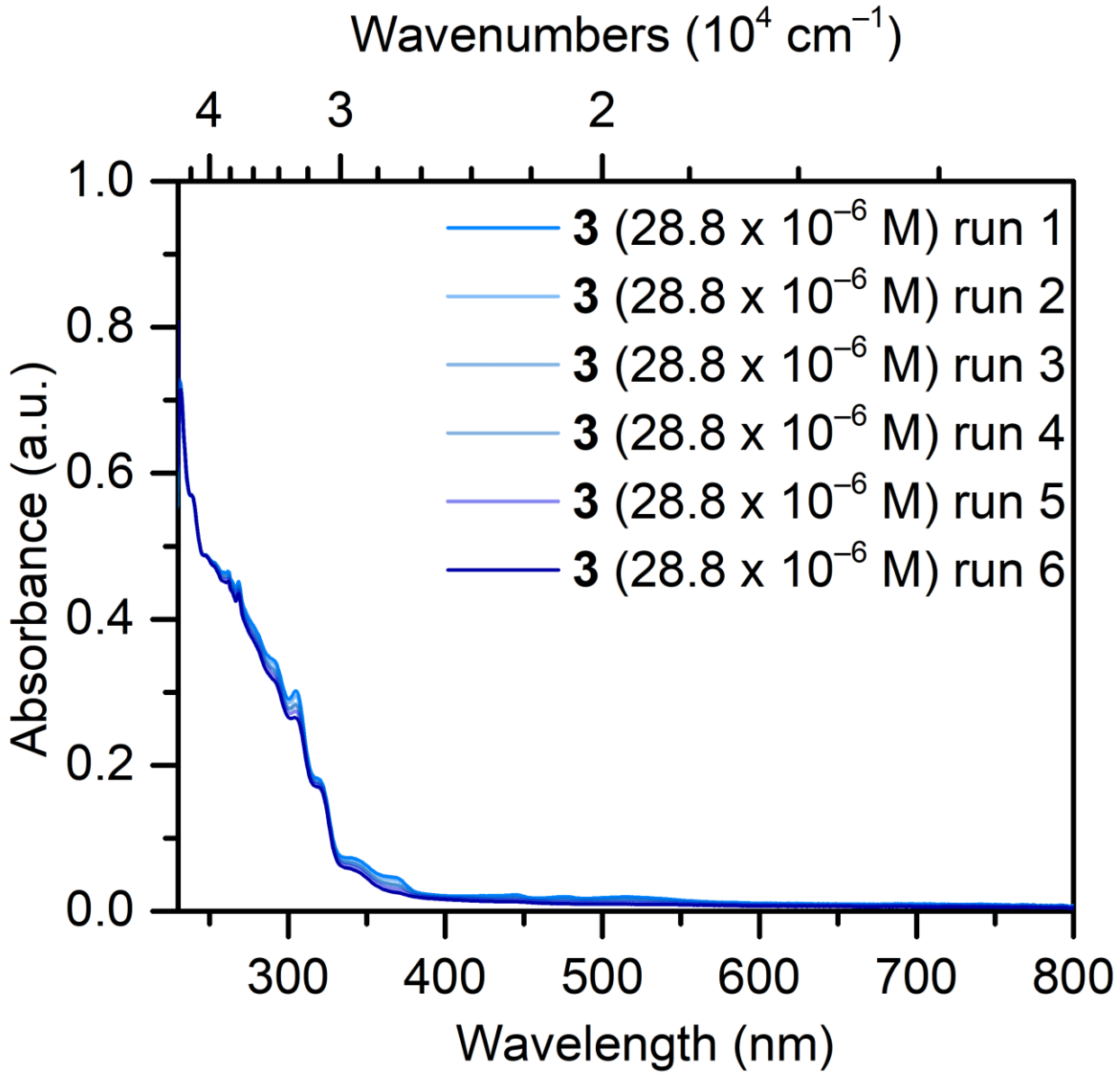

Figure S47. UV-Vis spectra of [K(crypt-222)][U(dbCOT)$_2$(THF)], **3**, taken in 2-MeTHF at 25.0 x 10^{-6} mol/L over the course of six scans.

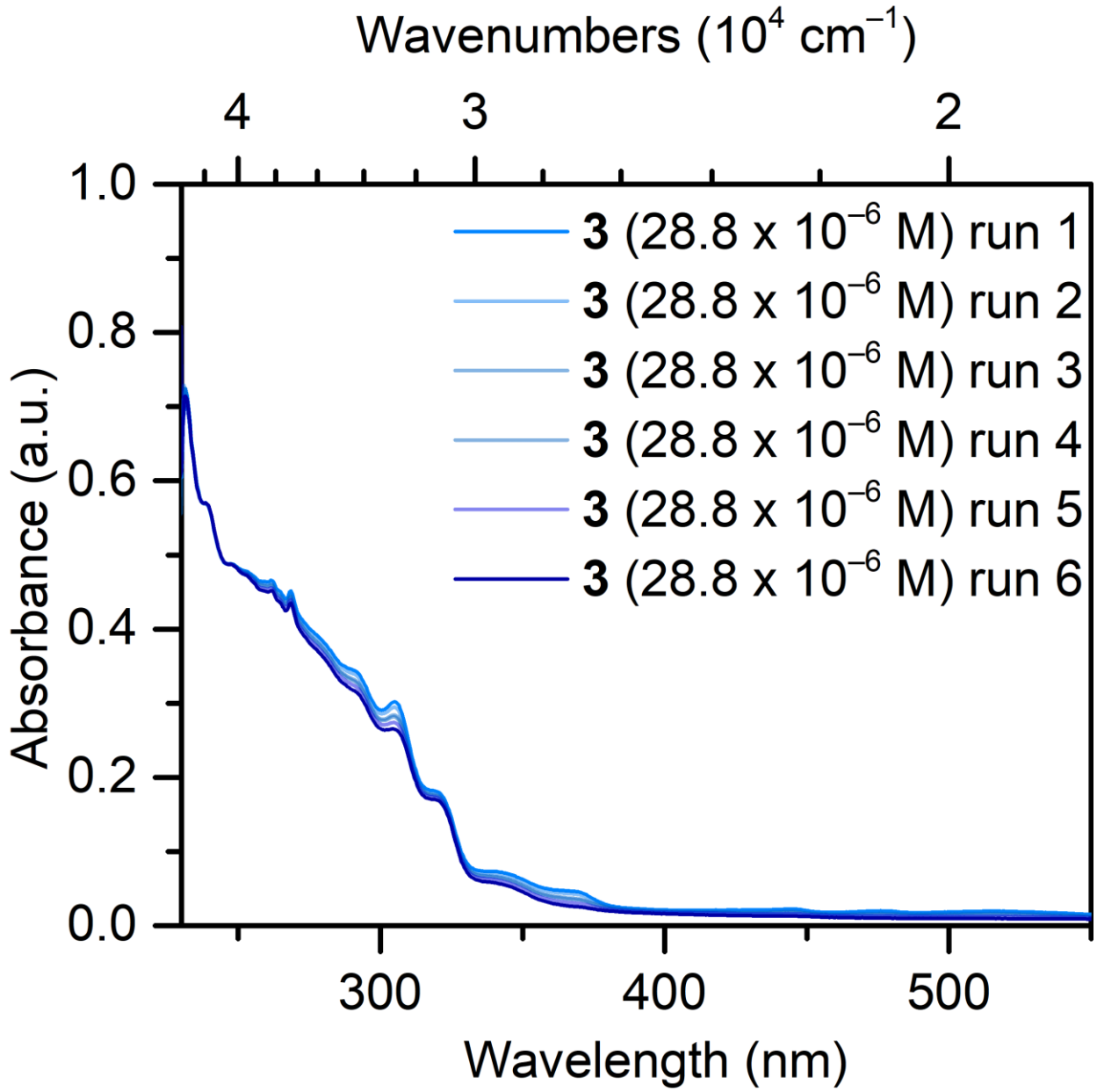

Figure S48. Magnification of the UV-Vis spectra of [K(crypt-222)][U(dbCOT)$_2$(THF)], **3**, taken in 2-MeTHF at 25.0 x 10^{-6} mol/L over the course of six scans.

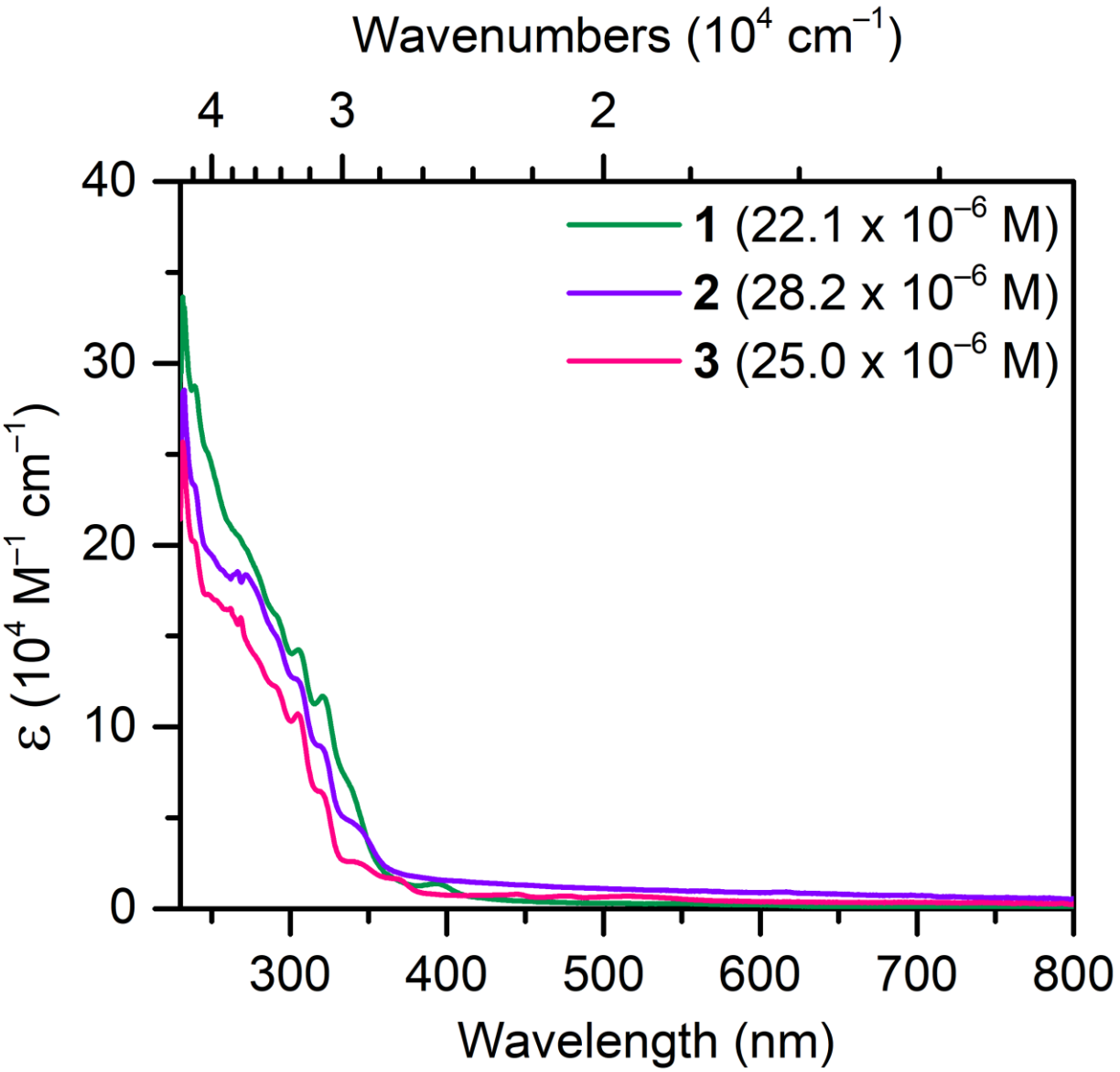

Figure S49. UV-Vis spectra of $[K(DME)_2][U(dbCOT)_2]$, **1** (green line), [K(crypt-222)][$U(dbCOT)_2$], **2** (purple line), and [K(crypt-222)][$U(dbCOT)_2$(THF)], **3** (pink line), taken in 2-MeTHF at 22.1 x 10^{-6} mol/L, 28.2 x 10^{-6} mol/L, and 25.0 x 10^{-6} mol/L, respectively.

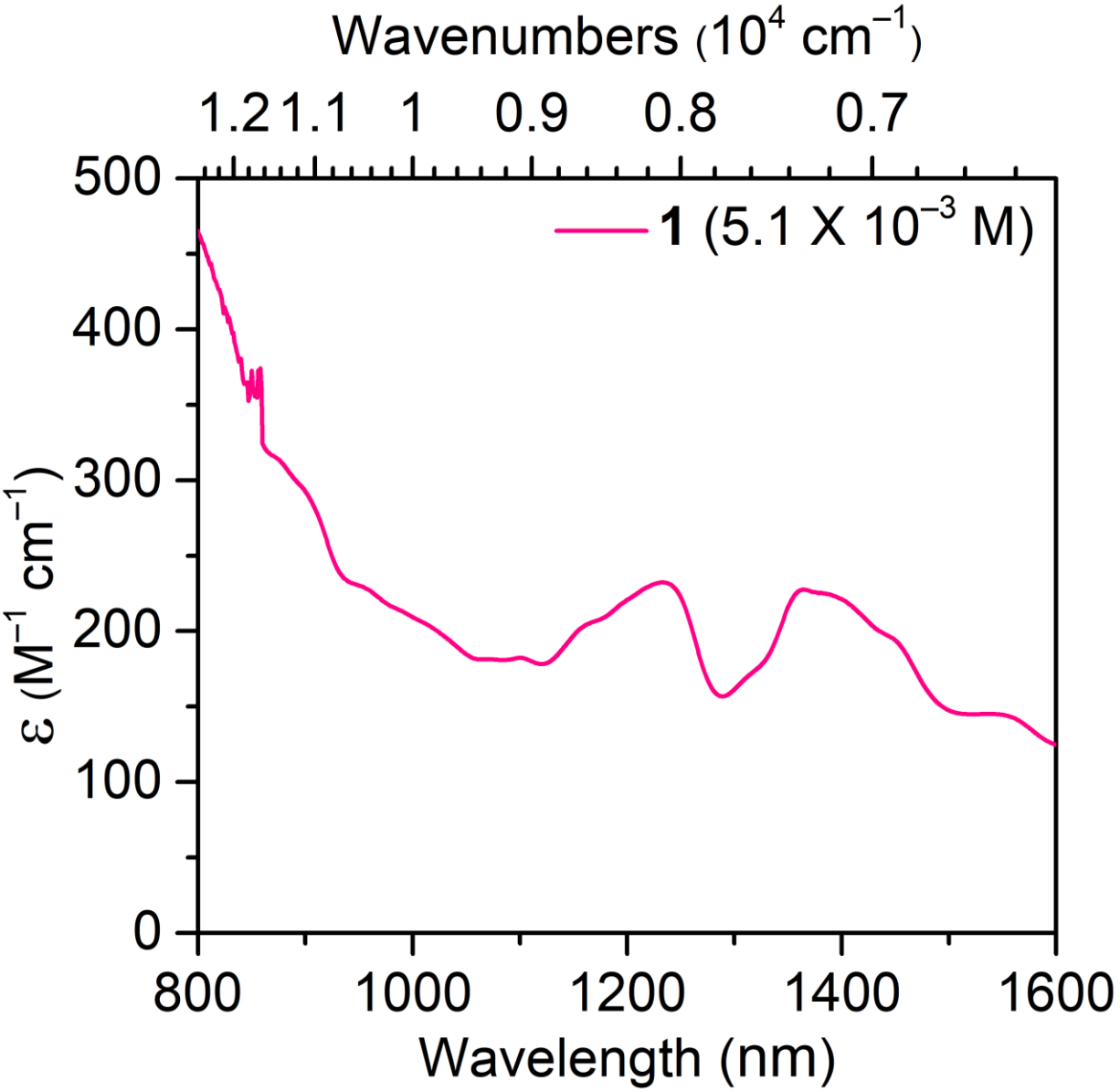

Figure S50. NIR spectrum of $[K(DME)_2][U(dbCOT)_2]$, **1**, taken in 2-MeTHF at 5.1 x 10^{-3} mol/L.

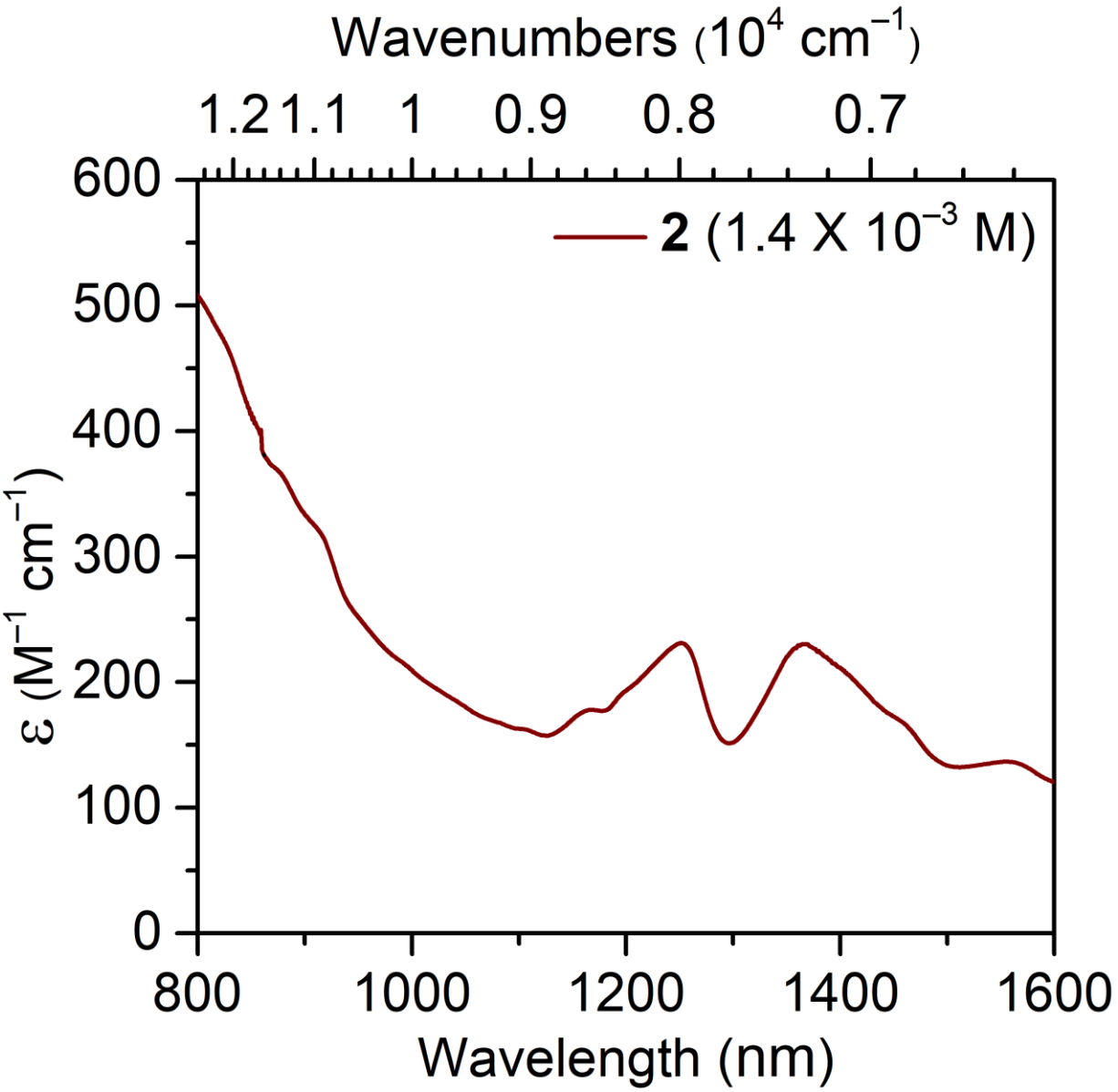

Figure S51. NIR spectrum of [K(crypt-222)][U(dbCOT)$_2$], **2**, taken in 2-MeTHF at 1.4 x 10^{-3} mol/L.

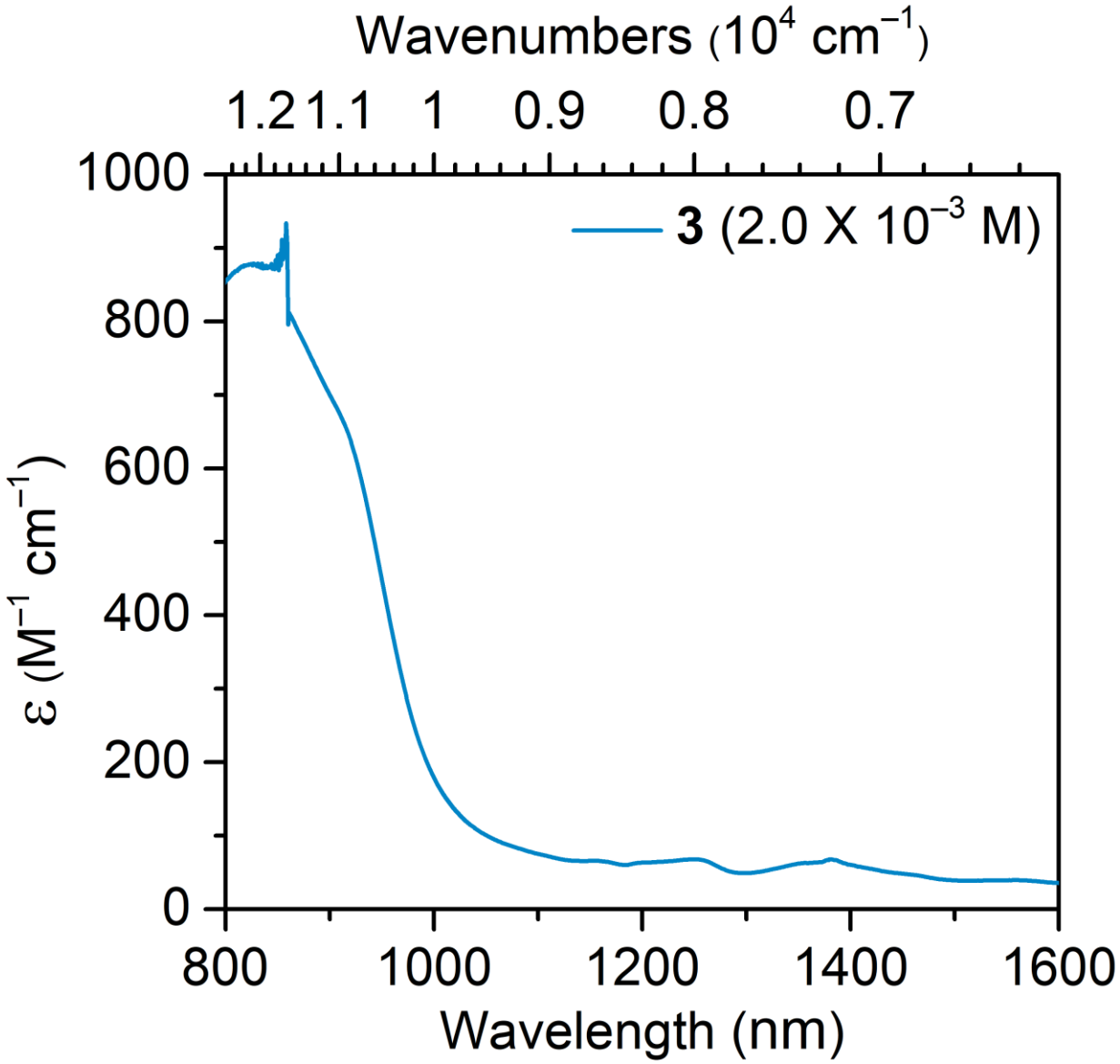

Figure S52. NIR spectrum of [K(crypt-222)][U(dbCOT)$_2$(THF)], **3**, taken in 2-MeTHF at 2.0 x 10^{-3} mol/L.

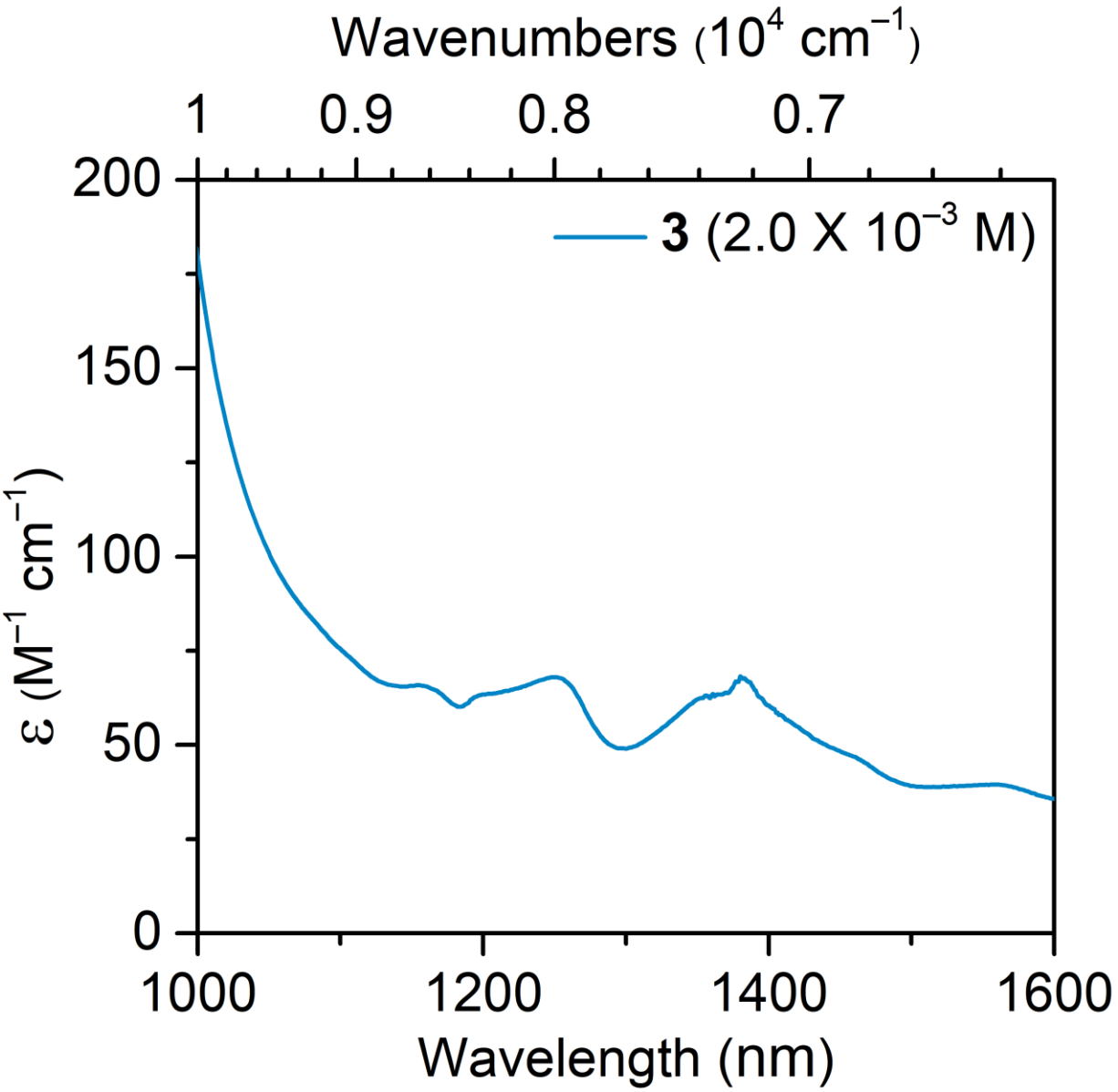

Figure S53. Magnification of the NIR spectrum of [K(crypt-222)][U(dbCOT)$_2$(THF)], **3**, taken in 2-MeTHF at 2.0 x 10^{-3} mol/L.

4 IR Spectroscopy

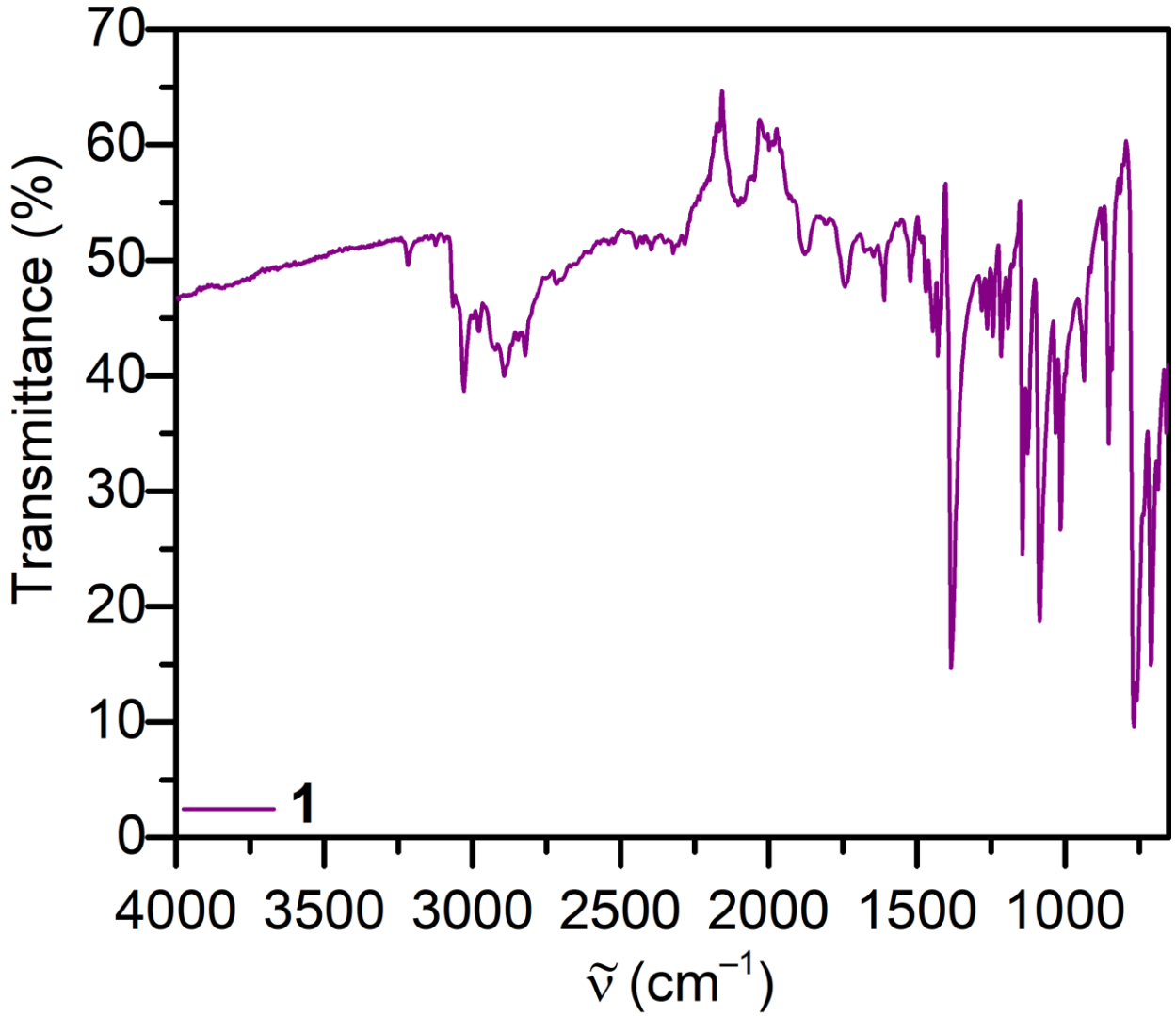

Figure S54. FTIR spectrum of $[K(DME)_2][U(dbCOT)_2]$, **1**, collected on crushed crystalline solids under a nitrogen atmosphere.

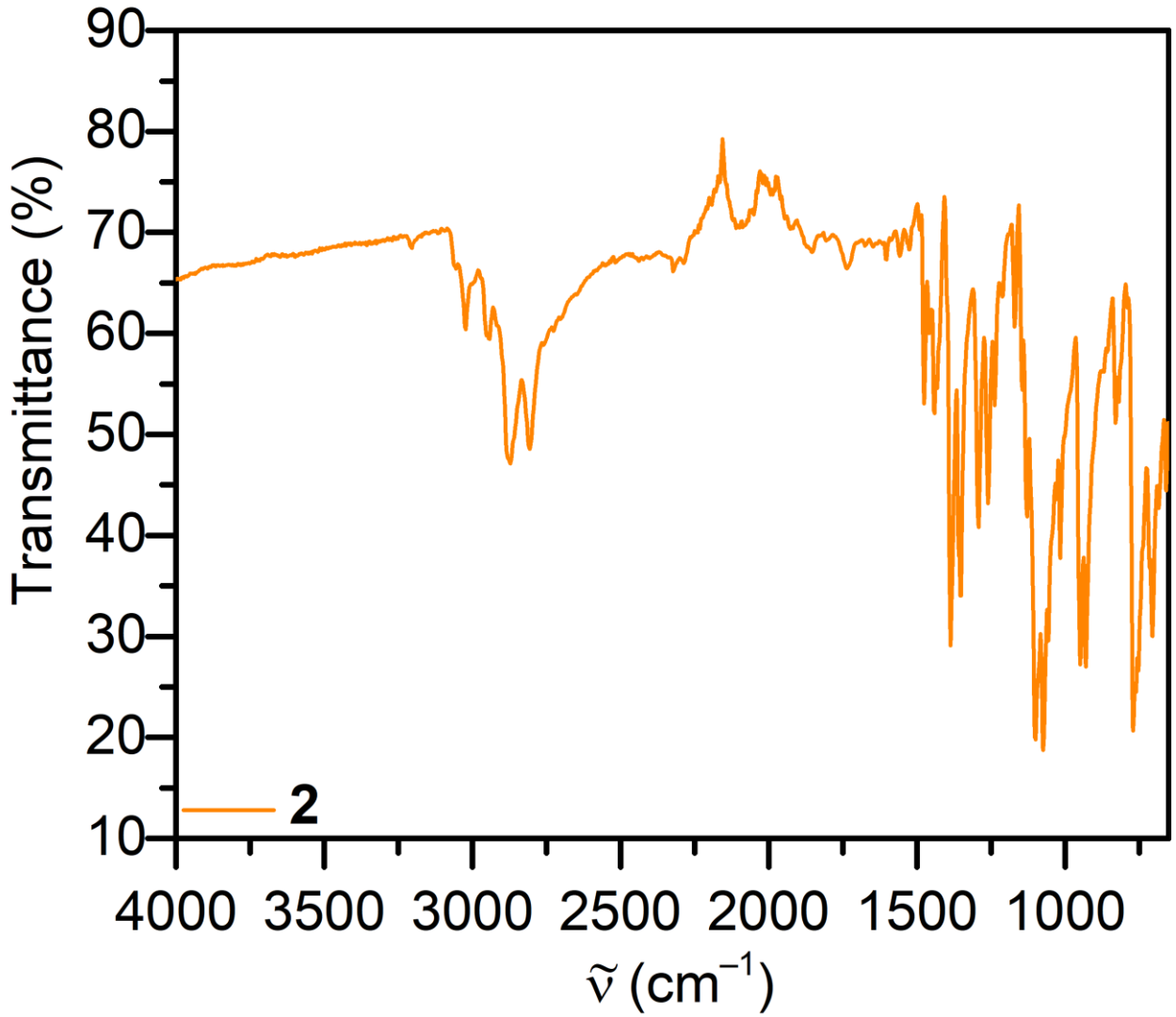

Figure S55. FTIR spectrum of [K(crypt-222)][U(dbCOT)$_2$], **2**, collected on crushed crystalline solids under a nitrogen atmosphere.

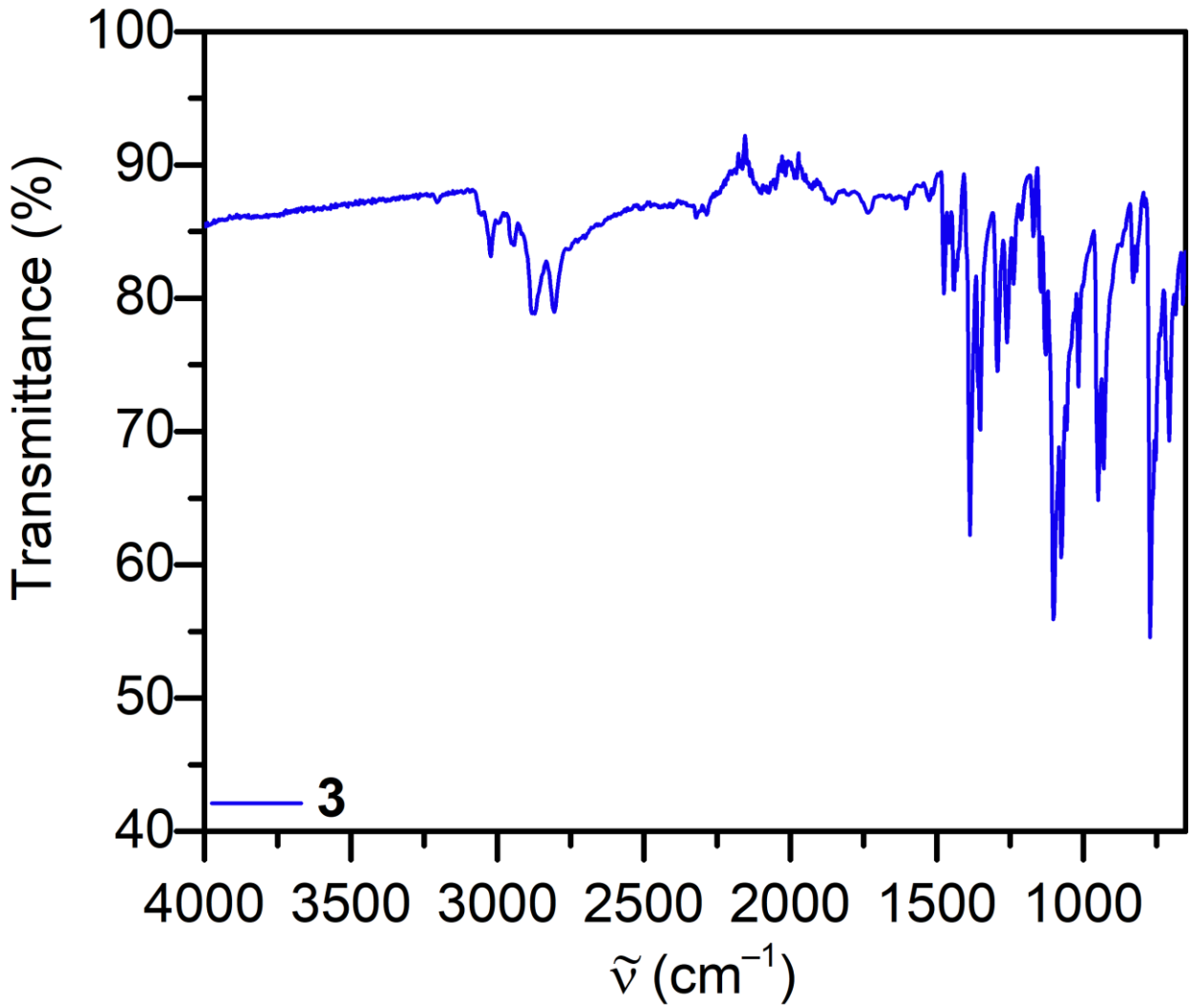

Figure S56. FTIR spectrum of [K(crypt-222)][U(dbCOT)$_2$(THF)], **3**, collected on crushed crystalline solids under a nitrogen atmosphere.

5 DFT Calculations

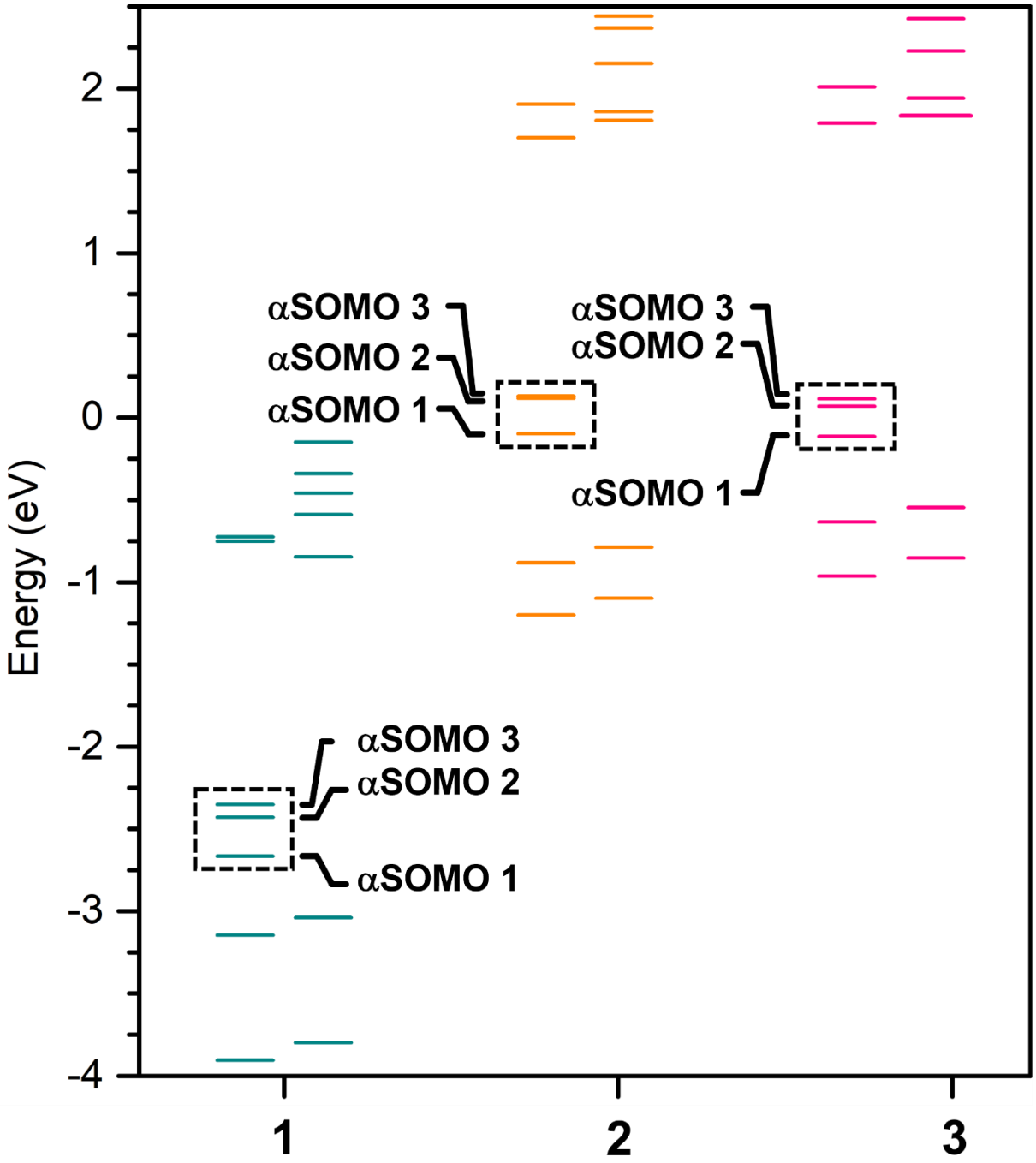

Figure S57. The calculated frontier alpha (α) and beta (β) spin orbital energies of the optimized structures of $[K(DME)_2][U(dbCOT)_2]$, **1** (teal lines), as well as the $[U(dbCOT)_2]^-$ anions in $[K(crypt\text{-}222)][U(dbCOT)_2]$, **2** (orange lines), and $[K(crypt\text{-}222)][U(dbCOT)_2(THF)]$, **3** (pink lines), respectively. The three α-spin singly occupied molecular orbitals (αSOMO) are highlighted for each complex. Energy levels are shown to scale.

Table S5. Spin polarization difference in the calculated frontier alpha (α) and beta (β) spin orbital energies of the optimized structures of $[K(DME)_2][U(dbCOT)_2]$, **1**, as well as the $[U(dbCOT)_2]^-$ anions in $[K(crypt\text{-}222)][U(dbCOT)_2]$, **2**, and $[K(crypt\text{-}222)][U(dbCOT)_2(THF)]$, **3**, respectively.

	Orbital	αSOMO E (eV)	βSOMO E (eV)	Δ E
1	αSOMO 1	–2.6649	–0.8452	1.8197
	αSOMO 2	–2.4290	–0.5892	1.8398
	αSOMO 3	–2.3509	–0.4598	1.8911
2	αSOMO 1	–0.0992	1.8068	1.906
	αSOMO 2	0.1171	1.8592	1.7421
	αSOMO 3	0.1295	2.1528	2.0233
3	αSOMO 1	–0.1161	1.8363	1.9524
	αSOMO 2	0.0704	1.9407	1.8703
	αSOMO 3	0.1118	2.2279	2.1161

Table S6. Calculated percent contributions of natural bonding orbitals (NBOs) to the parent canonical molecular orbitals in the optimized structure of $[K(DME)_2][U(dbCOT)_2]$, **1**.

Orbital Number	Orbital Label	NBO Composition	% Contribution
207	αHOMO–4	U (LV)	9.5
		C (LP)	12.7
		C–C (BD*)	38.2
209	αHOMO–2	U (LV)	9.9
		C (LP)	6.3
		C–C (BD)	35.5
210	αHOMO–1	U (LV)	7.4
		C–C (BD)	57.0
211	αHOMO	U (LV)	14.9
		C–C (BD)	27.2
		C–C (BD*)	32.0
212	αSOMO 1	U (LP)	89.7
213	αSOMO 2	U (LP)	85.1
214	αSOMO 3	U (LP)	93.1
215	αLUMO	U (LV)	18.8
		C–C (BD*)	33.0
216	αLUMO+1	C–C (BD*)	51.8
217	αLUMO+1	K (LV)	24.1

BD = bonding orbital; BD* = antibonding orbital; HOMO = highest occupied molecular orbital; LUMO = lowest unoccupied molecular orbital; LP = lone particle, LV = lone valence; NBO = natural bond orbital; SOMO = singly occupied molecular orbital.

Table S7. Calculated percent contributions of natural bonding orbitals (NBOs) to the parent canonical molecular orbitals in the optimized structure of the $[U(dbCOT)_2]^-$ anion in $[K(crypt\text{-}222)][U(dbCOT)_2]$, **2**.

Orbital Number	Orbital Label	NBO Composition	% Contribution
149	αHOMO–3	U (LV)	10.5
		C–C (BD)	15.5
		C–C (BD*)	32.8
150	αHOMO–2	U (LV)	8.0
		C–C (BD)	16.7
		C–C (BD*)	30.2
151	αHOMO–1	U (LV)	8.8
		C–C (BD)	43.5
		C–C (BD*)	12.7
152	αHOMO	U (LV)	14.6
		C–C (BD)	16.1
		C–C (BD*)	15.4
153	αSOMO 1	U (LP)	91.6
154	αSOMO 2	U (LP)	85.5
155	αSOMO 3	U (LP)	90.2
156	αLUMO	U (LV)	19.4
		C–C (BD*)	36.9
157	αLUMO+1	U (LV)	24.3
		C–C (BD*)	23.7

BD = bonding orbital; BD* = antibonding orbital; HOMO = highest occupied molecular orbital; LUMO = lowest unoccupied molecular orbital; LP = lone particle, LV = lone valence; NBO = natural bond orbital; SOMO = singly occupied molecular orbital.

Table S8. Calculated percent contributions of natural bonding orbitals (NBOs) to the parent canonical molecular orbitals in the optimized structure of the $[U(dbCOT)_2(THF)]^-$ anion in $[K(crypt\text{-}222)][U(dbCOT)_2(THF)]$, **3**.

Orbital Number	Orbital Label	NBO Composition	% Contribution
169	αHOMO–3	U (LV)	6.4
		C (LP)	6.4
		C–C (BD*)	46.7
171	αHOMO–1	U (LV)	6.9
		C–C (BD)	40.9
172	αHOMO	U (LV)	13.2
		C–C (BD)	32.3
173	αSOMO 1	U (LP)	89.3
174	αSOMO 2	U (LP)	88.5
175	αSOMO 3	U (LP)	87.8
176	αLUMO	U (LV)	10.6
		C–C (BD*)	47.0
177	αLUMO+1	C–C (BD*)	60.0

BD = bonding orbital; BD* = antibonding orbital; HOMO = highest occupied molecular orbital; LUMO = lowest unoccupied molecular orbital; LP = lone particle, LV = lone valence; NBO = natural bond orbital; SOMO = singly occupied molecular orbital.

Table S9. Calculated percent contributions of atomic orbitals to the natural bonding orbitals (NBOs) in the optimized structures of $[K(DME)_2][U(dbCOT)_2]$, **1**, as well as the $[U(dbCOT)_2]^-$ and $[U(dbCOT)_2(THF)]^-$ anions in $[K(crypt\text{-}222)][U(dbCOT)_2]$, **2**, and $[K(crypt\text{-}222)][U(dbCOT)_2(THF)]$, **3**, respectively.

	NBO	Occupancy	% Composition
1	**U (LP 1)**	0.98029	s (0.04%), p (1.02%), d (0.35%), f (98.59%)
	U (LP 2)	0.96538	s (0.00%), p (0.49%), d (0.08%), f (99.43%)
	U (LP 3)	0.89198	s (0.06%), p (0.34%), d (0.04%), f (99.62%)
2	**U (LP 1)**	0.95471	s (0.09%), p (0.53%), d (0.58%), f (98.80%)
	U (LP 2)	0.94653	s (0.01%), p (0.34%), d (0.13%), f (99.52%)
	U (LP 3)	0.93561	s (0.00%), p (0.21%), d (0.20%), f (99.59%)
3	**U (LP 1)**	0.97384	s (0.60%), p (0.12%), d (2.32%), f (96.96%)
	U (LP 2)	0.94997	s (0.00%), p (0.14%), d (0.28%), f (99.58%)
	U (LP 3)	0.94454	s (0.06%), p (0.00%), d (0.51%), f (99.43%)

LP = lone particle.